Synthesis and Properties of Transition Metal Complexes of new 3,7-Diazabicyclo[3.3.1]nonane Derivatives

INAUGURAL - DISSERTATION

zur

Erlangung der Doktorwürde

der

Naturwissenschaftlich-Mathematischen Gesamtfakultät

der

Ruprecht-Karls-Universität Heidelberg

vorgelegt von
Carlos López de Laorden
aus Madrid, Spanien

2006

INAUGURAL - DISSERTATION

zur

Erlangung der Doktorwürde

der

Naturwissenschaftlich-Mathematischen Gesamtfakultät

der

Ruprecht-Karls-Universität Heidelberg

vorgelegt von
Carlos López de Laorden
aus Madrid, Spanien

2006

Tag der mündlichen Prüfung: 24.03.2006

Synthesis and Properties of
Transition Metal Complexes of new
3,7-Diazabicyclo[3.3.1]nonane Derivatives

Abbreviations

CV	Cyclic voltammetry
EPR	Electron paramagnetic resonance
FAB$^+$	Fast-atom-bombardment mass spectrometry
NMR	Nuclear magnetic resonance
FT-IR	Fourier transform infrared
ppm	Parts per million
δ	Chemical shift
r.t.	Room temperature
bs	Broad singlet
bd	Broad doublet
s	Singlet
d	Doublet
t	Triplet
dd	Double doublets
dt	Double triplets
m	Multiplet
CH$_3$CN	Acetonitrile
CH$_3$OH	Methanol
m-**CPBA**	*m*-chloroperoxybenzoic acid
TFA	trifluoroacetic
Ts	*p*-toluene sulfonyl
^{t}**Bu**	*tert*-butyl
PhINTs	N-tosyliminobenzyliodinane
BuLi	Butyllithium
DMAE	Dimethylaminoethanol
DMF	Dimethylformamide
LDA	Lithium diisopropylamide
TMEDA	N,N,N',N'-Tetramethylethylenediamine

Index

Ligands Index^{a)}

N2Py2

N26MePy2

N26BrPy2

N25BrPy2
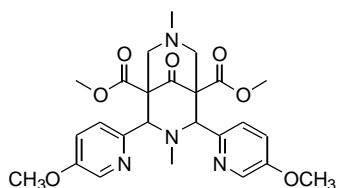
N25MOXPy2
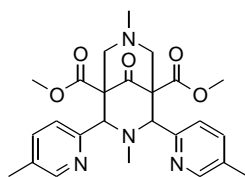
N25MePy2
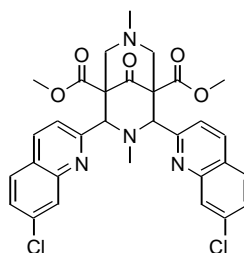
N2CQ2
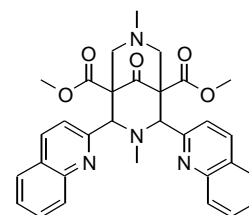
N2Q2
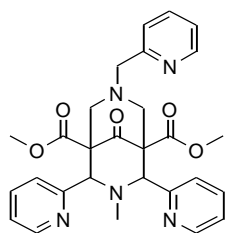
N2Py3o
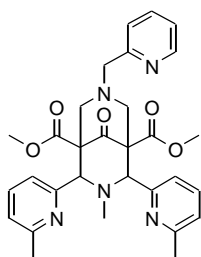
N2Pic6MePy
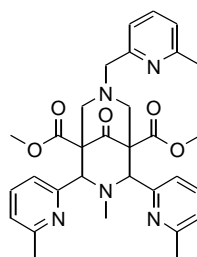
Tri6MePy
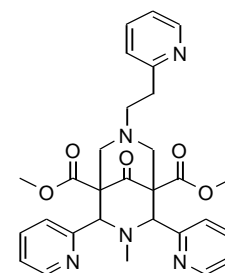
N2Py3Lo
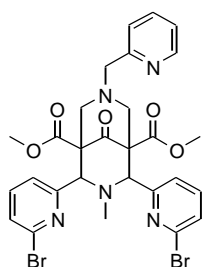
N26BrPy3o
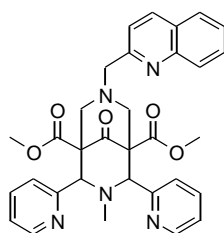
N2Py2Qo
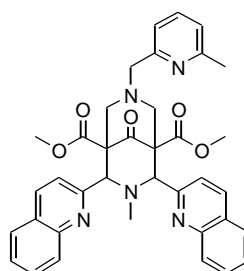
N26MePicQ2
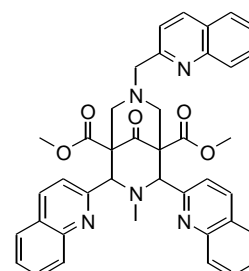
N2Q3o
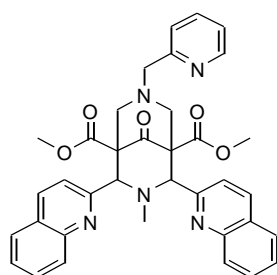
N2Q2Pyo
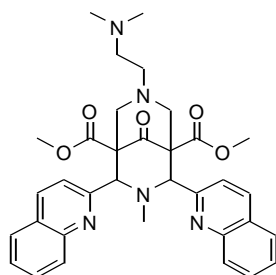
N2Q2DMEA

a)The names of the newly synthesized ligands are written in **bold-typeface** (throughout this work)

1. Abstract

The synthesis of 3,7-diazabicyclo[3.3.1]nonane derivatives is usually performed via a double Mannich reaction (Fig 1.1). The general bispidone synthesis offers a wide range of possibilities for modification of the ligands and, as shown in Chapter 4, it is possible to introduce substituents at three different positions in a relatively simple manner. However, new amino or aldehyde precursors are sometimes required, the synthesis of which may be considerably more difficult than that of the bispidone itself.
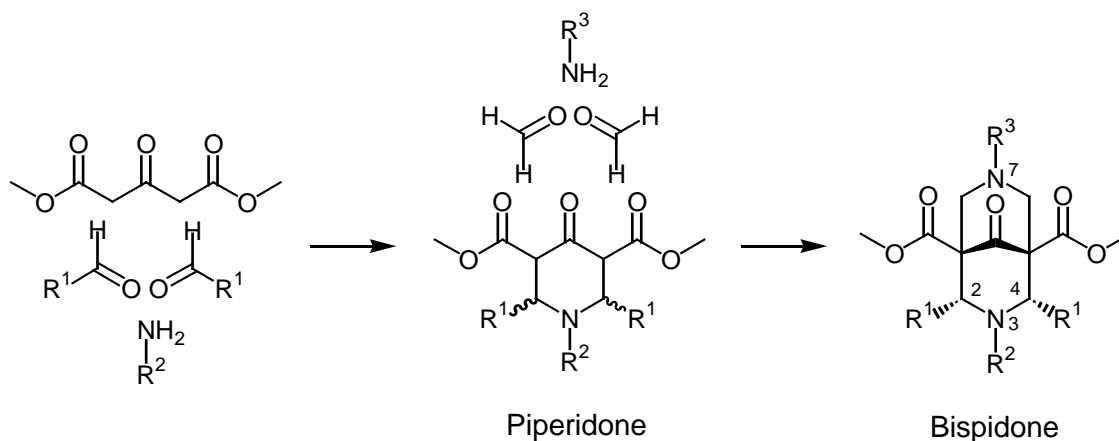
Fig. 1.1: General synthesis of 3,7-diazabicyclo[3.3.1]nonane derivatives

The main goal of the present research work was to develop a series of new 3,7-diazabicyclo[3.3.1]nonane derivatives in which only electronic (5-substituted pyridines at R_1), only steric (pyridine and 6-methyl substituted pyridines at R_1 and R_2) and both effects at the same time (quinoline derivatives and 6-substituted pyridines) were introduced (Fig. 1.2).

The intention of the proposed modifications was to obtain a series of new copper(II) and iron(II) complexes in which the electronic properties of the metal centre (redox potentials) are modified to produce new efficient and stable catalysts for the Cu-catalyzed aziridination of olefins with N-tosyliminobenzyliodinane (PhINTs) as nitrene source and the selective Fe-catalyzed oxidation of olefins with hydrogen peroxide.

Considering first the aziridination of styrene, the preliminary results shown in Fig. 1.3, suggest that an increase in the redox potential should lead to an improvement in activity (for both tetra- and pentadentate ligands). Following this hypothesis, a range of new 3,7-diazabicyclo[3.3.1]nonane copper(II) complexes were successfully synthesized and, although they still need to be tested, the observed increase in the redox potential is in some cases up to almost 600 mV (Chapter 5), promising interesting results (despite a possible increase in the steric demand leading to accessibility problems for the substrate in reaching the metal centre).
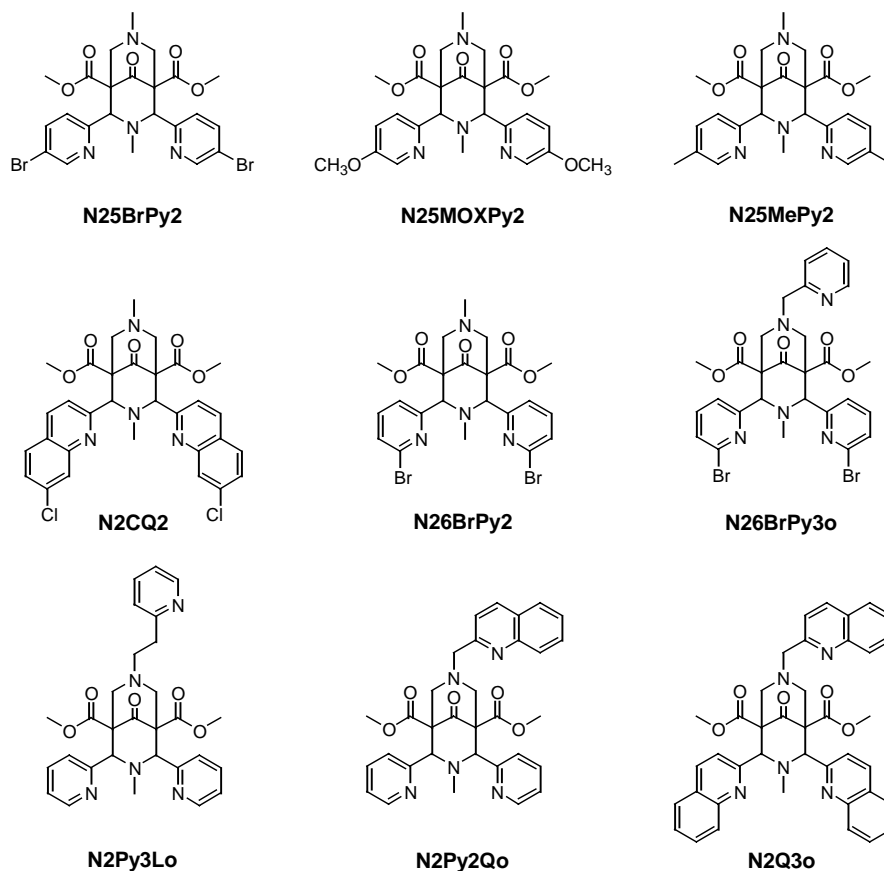
Fig. 1.2: New synthesized 3,7-diazabicyclo[3.3.1]nonane derivatives

Charge distribution calculations, using the potential-based CHELPG and Merz-Kollmann methodologies, were performed on the copper(II) complexes of a range of substituted 3,7-diazabicyclo[3.3.1]nonane derivatives at two different levels of accuracy. The results, presented in Chapter 5, provide an interesting and chemically intuitive picture of the bonding in copper(II) bispidine complexes, which is, however, not always in agreement with experiment. Possible reasons for this lack of correlation between experiment and theory could be effects such as solvation, which may influence properties such as redox potential, but are not included in the present theoretical model. A high level of theory is required to provide reasonable results for charge calculations, but has been shown to be less important for the geometries and relative energies of the complexes, with the exception of complexes with highly electronegative ligand substituents such as bromine.

	R_1				
R_2					
CH_3		6	9	19	**17**
		-440	-413	-94	-74
		-	0	**3**	-
		-	-603	-450	-383

TON
E^o (mV)

Preliminary results

N2Py3o
-603 mV

N2Q3o
-35 mV

N2Py2
-417 mV

N26BrPy2
+53 mV
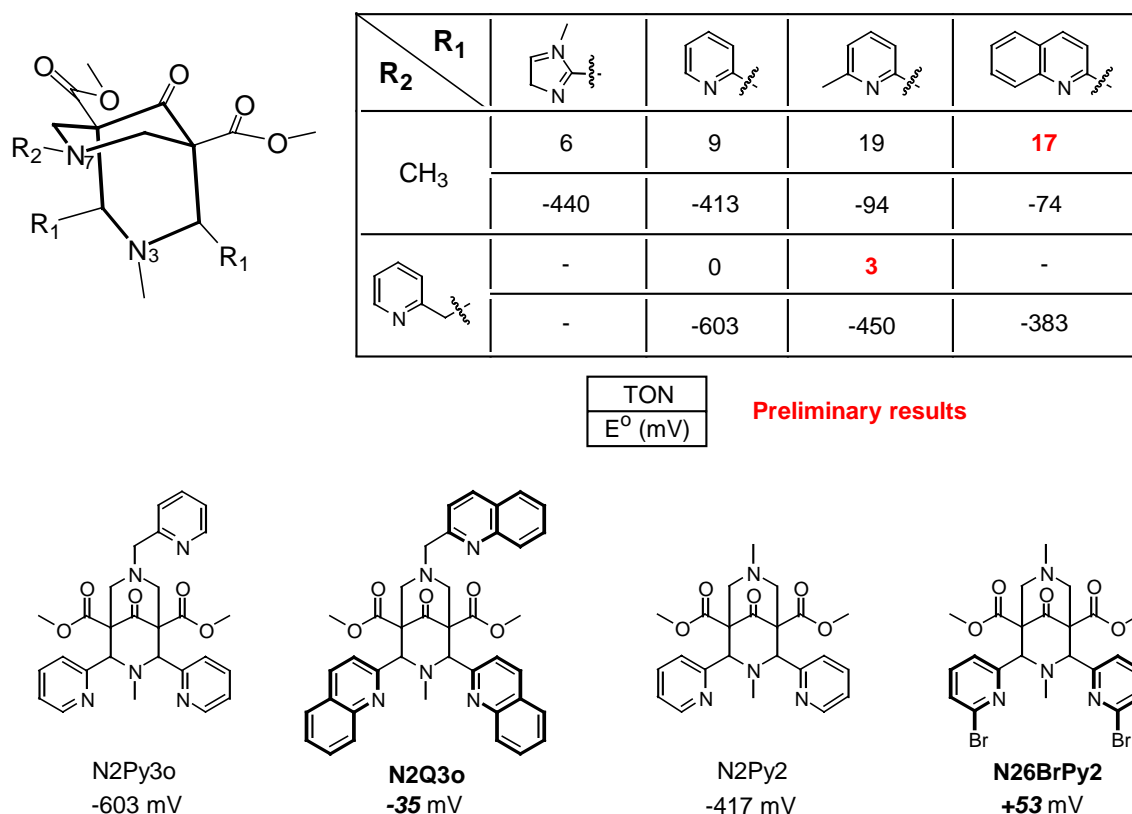
Fig. 1.3: Catalytic aziridination of styrene with 3,7-diazabicyclo[3.3.1]nonane derivatives and the largest shifts in redox potentials of selected new tetra- and pentadentate derivatives

With regard to the iron complexes, a rich oxidation chemistry was observed with both the pentadentate (N2Py3o and N2Py3u) and the tetradentate (N2Py2) ligands (Fig. 1.4). The most intensively studied of these was N2Py3o and, with the help of reactivity and labelling studies, a good understanding of the mechanism of the cyclooctene oxidation was achieved. As shown in Chapter 6, the activity of the complexes studied in the present work in the epoxidation and/or dihydroxylation of olefins using H_2O_2 as oxidant, is comparable to those of the best known catalysts of this kind.

N2Py2   **N2Py3o**   **N2Py3u**
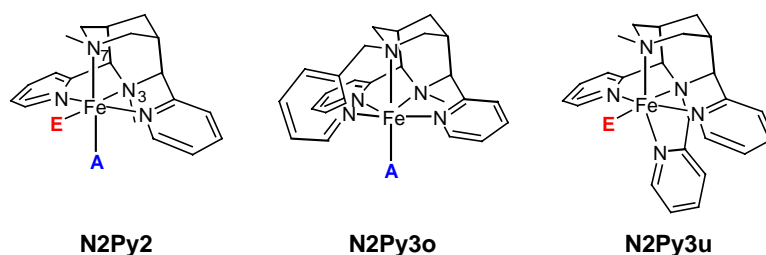
Fig. 1.4: Representation of the studied iron(II) complexes

The mechanism shown in Fig. 1.5 correlates well with the experimental results. From these it was possible to demonstrate the presence of intermediates **A** and **B**. The latter may follow three different decay pathways yielding: (i) epoxide upon reaction with oxygen, (ii) diol upon reaction with a highly reactive hydroxy radical or (iii) epoxide by decomposition. Regarding N2Py3o, the most surprisingly result was the extremely different behaviour under aerobic or anaerobic conditions, suggesting the presence of (carbon-based) radicals in the process of oxidation, as presented in path (i). The presence of these was confirmed by the oxidation results with 2-cis-heptene, where stereochemical scrambling in the epoxide (under aerobic conditions) was observed. Epoxide could also be obtained by oxidation with the in-situ prepared Fe(IV)=O intermediate (**A**) however, which implies a direct transfer of the ferryl oxygen atom to the C-C double bond. With regard to intermediate **A**, an exchange between coordinated water and the ferryl oxygen was shown, by observation of the labelling results.

The diol formation is proposed to take place via pathway (ii), in which the carbon-based radical **B** reacts with a highly reactive oxygen-based radical. The inhibition of diol formation In MeOH confirms the quenching of the later.
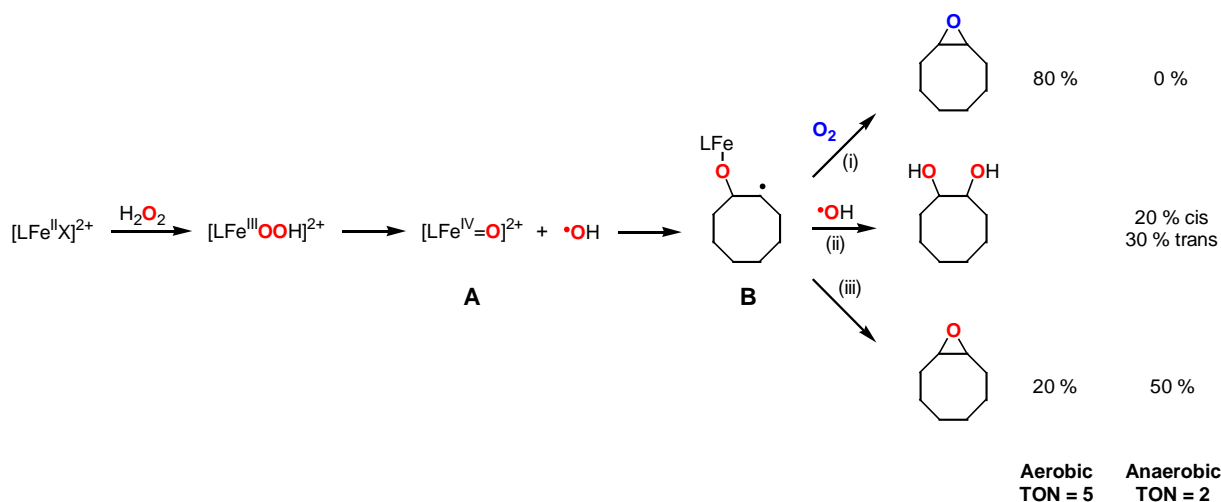
Fig. 1.5: Proposed mechanism for cyclooctene oxidation with N2Py3o iron(II) complex

The behaviour of N2Py2 in the oxidation of cyclooctene is completely different to that of N2Py3o and N2Py3u. The N2Py2-based catalyst demonstrates the same reactivity and selectivity (diol:epoxide ratio) under aerobic and anaerobic conditions, suggesting that oxygen is not required for catalytic activity. In MeOH, as for N2Py3o, complete and partial inhibition of diol and epoxide production, respectively, was observed. In this case, it is postulated that the MeOH functions, not as a radical quencher, but rather by blocking the second coordination site, thereby preventing the formation of the presumed catalytically active species shown in Fig. 1.6.

The most interesting result obtained from the ^{18}O-labeling experiments was the complete incorporation of the label coming from $H_2{}^{18}O_2$ into the diol, while tetradentate analogues like TPA (Fig. 6.3) for example, incorporate only fractions of the label. Density functional calculations suggest an Fe(II)/Fe(IV) pathway for diol formation, where the active species is an Fe(IV)-dihydroxo species (pathway (i) in Fig. 1.6).

A tentative mechanism for the epoxidation and dihydroxilation with the N2Py2 based catalyst is shown in Fig. 1.6. It involves the formation of an active Fe(IV)=O species, via Fe(II)(HOOH) and Fe(IV)-dihydroxo intermediates. This species is analogous to intermediate **A** in the N2Py3o mechanism (Fig. 1.5), but is formed without the release of OH radicals. The analogue of intermediate **B** can then be formed in a similar way to that proposed for N2Py3o. Due to the lack of OH radicals, this species cannot form diol, as for N2Py3o, but follows pathways (ii) and (iii) to form epoxide originating from H_2O_2 and O_2 respectively.

.
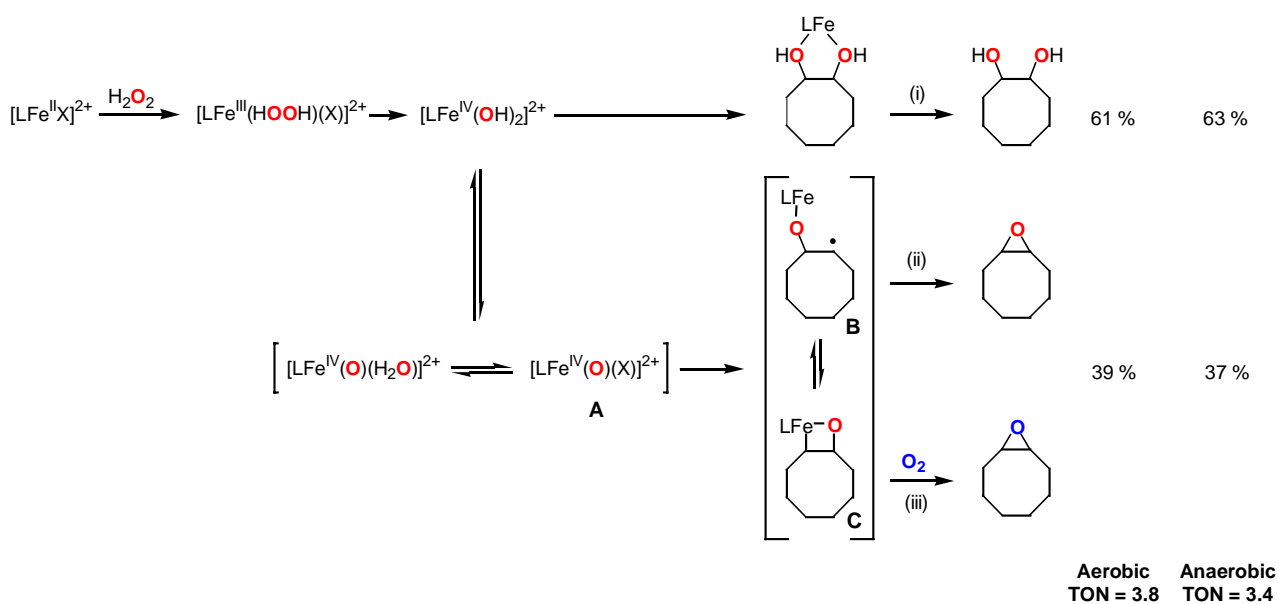
Fig. 1.6: Proposed mechanism for cyclooctene oxidation with N2Py2 iron(II) complex

Finally, a series of 3,7-diazabicyclo[3.3.1]nonanes were tested for antimalarial activity. The preliminary results, shown in appendix A, indicate that, while these compounds are not especially active against diverse protozoan malaria parasites, a rational tuning of the 3,7-diazabicyclo[3.3.1]nonanes backbone (by modification and/or substitution on the pendant residues at R_1 or R_2) could produce interesting and promising new lead structures and introduce these compounds to the field of the antimalarial drugs.

2. Zusammenfassung

Das Ziel dieser Arbeit war die Entwicklung einer neuen Reihe 3,7-Diazabicyclo[3.3.1]nonan Derivate, wo nur elektronisch (R_1 5-substituierte Pyridine), sterisch (pyridin und 6-methyl substituierte Pyridine an R_1 und R_2) und beide Effekte gleichzeitig (quinolin derivative) an dem Metallzentrum einwirken könnten. Die Synthese der substituierten 3,7-Diazabicyclo[3.3.1]nonanone erfolgt über eine zweifache Mannich-Reaktion. Im Verlauf dieser Arbeit konnten zahlreiche neue Derivate dargestellt werden (siehe Kap. 4 und Abb. 2.1.

Piperidone

Bispidone

N25BrPy2

N25MOXPy2

N25MePy2

N2CQ2

N26BrPy2

N26BrPy3o

N2Py3Lo

N2Py2Qo

N2Q3o
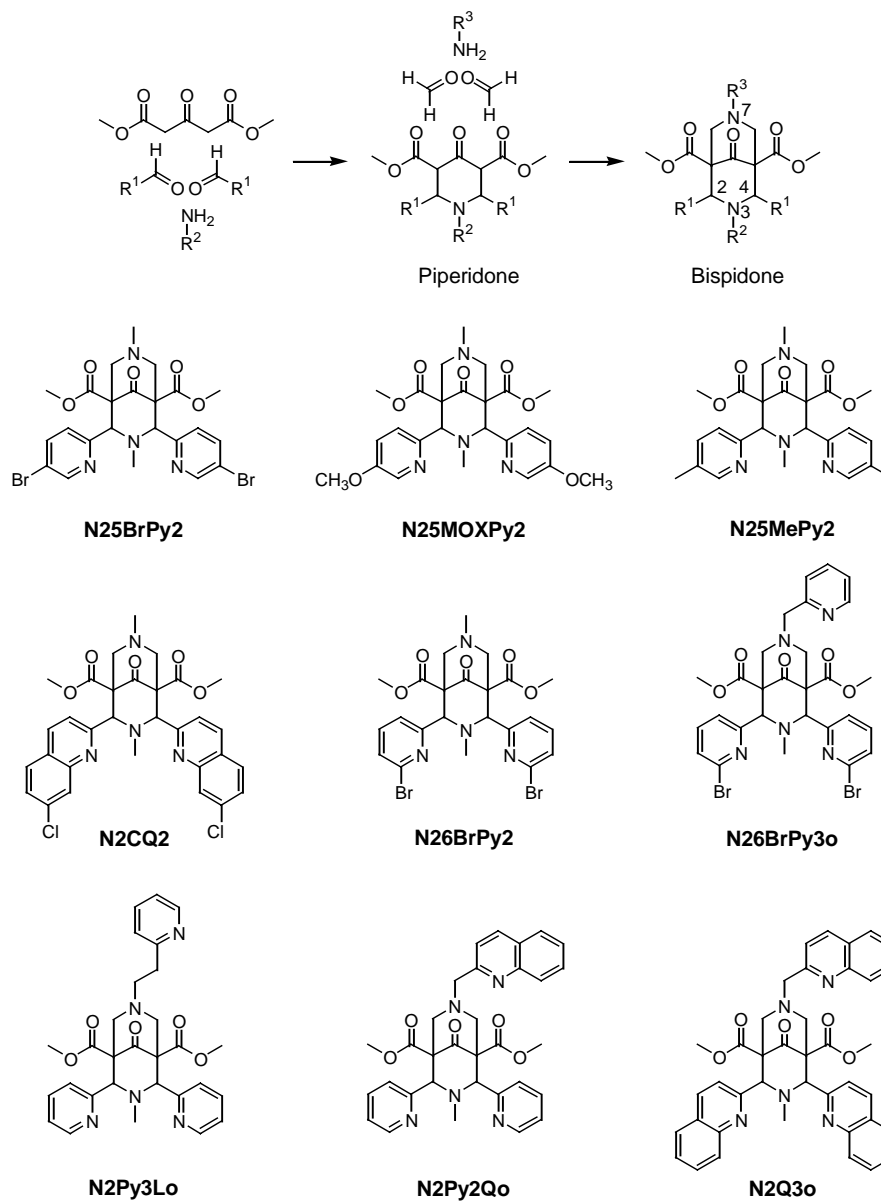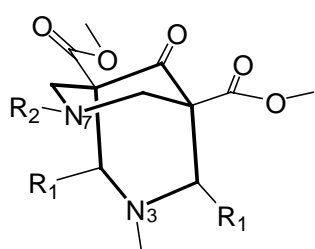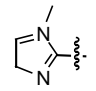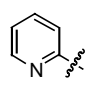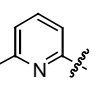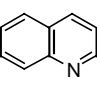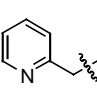
Abb. 2.1: Synthese der substituierten 3,7-diazabicyclo[3.3.1]nonan Derivate

Der Zweck solcher Modifikationen waren neue Kupfer(II) und Eisen(II) komplexe zu synthetisieren, wo die Elektronische Eigenschaften des Metallzentrums (Redoxpotentiale) modifiziert werden könnten, so dass eine neue Familie effektive und stabile Katalysatoren für die Aziridinierung von Olefine mit PhINTS als Nitrenquelle, beziehungsweise für die selektive Oxidation von Olefine, erreichbar werden könnte.

Die ersten Ergebnisse in der Styrol Aziridinierung mit den neuen Kupfer(II) komplexe (siehe Abb. 2.2) zeigten, dass eine Erhöhung des Redox Potentials des Kupfer(II) komplexes eine eindeutige Verbesserung der Ausbeute ergab (innerhalb vier- und fünfzähnige Liganden). Eine ganze Reihe viel versprechende neuer kupfer(II) Komplexe wurde erfolgreich synthetisiert, wo in manchen Fällen eine Steigung von ca. 600 mV in der Redox Potential möglich war (siehe Abb. 2.2). Die eingefügten Elemente (z.B. Quinoline), die die oben genannte Erhöhung ermöglichen, könnten wegen sterische Probleme auch der Zugang von Substraten an dem Metallzentrum leicht sperren. Trotzt diesem negativen Effekt und dank Ihrer hohen Redoxpotentialen, bleiben die neuen Kupfer(II) Komplexe als potenzielle attraktive Katalysatoren.

R_1 / R_2	(N-methylimidazole)	(pyridine)	(6-methylpyridine)	(quinoline)
CH$_3$	6	9	19	**17**
	-440	-413	-94	-74
(2-picolyl)	-	0	**3**	-
	-	-603	-450	-383

TON
E^o (mV)

Preliminary results

N2Py3o
-603 mV

N2Q3o
-35 mV

N2Py2
-417 mV

N26BrPy2
+53 mV

Abb. 2.2: Katalytischer Aziridinierung von Styrol mit 3,7-diazabicyclo[3.3.1]nonane Derivate und größte Verschiebung der redox Potentiale

Die Parametrisierung von Redoxpotentialen und Reaktivitäten mit Ladungsverteilungsrechungen wurde untersucht. Der Grund warum die Potential basierende Methoden benutzt wurden war der Kompromiss zwischen Genauigkeit, Simplizität der Methode und kürze Rechnerzeit. Chelpg und Merz-Kollmann wurden schon erfolgreich verwendet mit chemischen Modellen von blauen Kupferproteinen.

Die Oxidation von cis-Cycloocten mit dem Eisen(II) Komplexe (siehe Abb. 2.3) wurde gründlich untersucht. Durch Markierungsexperimente sowie H_2O_2 Konzentration / Zeit / Temperatur Abhängigkeitsversuche konnte der Oxidationsmechanismus gut verstanden werden.

In Kapitel 6 wurde schon erwähnt, dass Bispidon-Katalysatoren vergleichbare Aktivitäten sowie Reaktivitäten mit dem besten Eisen(II) Katalysatoren, die heute verfügbar sind, erreichen.
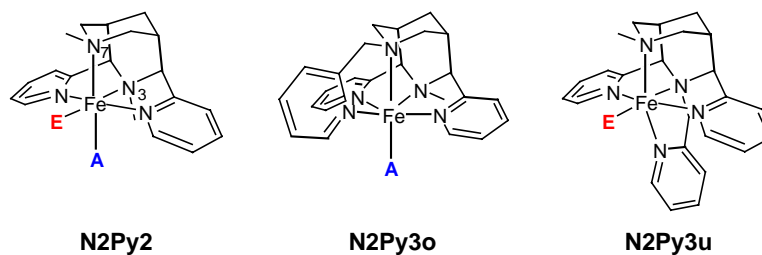
Abb. 2.3: Untersuchte Eisen(II) Komplexe

Der vorgestellte Mechanismus für N2Py3o (siehe Abb. 2.4) passt sehr gut zu den erhaltenen Ergebnissen. In diesem sind Intermediate **A** und **B** die aktive Spezies. Intermediat **B** kann folgendermaßen reagieren; (i) Epoxid wird durch Reaktion mit Sauerstoff, (ii) Diol wird durch Reaktion mit hochreaktiven Hydroxylradikalen oder (iii) Epoxid wird nach Zersetzung von **B** gebildet. Ein wertvoller Hinweis für die Anwesenheit von **B** ist, dass unter Argon die Ausbeute und die Selektivität deutlich sinken. Das deutet darauf hin, dass Kohlenstoff-basierte Radikale in dem Mechanismus involviert sind. Diese Radikale konnten nachgewiesen werden („*stereochemical scrambling*" wurde beobachtet) in der Reaktion mit 2-cis-Hepten als Substrat.

Intermediat **A** spielt aber auch eine wichtige Rolle in der Epoxid Bildung mit N2Py3o, wo eine direkte Sauerstoffübertragung an der C-C Doppelbindung beobachtet wurde. Laut Markierungsexperimente findet ein Austausch zwischen koordiniertes Wasser und der Sauerstoff der Ferryl Einheit statt.

Interessant ist auch, dass in Methanol kein Diol gebildet wird. Das deutet darauf hin dass die Diol Bildung mit Radikalen in Verbindung steht und diese werden durch das Methanol gequencht.
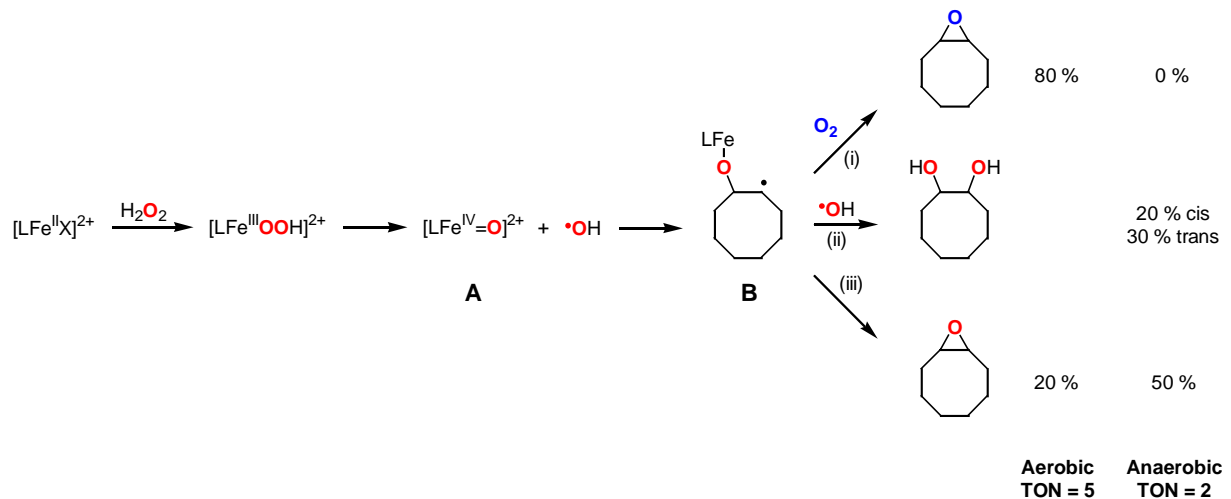
Abb. 2.4: Postulierte Cycloocten Oxidation Mechanismus mit N2Py3o

Im Gegensatz zu N2Py3o besitzt N2Py2 eine völlig unterschiedliche Reaktivität. Das liegt daran, dass der Eisen(II)-N2Py2 Komplex eine extra freie Koordinationsstelle zur Verfügung hat (siehe Abb. 2.3).

Der N2Py2 basierte Katalysator ist nicht selektiv (fast 1:1 Epoxid:Diol ratio), aber vergleichbar reaktiv wie N2Py3o. Unter O_2 sowie unter Argon die Selektivität und die Reaktivität waren fast identisch. In Methanol ist die Bildung von Diol (wie mit N2Py3o) verhindert. Der Grund dafür, hat hier aber nichts mit Radikalen zu tun. Man vermutet, dass Methanol durch Koordination zu dem Metallzentrum die aktive Spezies (siehe Abb. 2.5) blockiert. Wenn $H_2^{18}O_2$ statt H_2O_2 verwendet wurde, waren alle ^{18}O Atome in dem Diol eingebaut.

Der Einfluss von H_2O_2 Konzentration, Reaktionszeit und Temperatur an der TON wurde mit dem N2Py3o und N2Py3u Systeme untersucht. Es wurde dabei festgestellt, dass bei N2Py3o der einzige Faktor, der eindeutig die TONs erhöht, die Temperatur war. Mit N2Py3u ist eine längere Reaktionszeit nötig, um vergleichbare Reaktivitäten zu erreichen. Durch eine Erhöhung der H_2O_2 Konzentration bei N2Py3o erhöht sich die Ausbeute (bekommt man mehr Produkt), aber nicht der TON. Mit den Standard Reaktionszeiten wurde festgestellt, dass fast genau soviel Produkt erhalten worden ist wie auch nach 24 Stunden.

Zum Schluss und wie im Anhang A gezeigt, die 3,7-diazabicyclo[3.3.1]nonane Derivate wurden gegen Malaria getestet. Sie sind aber nicht besonders aktiv und auch nicht besonders ungiftig. Aber wie manche erste Ergebnisse zeigten, könnte man diese große

Familie von Verbindungen in diesem sehr interessanten Bereich der Antimalaria Medikamente weiter vorantreiben.
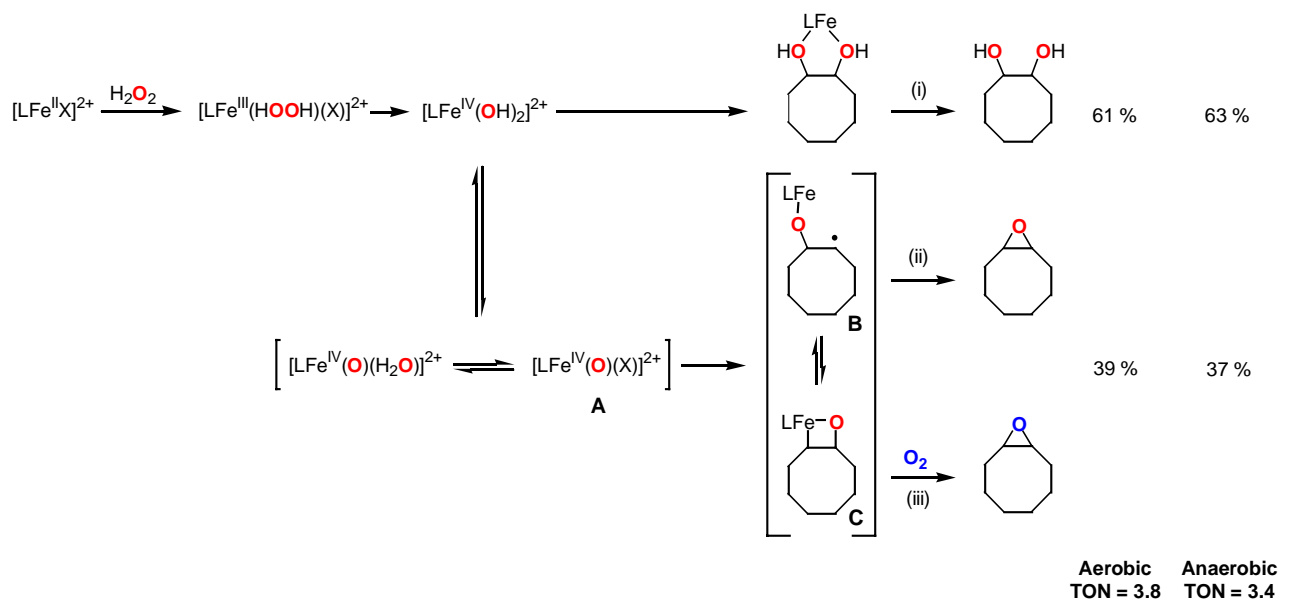
Abb. 2.5: Postulierte Cycloocten Oxidation Mechanismus mit N2Py2

3. Introduction

The present research work is dedicated to the synthesis of new bispidine-type ligands and the study of the properties and applications of their copper(II) and iron(II) complexes.

In coordination chemistry and particularly for ligands of this kind, preorganization and selectivity are concepts of great importance[1,2]. Preorganization compares the structures of the free and the coordinated ligand, with a highly preorganized ligand exhibiting almost the same structure when coordinated as in the metal-free form. Metal-ion selectivity refers to the relative stabilities of different metal ion complexes with a specific ligand, and is influenced by steric, electronic, kinetic and thermodynamic effects, as well as solvation. In terms of the 3,7-diazabicyclo[3.3.1]nonane backbone, bispidone ligands are highly preorganized, but in the metal-free form the two pyridine rings are most often rotated away from the coordination site by approximately 180° (torsion with a low energy barrier). Another important feature of these ligands is the high elasticity of the coordination sphere (flat potential energy surfaces), which, despite the rigidity of the backbone, leads to ligands less selective than expected[3,4,5], but for this very reason, to interesting and unexpected non Irving-Williams behaviour. These properties of the bispidone ligands, combined with the relative ease of modification (variation of steric and/or electronic effects) at all R positions shown in Fig. 3.1, offer a great variety of coordination geometries and electronic structures, leading to different stabilities and interesting properties of the corresponding metal complexes[6,7,8].
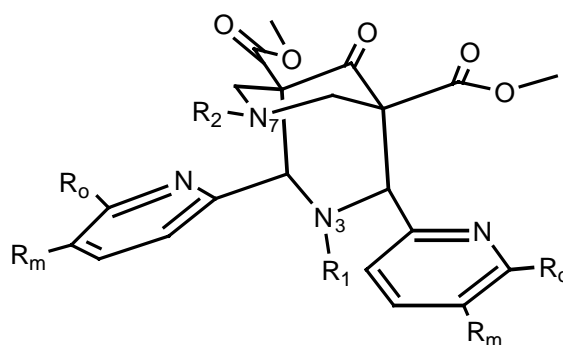
Fig. 3.1: The 3,7-diazabicyclo[3.3.1]nonane backbone

The scope of application of these ligands in coordination chemistry is mainly focused on biologically relevant transition metal ions such as copper and iron[3,4,6], although complexes with a number of other metals are known[9,10].The ability to tune the properties of these metal complexes at will is an important challenge in the development of new and active catalysts. Molecular modelling has become a useful tool in coordination chemistry, and various methods are used to improve the understanding of the electronic and steric influence of

substituents in metal complexes. By correlating calculations with experiment, molecular modelling can be used to develop criteria for synthesising ligands and complexes with specific properties required for effective catalysis.

The two main fields in *catalysis* in which bispidone complexes are involved are the selective oxidation of hydrocarbons[11] and the aziridination of olefins[7]. The former is of great interest due to the fact that, for a long time, the most common catalysts in this field were based on chromium[12], osmium[13], manganese[12] and other metals potentially harmful to humans and the environment. The development of iron-based oxidation catalysts is therefore an important alternative and most of those developed in recent years have been non-heme in nature[14-18]. Numerous examples of both heme and non-heme iron enzymes are found in nature, which are involved in a variety of hydrocarbon oxidations via C-H or C-C bond activation[19-22]. Examples of these are cytochrome P450 (mononuclear heme)[10], the anti-tumor drug bleomycin (mononuclear non-heme)[19-21,23,24] and methane monooxygenase (dinuclear non-heme)[19]. Within the recently developed class of synthetic, non-heme iron oxidation catalysts, the iron complexes of selected bispidone ligands show reactivities comparable to the best catalysts known.

Copper-based catalysts have long been used in the aziridination of olefins[25-28]. Aziridines are the nitrogen analogues of epoxides and exhibit similar reactivity patterns as electrophilic reagents. They undergo highly regio- and stereoselective transformations and are therefore useful building blocks in organic synthesis. In addition, some aziridines exhibit antitumor, antibiotic or other biological activites, which makes them attractive synthetic targets on their own. The basic reaction proceeds via the insertion of a nitrene source (a commonly used source is [*N*-(p-toluenesulfonyl)-imino]phenyliodinane) into the C-C double bond of the olefin. The copper complexes of selected bispidine ligands have shown interesting catalytic activity in the azidirination of olefins[7].

4. 3,7-diazabicyclo[3.3.1]nonane derivatives

4.1. Introduction

The diazaadamantane-derived 3,7-diazabicyclo[3.3.1]nonane backbone exists in nature as part of the natural product *Sparteine* (Fig. 4.1).

Sparteine   3,7-diazabicyclo[3.3.1]nonane
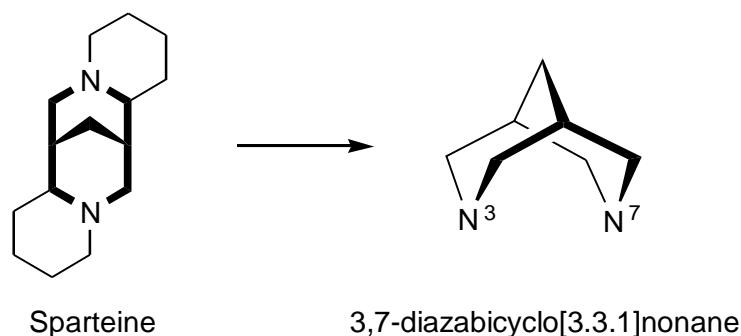
Fig. 4.1: Sparteine and the 3,7-diazabicyclo[3.3.1]nonane backbone

The 3,7-diazabicyclo[3.3.1]nonanes can be found in three different conformations: chair-chair, chair-boat and boat-boat (Fig. 4.2). The chair-chair conformation, with its diamond core like structure, is generally the most stable and, for coordination chemistry, the most interesting, due to its potential ability to act as a bidentate ligand.

Chair-Chair   Chair-Boat   Boat-Boat
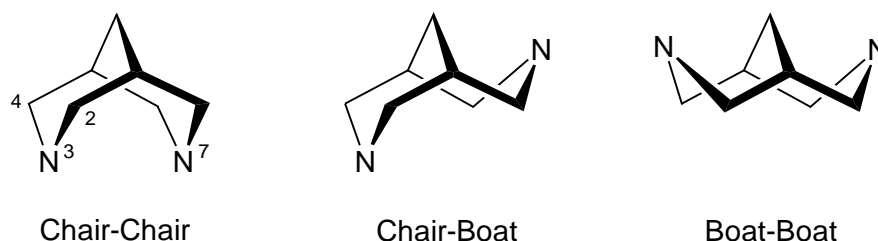
Fig. 4.2: Possible conformations of the 3,7-diazabicyclo[3.3.1]nonane backbone

The synthesis of 3,7-diazabicyclo[3.3.1]nonane derivatives is generally performed via a double Mannich reaction (Fig 4.3)[29]. In the first step, a piperidone is formed. Following a fairly simple synthetic procedure, it is usually possible to isolate the desired product as a white to pale yellow solid, in many cases with yields up to 90 %, by mixing all reactants at 0° C under ambient atmosphere and leaving the reaction mixture to stir for a couple of hours at room temperature. In the next step, the second ring is closed and the bispidone is obtained. For this step it is necessary to reflux all reactants for one to two hours. The work-up of the products depends on the substituents R_1, R_2 and R_3, but the most used methods are crystallization from polar, protic solvents like methanol or ethanol and precipitation with

diethylether. The yields for this reaction are much more variable, but in most cases lower than for the first step.

The general bispidone synthesis offers a wide range of possibilities for modification[30,31] of the ligands. It is possible to introduce substituents at three different positions in a relatively simple manner. However, new amino or aldehyde components are sometimes required, the synthesis of which may be considerably more difficult than that of the bispidone itself.
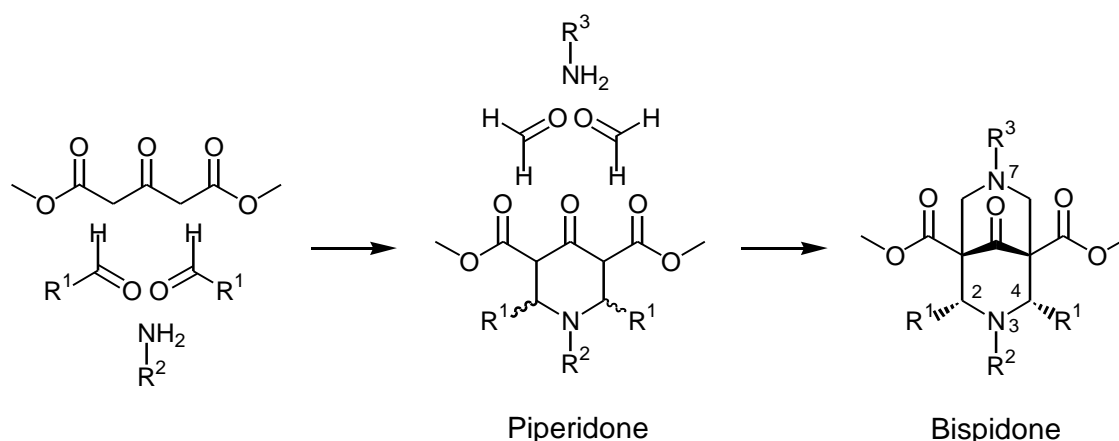
Fig. 4.3: General synthesis of 3,7-diazabicyclo[3.3.1]nonane derivatives

Not only is the introduction of the desired residues one of the most difficult tasks in this synthesis, but obtaining the desired configuration of these residues can also prove to be quite complicated. In the formation of the piperidone, both the cis- and the trans- isomers can be obtained and, as shown in Fig. 4.4, can be interconverted by refluxing the mixture in a polar and protic solvent (for example ethanol or methanol). The interconversion process is thought to proceed via an α,β-unsaturated carbonyl form which can be attacked[32] intramolecularly (as in a Michael addition) to yield either the starting form or its isomer.
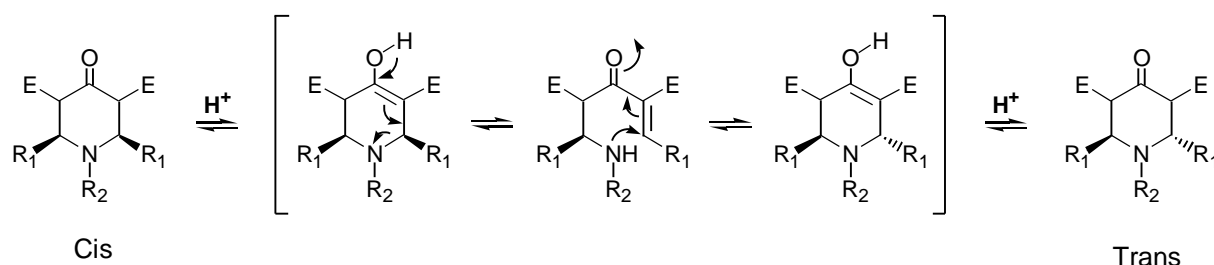
Fig. 4.4: Possible mechanism of isomerisation in protic solvents at C2/C4 position

Once the piperidone is obtained, whether in cis- or trans-, keto or enol form, it is used directly in the next step. Here, the relative orientation of the R_1 substituents becomes more important. If these substituents are not in the endo-endo form, as shown in Fig. 4.5, the

complexation will not be optimal. If this is the case, the endo-exo form can be converted into the desired endo-endo by refluxing the mixture of isomers in a polar protic solvent such as methanol or ethanol, and the desired bispidone obtained via a mechanism similar to that proposed for the isomerization of piperidones in protic solvents (Fig 4.4)[32].
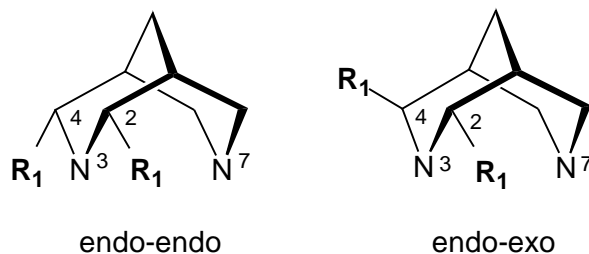
endo-endo   endo-exo

Fig. 4.5: Representation of the endo-endo and endo-exo form

4.2. Aldehyde synthesis

As mentioned before, one of the main difficulties in the preparation of bispidone derivatives lies in the synthesis of the corresponding amine and aldehyde components. One of the main goals of the present study was to vary the substituents R_1, R_2 and R_3. For R_1, various 5- and 6- member heteroaromatic aldehydes have been used. The amines needed for R_2 and R_3 are easier to obtain; most of them are commercially available or they can be prepared starting from the correspondent aldehyde[33]. The largest and best studied group of bispidone ligands has pyridine rings at R_1 and no extra donor atom, relatively simple short chain aliphatic amines or pyridine groups at R_2 and R_3.

In the present work one of the main tasks was to develop short and effective syntheses of new ortho-, meta- and para- substituted pyridine 2-carbaldehydes. The strategy was to modify the sterics and electronics of the donor groups in a rational way in order to gain a better understanding of their influence on the metal centre.

There are three basic approaches to the synthesis of pyridine 2-carbaldehydes and these are shown in Fig. 4.6.
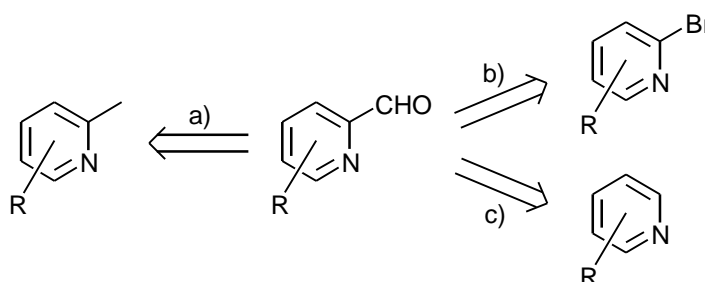
Fig. 4.6: Synthetic approaches to obtain pyridine 2-carbaldehyde derivatives

Approach a:

Starting from the corresponding substituted picoline derivatives there are two ways of synthesizing the desired aldehyde.

The aromatic methyl group can be oxidized to the aldehyde under relatively mild conditions, to avoid oxidation to the carboxylic acid[34]. The reaction can be considered a variation of an allylic oxidation, but although the oxidation of quinoline derivatives has been successfully performed[34], the reaction did not work as well with some pyridine analogues (see Fig. 4.7).
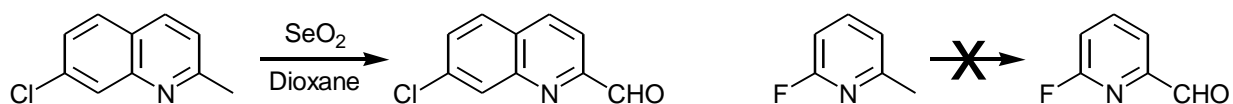
Fig. 4.7: The SeO$_2$ oxidation of N-heteroaromatic rings

Starting from a 2-methyl substituted pyridine derivative, the other possibility is via the so called *N-oxide rearrangement*. This method was successfully applied to the synthesis of 5-methoxy-2-pyridinecarbaldehyde[35] (see Fig. 4.8).
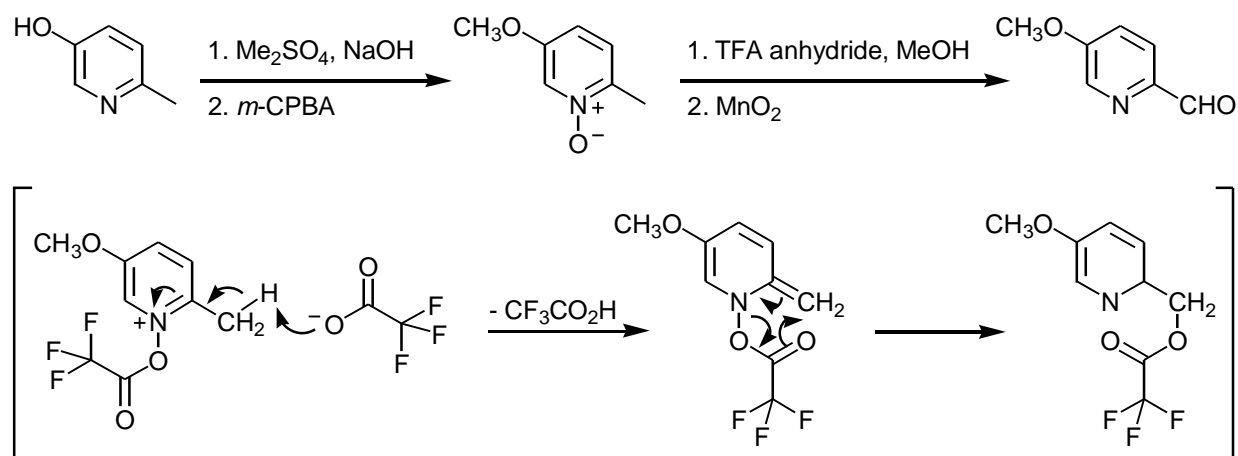
Fig. 4.8: Mechanism of N-oxide rearrangement of substituted pyridines

This synthetic route is a valuable alternative when the direct oxidation does not work. However, although the yields for the individual steps, apart from that of the first methylation step, are acceptable, the total yield is quite low and the reaction is time consuming.

Approach b:

This is a much more direct, selective and efficient method, but it requires an already brominated pyridine ortho to the nitrogen. The approach is based on a selective halogen-lithium exchange in toluene and the subsequent nucleophilic attack of the lithiated pyridine on the desired electrophile, in this case DMF. After a relatively simple work-up and

column chromatography, the desired aldehydes are obtained in acceptable yields (Fig. 4.9). Following this methodology and starting from a dibrominated species, it is even possible to obtain selectively the 5-bromo-2-pyridinecarbaldehyde. For this purpose the right non polar solvent and the right concentration of substrate to be lithiated are necessary[36]. It has been shown that, by playing with different solvent/substrate concentrations, it is possible to invert completely the bromine which is being lithiated in such 2,5-dibromo species[36]. In Fig. 4.9 the aldehydes obtained using this method are shown:
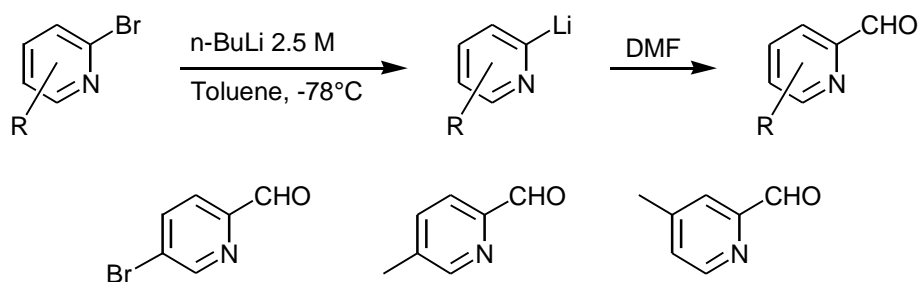
Fig. 4.9: The selective lithiation approach and the aldehydes obtained with this method

Approach c:

The idea of the direct introduction of a formyl group into heteroaromatic bases has been around for more than 30 years. However, at the time that this idea was being developed, it became apparent that this route would not be viable using the usual techniques. One of the novel alternatives was to use a two-step route[37]. In the first step, the addition of a trioxanyl radical to the aromatic substrate was performed, with subsequent hydrolysis of the formed intermediate to the formyl product (Fig. 4.10).
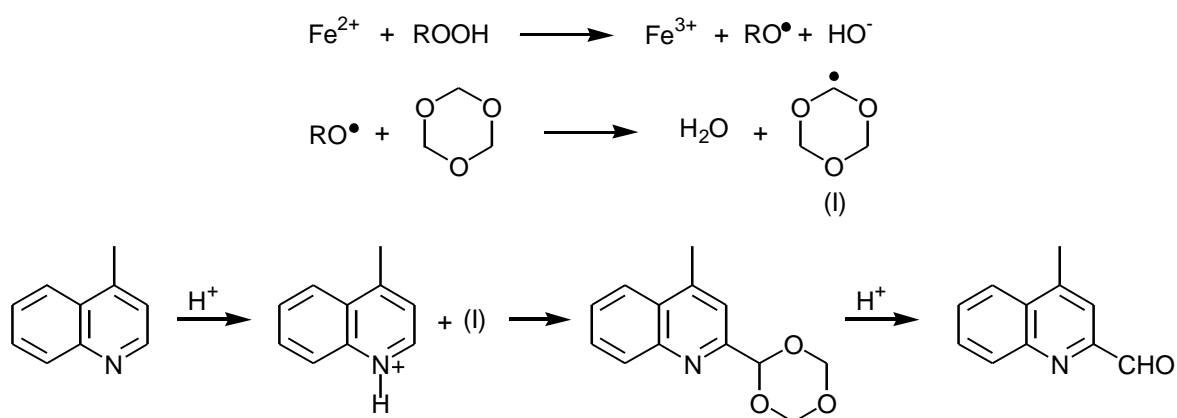
Fig. 4.10: Aldehyde synthesis via a trioxanyl radical intermediate

This procedure, however, provides fairly low total yields (up to 20 %), and for this reason lithium chemistry began to be used for the addition of a formyl group into a heteroaromatic base, as discussed below.

This method proceeds in the same direction as that of *approach b*. The direct lithiation of aromatic compounds has been known for many years, but selectivity has always been a problem. One powerful alternative, the functionalization of aromatic rings derived from direct lithiation, is the so called *directed ortho-methalation* (DOM) method[38] (see Fig. 4.11).
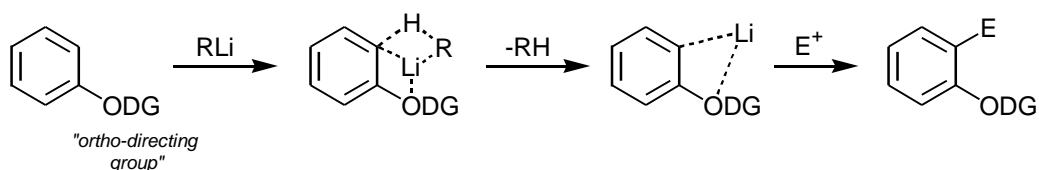
Fig. 4.11: Directed ortho-methalation

The DOM mechanism becomes more complicated with N-containing heteroaromatic compounds like pyridines, since the nitrogen atom is expected to modify inductive effects, while at the same time offering an additional lithium complexation site.

Although halogen-lithium exchange on bromo- or iodopyridines has proven to be an efficient process[39], hydrogen-lithium exchange represents a more direct way to functional derivatives. Unfortunately, the π-deficiency of pyridines limits the scope of the proposed hydrogen-lithium exchange. Indeed, reaction of pyridine derivatives with alkyllithium compounds has usually resulted in nucleophilic attack on the azomethine bond[40]. To overcome this side reaction and to favour lithiation, sterically hindered non-nucleophilic lithium dialkylamides like LDA have been proposed. This type of reagent improves the reactivity and selectivity, but also has some disadvantages. They often need to be used in excess (2 to 4 eq.) and their synthesis sometimes requires expensive starting amines. Equilibrated reactions (see Fig. 4.12) are also observed in some cases and imply in-situ trapping of lithio intermediates.
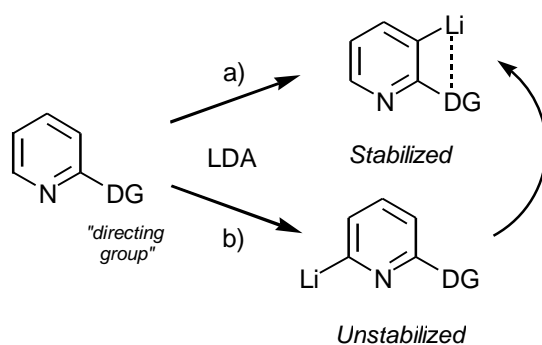
Fig. 4.12: Hydrogen-lithium exchange in pyridines

For this reason[41], the strongly basic alkyllithium compounds remain of interest, and the idea is to improve the reactivity and selectivity by increasing their basicity/nucleophilicity ratio, with a particular focus on the most common and easily handled n-BuLi.

One way of increasing this ratio is to enhance the basicity through association of n-BuLi with a lithium-chelating diamine such as TMEDA, while another approach employs the superbase known as LiCKOR (n-BuLi/'BuOK)[42,43]. It has been shown, however, that the best method[41] is to use a new class of lithium-containing unimetallic superbases, which combine a chelating amino group and an electron-rich alkoxide in the same species. The idea of an association between n-BuLi and a lithium aminoalkoxide is to enhance the basicity by complexation and inhibit the nucleophilicity by formation of sterically hindered aggregates. The mechanism is shown in Fig. 4.13.
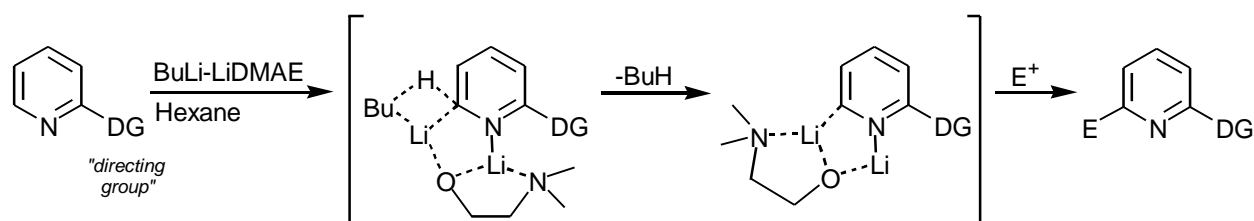
Fig. 4.13: n-BuLi-LiDMAE reaction mechanism

Using this methodology, it is in theory possible to synthesize a great variety of 2- and 4-substituted pyridine analogues (see Fig 4.14).
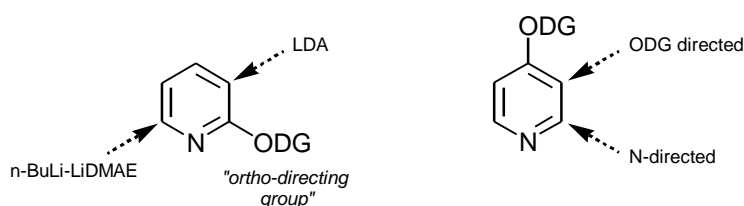
Fig. 4.14: Selectivity on 2- and 4- substituted analogues

In synthesis of the 2- and 4-substituted derivatives using the newly developed method with n-BuLi-LiDMAE, selectivities and reactivities are quite optimal[41]. Using the n-BuLi-LiDMAE methodology, the 4-dimethylamino-pyridine-2-carbaldehyde was obtained[44].

4.3. Synthesis of new 3,7-diazabicyclo[3.3.1]nonane derivatives

Using the methods described above for the synthesis of the aldehyde precursors, a number of new 3,7-diazabicyclo[3.3.1]nonane derivates could be synthesized and characterized. An overview of the ligands synthesized in this work is given in Fig. 3.16.

For the ligands N26BrPy2, N26BrPy3o, N2Q3o, N2Py2Qo and N2Py3Lo, the corresponding aldehyde was commercially available and the ligands were synthesized according to the general procedure for bispidines.

For the ligands N25MOXPy2 and N2CQ2 *approach a* and for N25BrPy2, N25MePy2 *approach b* were used in the aldehyde synthesis and the general procedures for the formation of the piperidone and bispidine were followed.

Using *approach b*, 4-methyl-2-carbaldehyde was successfully synthesized. However, preliminary attempts to synthesize the piperidone failed (no solid product was isolated), for unknown reasons. Using *approach c* 4-dimethylamino-pyridine-2-carbaldehyde was successfully synthesized but again, the preliminary attempts at piperidone synthesis failed. A possible reason could be the presence of an extra amine, which could modify the pH conditions for the condensation reaction, perhaps forcing a different sequence of addition of the educts.
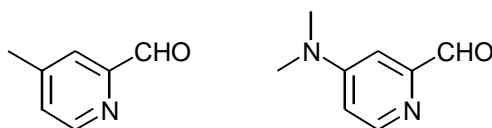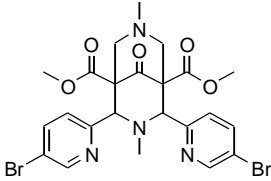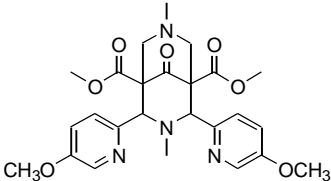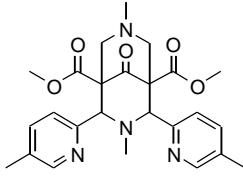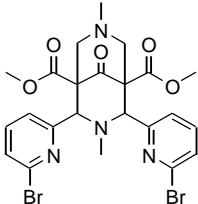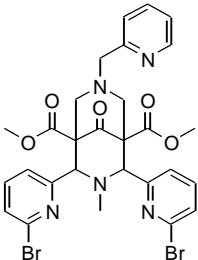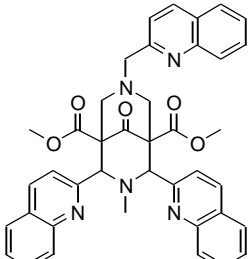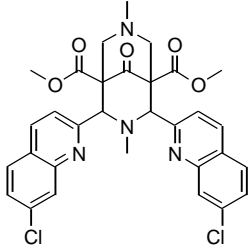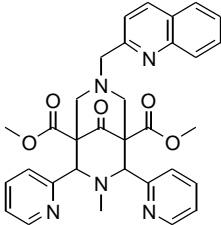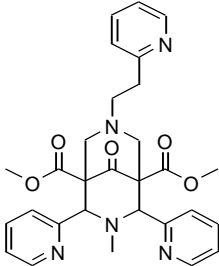
Fig. 4.15: Successfully synthesized aldehydes where the ligand synthesis failed

The ligands presented in Fig. 4.16 where characterized by means of NMR spectroscopy. When the right (endo-endo) conformation is obtained (see Fig. 4.5), the C2/C4 protons appear as a singlet due to a plane of symmetry through N3-N7. Further details are given in the experimental section. No X-Ray crystal structure data was obtained.

It has been shown that, from a variety of synthetic strategies, interesting aldehydes for the bispidone chemistry can be obtained. Once the aldehyde is obtained, there is still a long way to go before the corresponding 3,7-diazabicyclo[3.3.1]nonane derivative is synthesized. If reaction condition and product isolation problems can be overcome, it should be possible to optimize new attractive bispidone syntheses.

Fig. 4.16: Overview of new synthesized 3,7-diazabicyclo[3.3.1]nonane derivatives

	N25BrPy2	**N25MOXPy2**	**N25MePy2**
Aldehyde Synthesis	Approach b)	Approach a)	Approach b)
Aldehyde yield (%)	35	< 10	45
Piperidone yield (%)	66	27	34
Bispidone yield (%)	74	38	49

	N26BrPy2	**N26BrPy3o**	**N2Q3o**
Aldehyde Synthesis	Available	Available	Available
Aldehyde yield (%)	-	-	-
Piperidone yield (%)	82	82	66[7]
Bispidone yield (%)	50	35	28

	N2CQ2	**N2Py2Qo**	**N2Py3Lo**
Aldehyde Synthesis	Approach a)	Available	Available
Aldehyde yield (%)	90	-	-
Piperidone yield (%)	65	68	68
Bispidone yield (%)	78	28	46

5. Copper(II) complexes of 3,7-diazabicyclo[3.3.1]nonane derivates

5.1. Introduction

Copper plays an important role in biological systems as well as in the chemical industry. In nature, copper can be found in diverse areas, oxidation, oxygenation, electron transfer and oxygen transport being its most important and well studied fields of action.

Blue copper proteins are known to perform very fast electron transfer reactions[45]. This is closely related to the environment of the metal ion. In these kinds of compounds, the cavity where the metal lies favours, from a structural point of view, neither Cu(II) nor Cu(I), but a mixture of them. This implies that neither the reduced nor the oxidized form of copper in the protein is stabilized, making the transition state closer in energy to the initial state, not by reducing the energy of the former, but by increasing the energy of the latter (*entatic state,* Fig. 5.1)[46].
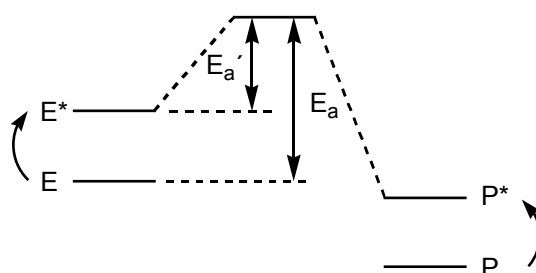
Fig 5.1: Diagrammatic representation of the entatic state principle, showing the educts, products and activation energy for both the catalyzed and uncatalyzed reactions

Copper is also important in oxygen transport however, and *hemocyanin* is a good example[47]. The dioxygen binding reaction in this dinuclear copper protein involves oxidative addition of the dioxygen molecule to the dicopper(I) center to form a dicopper(II) coordinated peroxide. In an attempt to mimic the reactions of such proteins, mono and dinuclear copper(I) 3,7-diazabicyclo[3.3.1]nonane derivatives were synthesized and tested in presence of oxygen. The results with the copper(I) complexes of some bridged ligands show unusual and very stable (μ-peroxo)-dicopper(II) complexes[48,49].

The previously discussed ligand properties, coupled with the high rigidity of the 3,7-diazabicyclo[3.3.1]nonane backbone, result in series of ligands suitable for many metal ions, but particularly for Jahn-Teller active centers like copper(II). Following on the idea of the entatic state discussed above, in order to obtain similar effects in catalysis, the corresponding ligand must have the right form and size (*complementarity*)[50] and a relatively high degree of rigidity, in order to avoid conformational changes upon coordination of the

substrate to the metal complex. The 3,7-diazabicyclo[3.3.1]nonane derivatives fulfill these two prerequisites and are therefore adequate to be applied in catalytic reactions such as the copper-catalyzed aziridination of olefins.

As mentioned above, copper plays a very important role in the chemical industry, largely in the field of catalysis, with applications ranging from numerous types of coupling reactions to carbene/nitrene insertion into double bonds (aziridination of olefins[25]). This last field of application is very important, since aziridines, as subunits in several natural products and versatile synthetic intermediates are very attractive molecules.

Although the synthesis of aziridines from the addition of photochemically or thermally generated nitrenes to olefins is a well-known reaction, the yields of the desired products are generally fairly low (competitive reactions like hydrogen abstraction and insertion processes take place)[26]. This is the main reason why the catalytic addition of a carbene moiety to an imine or the transfer of a nitrogen atom (nitrene) to an olefin (which is even possible in an enantioselective way) has become of great importance in the last years.

From a more theoretical point of view, it is important to keep in mind that the electronic configuration of copper(II) is d^9, which implies that copper(II) complexes are Jahn-Teller[51,52] active. This electronic effect produces a modification in the original geometry of the corresponding metal complex, by means of a stabilization of the energy of the orbitals of the metal ion. The observed distortion is produced by the interaction of the d orbitals of the metal center with the normal vibrations modes of the same symmetry (O_h).

The theoretical and most regular geometry for six donors around a copper(II) centre is an octahedron. In this case, the unpaired electron lies in one of the doubly degenerate e_g orbitals. In order to decrease the total energy of the system, the "ideal" octahedral geometry needs to be compressed or elongated along a specific axis. The corresponding modification of the orbital energies is represented in Fig. 5.2.
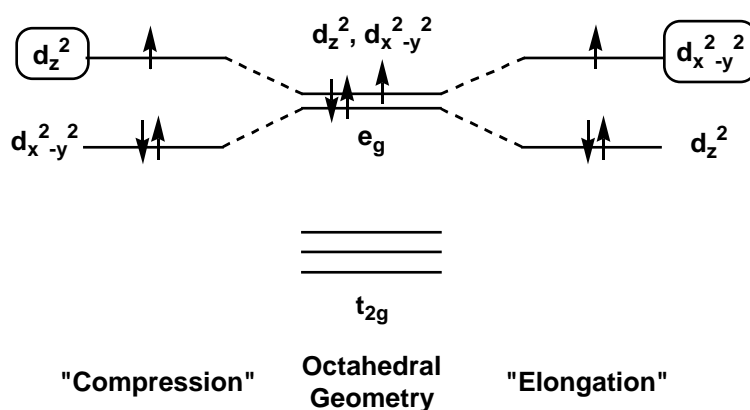
Fig. 5.2: Diagrammatic representation of the d orbital splitting in a d^9 configuration

For d^9 octahedral complexes there is only one Jahn-Teller active vibration, which has e_g symmetry and is therefore doubly degenerated and separated into a tetragonal (Q_θ) and a rhombic (Q_ε) distortion.

In Fig. 5.3 the so-called "Mexican hat" potential is represented, where the rim of potential energy surface corresponds to linear combinations of the tetragonal and rhombic distortions, with minima at ϕ = 0, 120 and 240°. Each of these minima corresponds to a tetragonally elongated structure, whereas the maxima represent the tetragonally compressed ones.
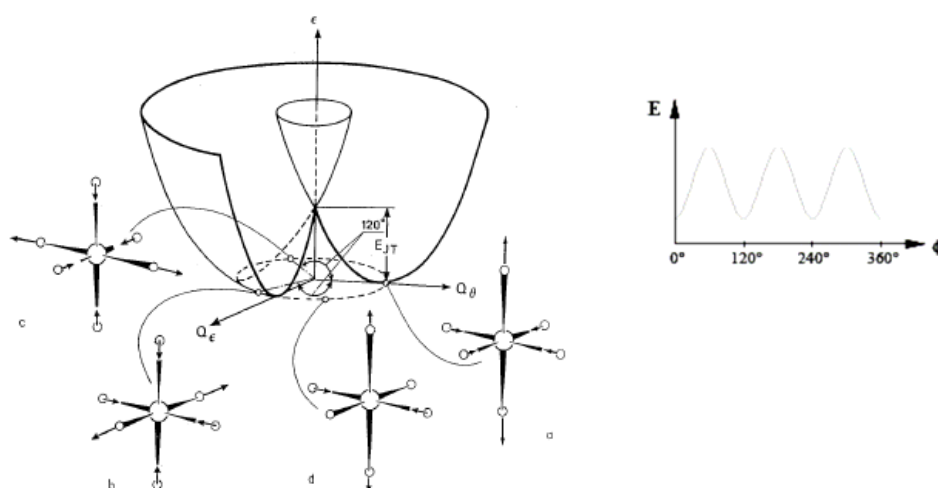
Fig. 5.3: "Mexican hat" representation of the Jahn-Teller distortion in pseudo-octahedral complexes, with the Q_θ and Q_ε components (left) and an energy profile of the a linear combination of both (right)[52]

5.2. Results and discussion

The main mechanistic issues in the Cu-catalyzed aziridination of olefins are the formation of a metal-nitrene intermediate, the oxidation state of the metal and the nature of the nitrene transfer. A very interesting point concerning this kind of catalytic reaction is the fact that copper(II) derivatives are sometimes just as active as those of copper(I). The copper(II)-catalyzed reactions are of special interest since, in contrast to most copper(I) complexes, the corresponding Cu(II) complexes are air stable. From recently acquired data (experimental[27] and theoretical[28] studies) involving the aziridination of olefins with [N-(*p*-toluenesulfonyl)imino]phenyliodinane (PhINTs) as nitrene source (Fig 5.4), it has been proposed that the copper(I) complexes are the active species. It has been suggested that the copper(II) complexes enter the catalytic cycle (supposed to be a Cu(I)-Cu(III) cycle[27]) via an *in situ* reduction to form the catalytically active copper(I) analogues, with a formal copper(III)-nitrene being the reactive intermediate.
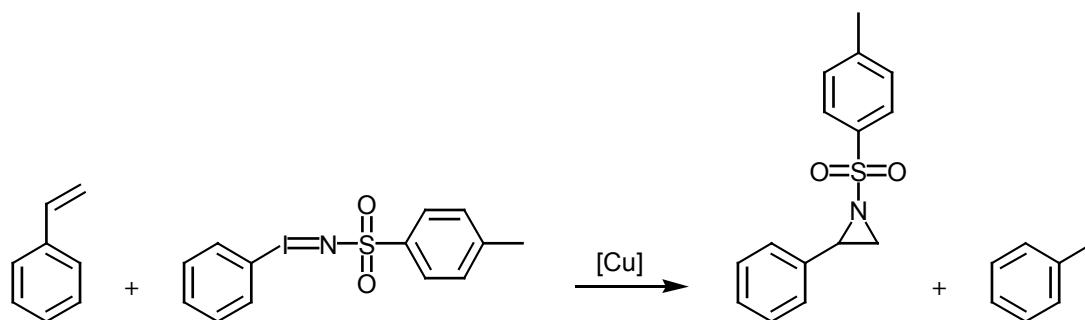
Fig 5.4: Aziridination of styrene using [N-(*p*-toluenesulfonyl)imino]phenyliodinane

The published results on copper(I) and copper(II) 3,7-diazabicyclo[3.3.1]nonane derivatives[7] follow the idea that the active catalyst is the corresponding Cu(I) complex. When performing the catalytic reaction with copper(II) complexes, the active catalyst is obtained by *in situ* reduction of the Cu(II) analogue. In support of the above interpretation, the 3,7-diazabicyclo[3.3.1]nonane copper(I) complexes were more active than their copper(II) analogues.

For the copper(II) precatalysts, a series of tetra- and another of pentadentate ligands were tested[7], and the nature of the substituents at the R_1 position (Fig 4.3) was shown to be of importance. Within the tetradentate series, which included ligands with 1-methylimidazol, pyridine and 6-methylpyiridine at R_1, the 6-methylpyridine derivative was by far the most active catalyst, followed by the pyridine and the 1-methylimidazol derivatives. If we compare the redox potentials of the copper(II) species with these three ligands (Fig 5.5), it appears

that the yield (and rate) of the catalytic reaction increases with an increase in the redox potential of the corresponding copper(II) complex (stabilization of the copper(I) species).

	N2Py2	N2Im2	N26MePy2
E^o (mV vs. Ag/AgNO$_3$)	-413	-440	-94
TON	9	6	19
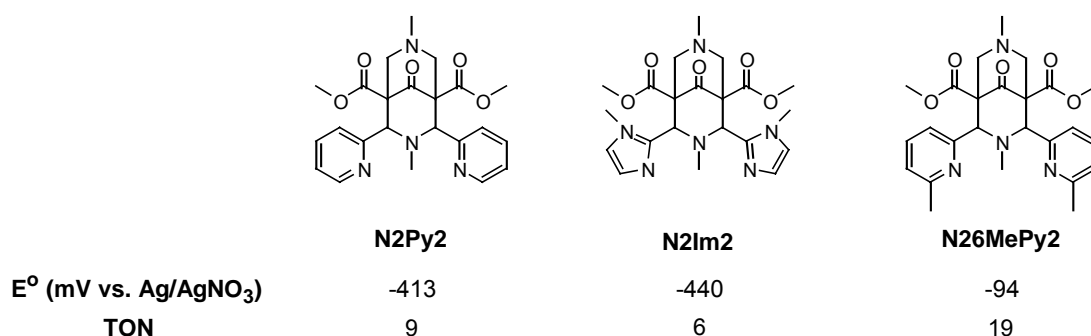
Fig 5.5: Comparison of the Cu$^{II/I}$ redox potentials in acetonitrile and the TON in the catalytic aziridination of styrene with PhINTs as nitrene source, within a series of tetradentate 3,7-diazabicyclo[3.3.1]nonane derivatives

With N2Py2 and N2Im2 a relationship exists between the basicity of the heteroaromatic ring and the corresponding redox potential. The pK$_a$ value of pyridine is 5.2, while that of imidazole is close to 7. This means that, with these two ligands, the copper(II) species is stabilized relative to the desired copper(I) species by an increase in the basicity of the aromatic ring. If electronic effects alone were responsible for the reactivity, one would expect the activity of the 6-methyl analogue to lie between those of the pyridine and the methylimidazole-based catalysts (the pK$_a$ of 6-methylpyridine is 6.0). However, as shown in Fig. 5.5, the redox potential of the copper(II) complex is more than 300 mV higher than that of the complexes with the other two ligands. Here, the two methyl groups play an important steric role. The square pyramidal structure of the copper(II) complex with a solvent molecule coordinated to the metal center is destabilized by the two methyl groups at the 6-position. In the copper(II) chloro complexes of N26MePy2, this steric strain is large enough to force the Cl into coordinating in the electronically unfavourable trans N7 position. This leads to a partial quenching of the Jahn-Teller stabilization, due to the restraints of the rigid ligand backbone, which do not allow the Cu-N3 bond (the Jahn-Teller axis in this case) to elongate as much as the Cu-N7 bond is able to. Acetonitrile, on the other hand, is small enough that the Jahn-Teller stabilization gained from coordinating trans to N3 overcomes the steric strain induced by the methyl groups, which nonetheless destabilizes the complex as a whole relative to N2py2[49]. As seen in Table 3, the main structural differences between the copper(II) complexes with N2Py2 and N26MePy2 and acetonitrile as co-ligand are the distances between the aromatic rings and the metal center. The Jahn-Teller axis remains the same, however, and the Cu-N7 bond in the N26MePy2 complex is even slightly longer than in the N2Py2 complex.

Within the series of pentadentate complexes, similar factors are of importance. The two ligands tested contain as heteroaromatic donors only pyridine rings. The redox potentials of these copper(II) complexes are even lower and, as shown in Fig 5.6, they are not active catalysts. Here, the reason for the loss of activity could be related to the relatively low redox potential alone, but the fact that an additional coordination site of the metal center is occupied by a pyridine donor may also play an important role.

	N2Py3u	N2Py3o
E^o (mV vs. Ag/AgNO$_3$)	-489	-603
TON	0	0
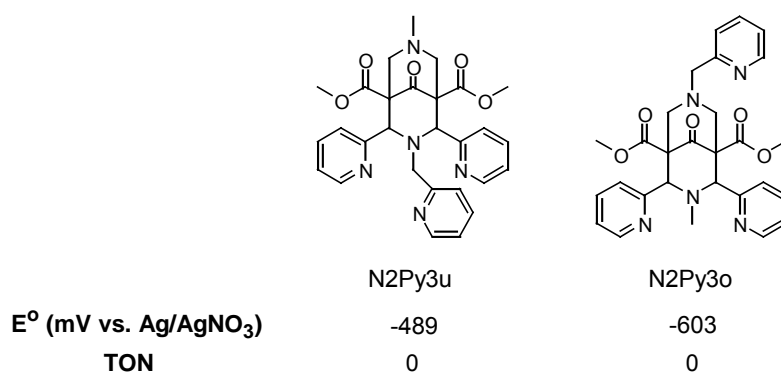
Fig 5.6: Comparison of the Cu$^{II/I}$ redox potentials in acetonitrile and the TON in the catalytic aziridination of styrene with PhINTs as nitrene source, for two pentadentate 3,7-diazabicyclo[3.3.1]nonane isomers

In order to gain a better understanding of the steric and electronic influence of the ligand substituents on the reactivity of the copper(II) center, a new set of complexes, using ligands with various 5- and 6-substituted pyridine rings, as well as quinoline based ligands, were synthesized, and preliminary aziridination experiments were performed with selected compounds. Specifically, the copper(II) complexes of tetradentate N2Q2 and pentadentate N2Pic6MePy, were tested as catalysts. The preliminary results are shown in Fig. 5.7:

	N2Q2	N2Pic6MePy
E^o (mV vs. Ag/AgNO$_3$)	-74	-450
TON	17	3
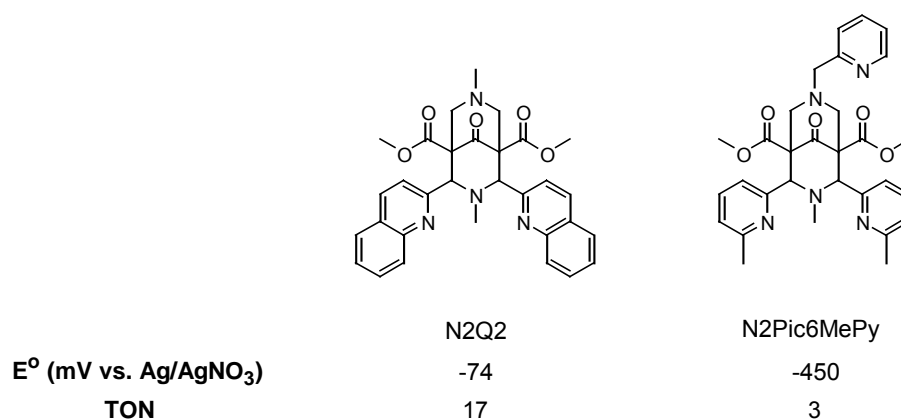
Fig. 5.7: Comparison of the Cu$^{II/I}$ redox potentials in acetonitrile and preliminary TON's in the catalytic aziridination of styrene with PhINTs as nitrene source, for two new 3,7-diazabicyclo[3.3.1]nonane derivatives

From these results it is clear that there are big differences between the tetra- and pentadentate ligand-based catalysts. The copper(II) complex with N2Q2 has a comparable redox potential (-74 mV) to that with N26MePy2 (-98 mV). This similarity implies, as described above for the tetradentate series, a similar stabilization of the copper(I) intermediates and consequently a comparable reactivity (note that the TONs shown in Fig. 5.7 are based on single experiments and need to be confirmed).

More interesting is the result obtained with the pentadente ligand N2Pic6MePy. This is the first case where a pentadentate ligand based catalyst has shown some activity, which implies that a main reason for reactivity is a relatively high redox potential (increase from -603 mV to -450 mV vs. N2Py3o). A similar effect was observed within the tetradentate series between N2Py2 (-417 mV) and N26MePy2 (-98 mV). This suggests that the destabilizing capacity of a residue at the 6-position on the pyridine rings is required to increase the redox potential. However, the available space and the position of the free coordination site with respect to the metal centre, where the substrate may coordinate, probably also play an important role. This implies that the redox potential may not be the only determining factor in the activity of the respective copper(II) complexes, a supposition which is confirmed by comparison of the redox potentials of N2Py3u and N2Pic6MePy (-489 versus -450 mV). It is unlikely that this small difference is the only reason for the presented reactivity of N2Pic6MePy. In the copper(II) complexes of N2Py3o and N2Pic6MePy, the free coordination site is along the elongated Jahn-Teller axis. This means that the only possible substrate coordination site in these two complexes is more labile than that of the N2Py3u complex, where the bond lengths of the coordinated co-ligands in crystal structures (when the Jahn-Teller axis lies along the Cu-N_7 bond) are, on average, 0.3 Å shorter.

It has been shown that structural changes, either in the heteroaromatic rings at C2/C4 positions (see Fig. 4.3) or in the position of the fifth donor group, can afford great changes in reactivity. The next step is to synthesize the copper(II) complexes of the new 3,7-diazabicyclo[3.3.1]nonane derivatives with different combinations of substituents, where the heteroaromatic rings are not only pyridine derivatives (methyl-, bromo- or methoxi-substituted), but also quinoline derivatives.

pK$_a$	7.0	6.0	5.2	4.9	4.9	0.9
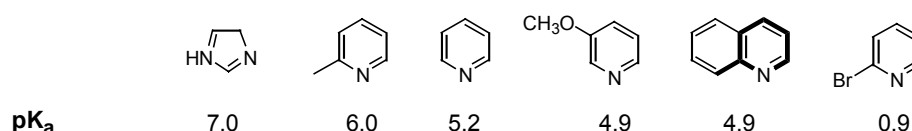
Fig. 5.8: pK$_a$ values and structures of various N-heterocycles[53]

Quinoline possesses a pK$_a$ value of 4.9, lower than all the previously discussed heterocycles (Fig. 5.8). Furthermore, it possesses two very interesting features concerning the

3,7-diazabicyclo[3.3.1]nonane group of ligands. Firstly, the lower pK_a is expected to lead to a destabilization of the corresponding copper(II) complexes. As highlighted in Fig. 5.8, there are also structural similarities with 2-methylpyridine, which implies that the steric effect of these two substituents should be similar. These two factors, in combination with the properties of the other heterocycles used here, offer a broad range of possibilities for varying the properties of the synthesized bispidine ligands. It should be possible to observe clear trends in the redox potential and other important properties, allowing the directed synthesis of effective ligands for catalysis, with which a new family of attractive copper(II) complexes for the catalytic aziridination of olefins may be synthesized.

Pentadentate series

In order to better understand the influence of the different substituents as well as the influence of their position in the 3,7-diazabicyclo[3.3.1]nonane backbone, a series of Cu(II) complexes with pentadentate 3,7-diazabicyclo[3.3.1]nonane derivatives containing mixed donor sets, involving as heterocycles pyridine, 2-methylpyridine, 2-bromopyridine and quinoline, were synthesized. The changes were introduced at the C2/C4 and N7 positions. As already discussed, the introduction of quinoline as donor yields interesting copper(II) complexes with higher redox potentials than those with pyridine, 6-methylpyridine and even 6-bromopyridine residues (Fig. 5.9).

	N2Py3o	N2Pic6MePy	**N26BrPy3o**	N2Q2Pyo
E^o (mV vs. Ag/AgNO$_3$)	-603	-450	-389	-383
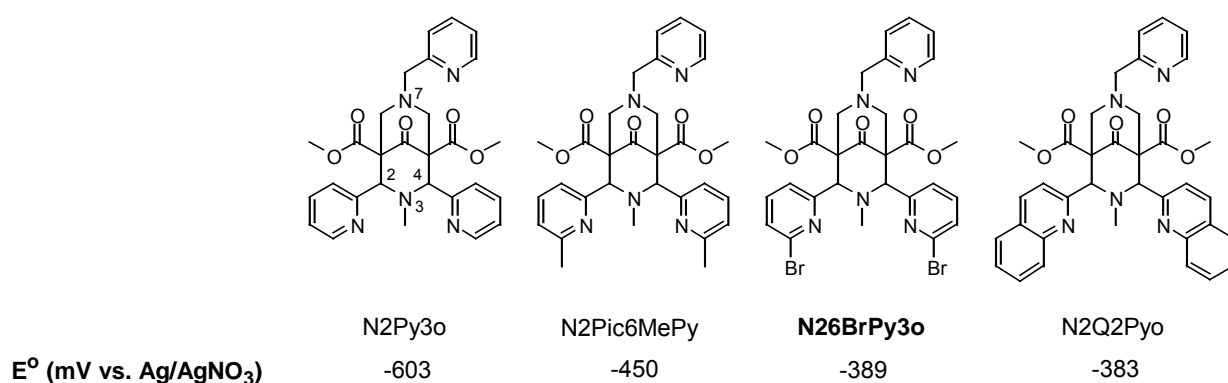
Fig. 5.9: Comparison of the Cu$^{II/I}$ redox potentials in acetonitrile within the N2Py3o C2/C4 modified series

These results confirm the interesting electronic and structural properties of the quinoline ring. With pyridine-derived donors alone it is possible to increase the redox potential of the corresponding copper(II) complex by 214 mV to -389 mV. N2Pic6MePy already leads to an increase of the redox potential by 153 mV with respect to N2Py3o. As expected, when the methyl group is substituted by bromine, due to its electron withdrawing capacity, it is possible to increase the redox potential by an additional 60 mV. However, the surprisingly result is that the copper(II) complex of N2Q2Pyo has a comparable redox potential to N26BrPy3o (Fig. 5.9), which implies that the quinoline ring has similar electronic properties to a clearly deactivated pyridine derived ligand, despite the fact that the pK$_a$ value of 2-bromopyridine is much smaller than that of quinoline (Fig. 5.8).

As important as the properties of the different residues, is the position of these in the 3,7-diazabicyclo[3.3.1]nonane backbone. The question now is whether the effect of the substituents is similar when substituted at N7 instead of at C2/C4. For this reason the copper(II) complex with N2Py2Qo was synthesized. The influence on the redox potential is

significantly smaller when the quinoline ring is substituted at N7, as seen by a shift in the redox potential of only 51 mV from N2Py3o to N2PyQo (Fig. 5.10).

	N2Py3o	**N2Py2Qo**	N2Q2Pyo
E^o (mV vs. Ag/AgNO$_3$)	-603	-552	-383
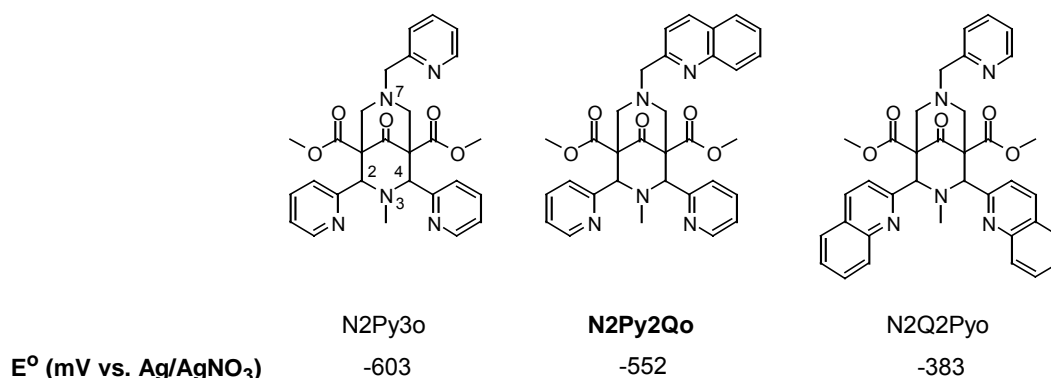
Fig. 5.10: Comparison of the effect of N7 vs. C2/C4 substitution in the Cu$^{II/I}$ redox potentials in acetonitrile within the N2Py3o series

Although the effect is much smaller with a substitution at N7 than that at C2/C4, it is nevertheless possible to increase the redox potential by substitution at N7. A set of *doubly* substituted 3,7-diazabicyclo[3.3.1]nonane derivatives were therefore used to investigate the possibility of further increasing the redox potential of the corresponding copper(II) complexes. As shown in Fig. 5.11, it is possible to obtain a redox potential of -35 mV when all residues are quinolines. It is important to note the possibility of fine tuning the redox potential in the *doubly* modified series, where the selection of the correct 6-methylpyiridine/quinoline ratio allows one to change the redox potential in approximately 30 mV intervals.

	Tri6MePy	N26MePicQ2	**N2Q3o**
E^o (mV vs. Ag/AgNO$_3$)	-94	-69	-35
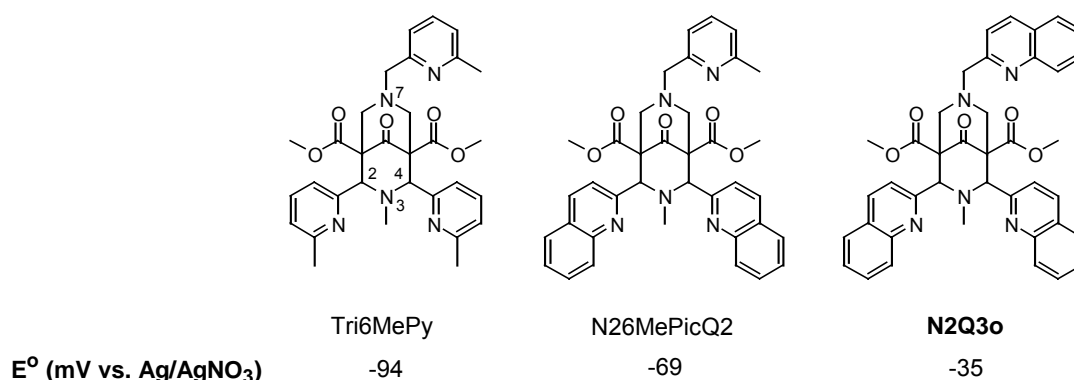
Fig. 5.11: Comparison of the Cu$^{II/I}$ redox potentials in acetonitrile within the N2Py3o *double* modified series

To conclude the discussion of the pentadentate series and its redox potentials, it is important to point out the very rich possibility of variation on the 3,7-diazabicyclo[3.3.1]nonane

backbone and consequently, the possibility of tuning the redox potential within a range of almost 600 mV, from N2Py3o to N2Q3o.

All data on redox potentials discussed above, and the various structural and electronic properties of the ligands, can also be analyzed on the basis of the crystal structures obtained for the copper(II) complexes of some 3,7-diazabicyclo[3.3.1]nonane derivatives (see crystallographic data in Table 5.1).

The most interesting point is that the introduction of elements such as quinoline residues into the 3,7-diazabicyclo[3.3.1]nonane backbone induces a clear destabilization of the pseudo D_{4h} geometry with a Jahn-Teller axis along Cu-N7. This destabilization can also be explained by noting that, within the obtained X-Ray structures with quinoline-derived ligands, the Jahn-Teller axis always lies along the rings substituted at C2/C4, where, as discussed before, the biggest influence on the electronic properties of the metal center is exerted. As shown in Table 5.1, the N_{ar1}-N_{ar2} distances vary from approximately 4 Å in the N2Py3o complex to almost 5 Å in the complexes with quinoline-derived ligands (see Fig. 5.12. for a comparison of the X-Ray structures of the copper(II) chloro complexes with N2Py3o, N26MePicQ2 and N2Q2Pyo). This large variation demonstrates that, when quinoline rings are present at C2/C4, the electron density from the nitrogen donors cannot be used to stabilize the corresponding copper(II) complex, leading to the previously mentioned destabilization of the oxidized copper species.

Another important feature is the effect observed in the substituents at N7 (see Fig. 5.12). The change in position of the coordinating nitrogen donor upon moving from pyridine to 6-methylpyridine (red and blue structures vs. green in Fig. 5.12) can be clearly seen. The change from pyridine to quinoline at C2/C4 already induces a clear displacement of the coordination site of the copper (right picture) as well as the already discussed Jahn-Teller effect along both quinoline rings (left picture).
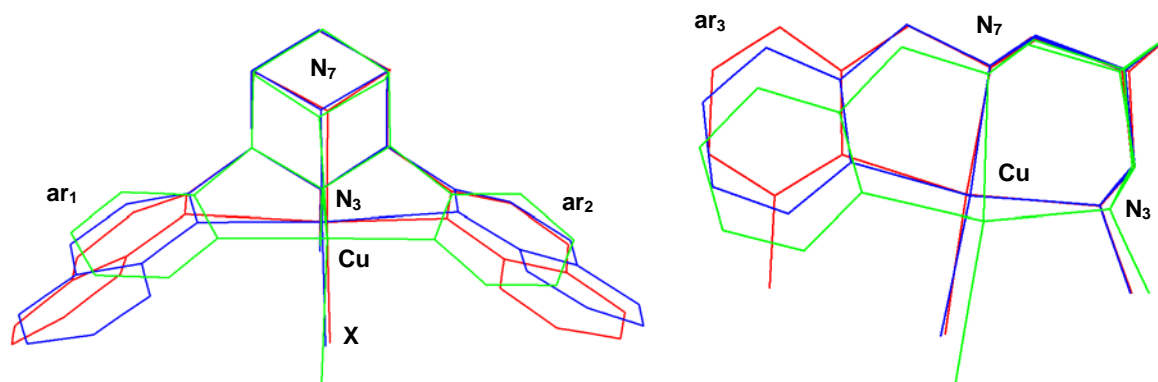
Fig. 5.12: Overlays of the X-Ray structures of the N2Py3o (green), N26MePicQ2 (red) and N2Q2Pyo (blue) copper(II) chloro complexes

The copper(II) complex of N2Q3o could also be crystallized (Fig. 5.13), in which one of the largest copper-nitrogen distances (Cu-N_{ar2} in Table 5.1) ever observed in complexes with pentadentate bispidine ligands was found (over 2.9 Å). This structure shares the other important features, such as the direction of the Jahn-Teller axis, with the quinoline analogues discussed in Table 5.1[10]. The exceptionally long Cu-N_{ar2} bond length implies that the cavity is too large to comfortably accommodate the Cu(II) ion and is a further indicator that the Cu(I) complex of this ligand should be stabilized with respect to the Cu(II) complex, as is reflected in the high redox potential.
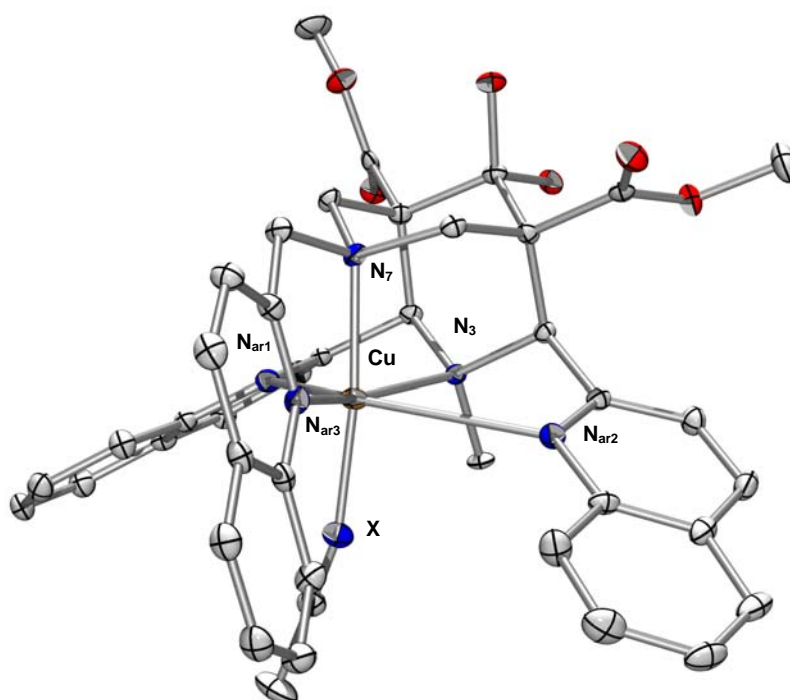
Fig. 5.13: Plot of the X-Ray structure of [Cu(**N2Q3o**)(CH$_3$CN)]$^{2+}$

Table 5.1

	[Cu(N2Py3o)(Cl)]$^+$	[Cu(**N2Q3o**)(CH$_3$CN)]$^{2+}$	[Cu(N2Q2Pyo)(Cl)]$^+$	[Cu(N26MePicQ2)(Cl)]$^+$
Bond lengths(Å)				
Cu-N$_3$	2.036(2)	2.122(2)	2.0888(14)	2.159(3)
Cu-N$_7$	2.368(2)	2.015(2)	2.1142(15)	2.079(3)
Cu-N$_{ar1}$	2.028(2)	2.288(2)	2.3449(15)	2.687
Cu-N$_{ar2}$	2.029(2)	2.929	2.609	2.320(3)
Cu-N$_{ar3}$	2.029(2)	2.108(2)	2.0192(15)	2.159(3)
Cu-X	2.717(1) (X = **Cl**)	1.988(3) (X = **N**CCH$_3$)	2.3054(5) (X = **Cl**)	2.2641(9) (X = **Cl**)
N$_3$…N$_7$	2.915	2.8176	2.8529	2.8356
N$_{ar1}$…N$_{ar2}$	3.995	4.968	4.7952	4.8204
Angles (°)				
N$_3$-Cu-N$_7$	82.53(6)	85.80(9)	85.51(6)	83.99(11)
N$_3$-Cu-N$_{ar1}$	81.39(7)	77.48(9)	76.58(5)	73.05
N$_3$-Cu-N$_{ar2}$	80.94(7)	68.06	74.69	75.91(10)
N$_3$-Cu-N$_{ar3}$	160.82(7)	155.18(9)	164.80(6)	160.09(11)
N$_7$-Cu-N$_{ar1}$	88.33	90.00(9)	92.70(5)	89.77
N$_7$-Cu-N$_{ar2}$	98.43	97.05	89.84	91.04(10)
N$_7$-Cu-N$_{ar3}$	79.27(7)	83.69(9)	83.29(6)	83.46(11)
N$_{ar1}$-Cu-N$_{ar2}$	160.07(7)	144.10	150.87	148.68
N$_{ar1}$-Cu-N$_{ar3}$	104.01	124.83(9)	114.13(6)	91.47
N$_3$-Cu-X	105.30(5)	95.20(9)	97.35(4)	93.76(8)
Torsion angles (°)				
N$_{ar1}$-C-C-N$_3$	31.43	49.16	46.53	60.19
N$_{ar2}$-C-C-N$_3$	-34.86	-53.02	-54.97	-48.57

Tetradentate series

Following the same methodology as for the pentadentate series discussed above, a new series of tetradentate 3,7-diazabicyclo[3.3.1]nonane derivatives was developed. Up to now it has been possible to synthesize various 6- and 5-substituted pyridine derivatives of N2Py2, as well as two tetradentate quinoline-based ligands. The structural and electronic elements discussed for the pentadentate series can also be applied to the tetradentate ligands.

	N2Py2	N26MePy2	**N26BrPy2**
E^o (mV vs. Ag/AgNO$_3$)	-417	-98	+53
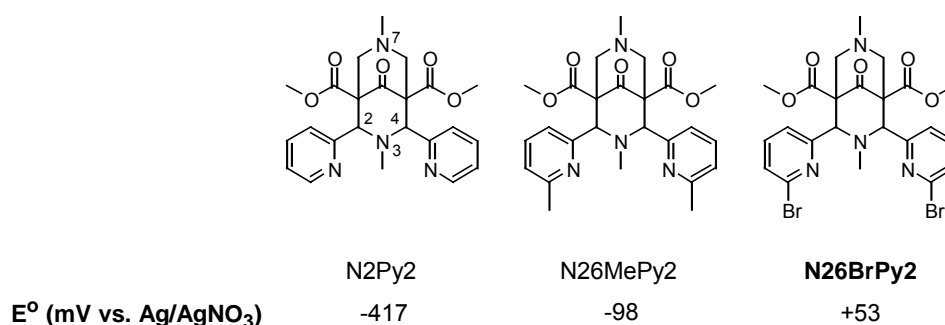
Fig. 5.14: Comparison of the Cu$^{II/I}$ redox potentials in acetonitrile within the 6-substituted N2Py2 series

As shown in Fig. 5.14, the shift of the redox potential of the corresponding copper(II) complexes follows the same trend as observed in the complexes of the pentadentate ligands. The introduction of any kind of substituent at the 6-position induces a destabilization of the copper(II) complexes, increasing the redox potential. Interestingly, between the N26MePy2 and the N26BrPy2 complexes there is an additional shift. This can be interpreted as follows: Both substituents (methyl and bromine) exert similar steric strain on the copper(II) complex because of the similarity in their size. This structural destabilization increases the redox potential substantially. If these bulky groups have an additional electron withdrawing function, as is the case with bromine (the pK$_a$ of 2-bromopyridine is five units lower than pyridine, see Fig. 5.8), the two effects (steric and electronic) reinforce each other, causing an additional increase of 151 mV and a total shift of more than 450 mV from N2Py2 to N26BrPy2. However, since no X-ray crystal structure could be obtained for the copper(II) acetonitrile complex of N26BrPy2, the possibility that the actonitrile coordinates trans to N7 and not trans to N3, as in the copper(II) acetonitrile complexes of N2Py2 and N26MePy2, cannot be excluded. This would lead to a change in the Jahn-Teller axis from Cu-N7 to Cu-N3 and a partial quenching of the Jahn-Teller stabilization, which would also have an effect on the redox potential. Computational studies (see Section 5.3.3) indicate that the two isomers (*trans N3* and *trans N7*) are close to degenerate for both complexes (with N26MePy2 and N26BrPy2), so that no definite conclusion can be drawn from this information.

The results obtained for the quinoline substituted analogues follow and reproduce the effect of substitution at the 6-position and the electronic properties of quinolines. As shown in Fig. 5.15, the complex with N2Q2 has a similar redox potential to that of N26MePy2, but the introduction of an electron withdrawing group like chlorine into the quinoline ring causes a further increase of almost 100 mV, indicating that even at such a distance from the donating nitrogen atom, the electronic properties of the aromatic ring have been strongly modified.

	N2Py2	N2Q2	N2CQ2
E^o (mV vs. Ag/AgNO$_3$)	-417	-74	+17
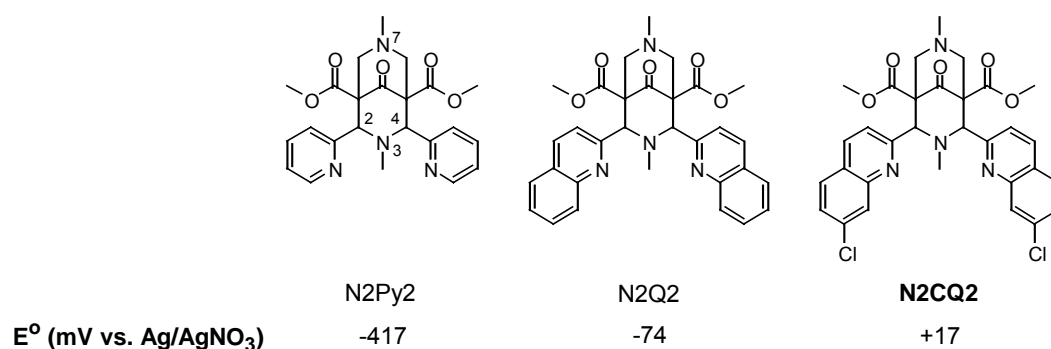
Fig. 5.15: Comparison of the Cu$^{II/I}$ redox potentials in acetonitrile within the 6-quinoline substituted N2Py2 series

Also of interest are the results obtained for the 5-substituted N2Py2 derived complexes. At this point it is important to note that, in principle, the positions of the substitution on the aromatic ring which are expected to exert a bigger electronic effect on the donating nitrogen atom, are 4- (*para*-) and 6- (*ortho*-). The reasons why we concentrate here on the 6- (*ortho*-) and 5- (*meta*-) substituted derivatives is due to preparative limitations (availability of the aldehydes or aldehyde precursors) and time constraints. In principle the synthesis of the 4- (*para*-) substituted derivatives should also be possible, using analogous synthetic methods. It is nonetheless interesting to compare the 5- and 6- substituted isomers and doing so can provide insight into the effects governing the reactivity of such compounds, as well as into the properties of possible 4-substituted isomers.

	N2Py2	N25MePy2	N25MOXPy2	N25BrPy2
E^o (mV vs. Ag/AgNO$_3$)	-417	-410	-387	-272
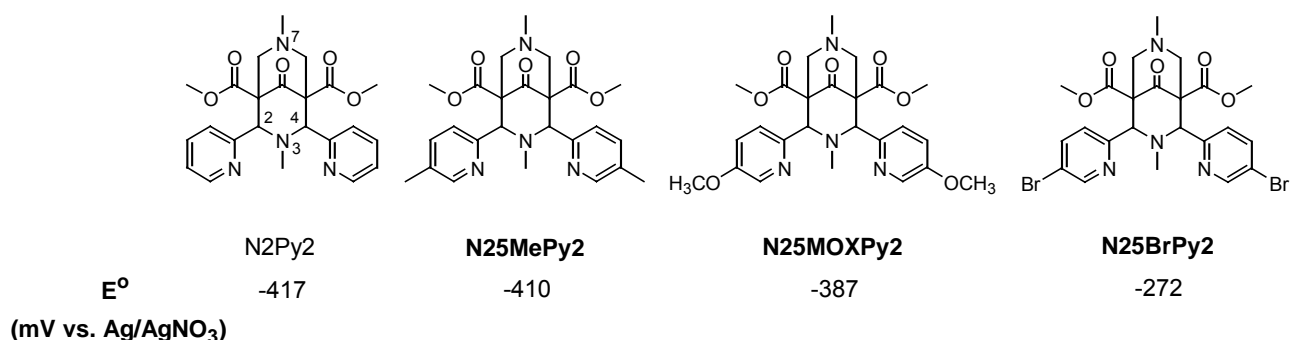
Fig. 5.16: Comparison of the Cu$^{II/I}$ redox potentials in acetonitrile within the 5-substituted N2Py2 series

As shown in Fig. 5.16, the relative differences between N2Py2 and the 5-substituted ligands, as well as between the 5-substituted ligands themselves, are quite small in comparison with the already discussed sets of penta- and tetradentate ligands, confirming the smaller electronic influence of the different groups in the *meta-* position. Using N2Py2 as reference, the idea was to synthesize 3,7-diazabicyclo[3.3.1]nonane analogues based on N2Py2, introducing weak and moderately donating groups like methyl and methoxy, as well as a moderately electron withdrawing group like bromine. The only expected result was that obtained for N25BrPy2, where the electron withdrawing capacity of bromine clearly destabilizes the copper(II) complex, producing a significant increase in the redox potential. For the supposedly electron donating residues, the obtained results show the opposite trend to what was expected.

The methyl group on N25MePy2 exerts neither an electronic nor a steric effect and consequently the redox potential remains practically identical to that of N2Py2. Even more interesting is the result obtained with N25MOXPy2, where the methoxy group acts as weakly electron withdrawing (the pK_a value of 3-methoxypyridine is 4.9, slightly lower than pyridine, see Fig. 5.8), upshifting slightly (30 mV) the redox potential of its copper(II) complex with respect to N2Py2. The same observation can be made by considering the small differences in the corresponding d-d transitions in the UV-Vis spectra (Table 5.2).

Compound	$E_{1/2}$ (mV)	ν_1 (cm^{-1})
[Cu(N2Py2)(CH$_3$CN)]$^{2+}$	- 417	15870
[Cu(**N25MePy2**)(CH$_3$CN)]$^{2+}$	- 410	16025
[Cu(**N2MOXPy2**)(CH$_3$CN)]$^{2+}$	- 387	15950
[Cu(**N25BrPy2**)(CH$_3$CN)]$^{2+}$	- 272	15800
[Cu(N26MePy2)(CH$_3$CN)]$^{2+}$	- 98	16300

Table 5.2: Comparison of redox potentials and d-d transitions within the N2Py2 series

One possible explanation for this behaviour is given in Fig. 5.17, where, as described above, the position of the substitution plays a key role in influencing the electronic effects on the nucleophilicity of the nitrogen atom. With regard to the methyl substituted analogue, the only possible electronic effect is the +I (inductive) effect, which is too weak at this position to significantly alter the electronic properties of the donor atom. Due to the electronegativity of oxygen and bromine, both groups (methoxy and bromine) possess a –I (inductive) effect.

Because of the presence of unpaired electrons on both atoms however, a +M (mesomeric) effect may appear. The –I effect is always present, but the further away the group with respect to the atom which we are focusing our attention on, the less the effect will be felt. Therefore, from a purely electronic point of view, the effect of the bromine atom in N26BrPy2 on the Cu$^{II/I}$ redox potential should be larger than in N25BrPy2. The +M effect can only produce a change on the nitrogen donor of the pyridine ring when the groups with unpaired electrons are disposed at *o-* or *p-* position with respect to it. For bromine, the –I effect dominates and the overall effect is electron withdrawing, whereas for methoxy, the +M effect dominates and the overall effect is electron donating. At the *m-* position however, the +M effect does not increase the electron density on the nitrogen atoms, only the -I effects of the substituents can be felt and both groups have an electron withdrawing effect. Due to electronegativity differences, the redox potential of the copper(II) complex is higher when bromine is attached than with a methoxy group.
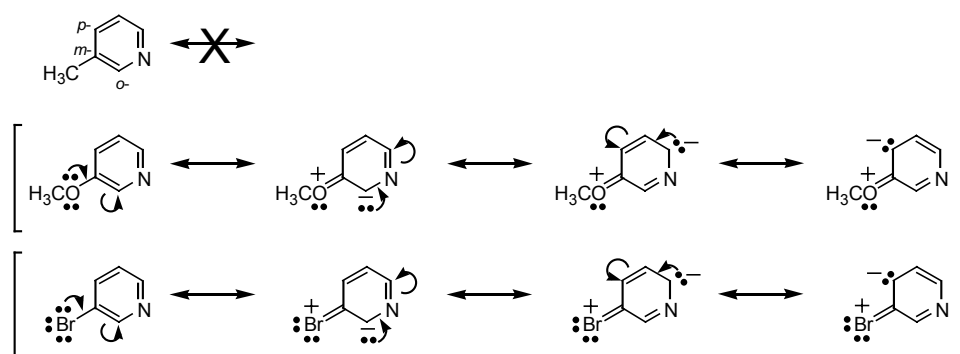
Fig. 5.17: Resonance structures in substituted pyridines

X-Ray crystal structures of the copper(II) complexes of N2CQ2, N25BrPy2 and N25MePy2 were obtained (Fig. 5.19 to 5.21) and compared to crystal structures of known copper(II) bispidine complexes (Table 5.3). Overlays of the copper(II) acetonitrile complexes of N2Py2, N26MePy2, N25MePy2 and N25BrPy2 (left) and the copper(II) complexes of N2Py2, N2Q2 (two isomers, *trans N3* and *trans N7*) and N2CQ2 with various co-ligands (right) are shown in Fig. 5.18. The most particular feature observed for the obtained X-Ray structures is the out of plane distortion of the quinoline rings at C2/C4, relative to N2Py2. This effect is most extreme for N2CQ2, a possible reason being the steric interaction of the two chlorine atoms.

From the left overlay plot of Fig. 5.18, it is clear that the structural differences between the pyridine analogues are smaller than for the pentadentate series (see Fig. 5.12). The largest separation between the aromatic nitrogen donors, within all the structures shown in the left overlay of Fig 5.18, is around 0.3 Å. In contrast, among the quinoline analogues, these

differences are more significant (right overlay of Fig. 5.18) and the largest separation between nitrogen donors is close to 0.6 Å.
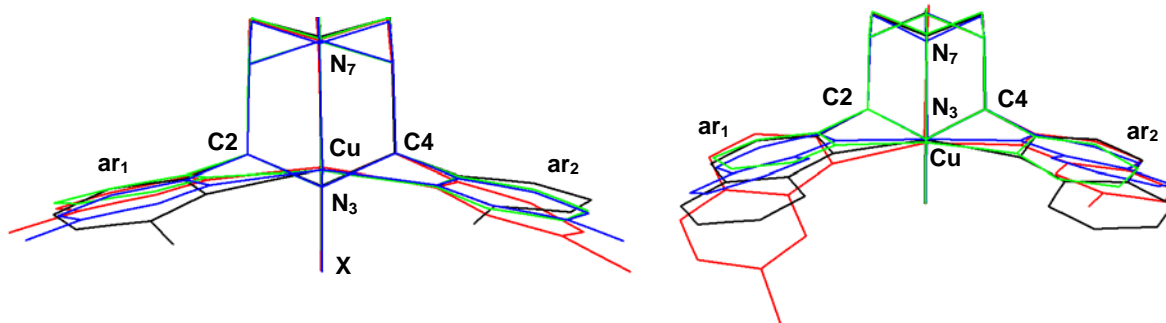
Fig. 5.18: Overlays of the X-Ray structures of tetradentate pyridine-derived (left) and quinoline-derived (right) copper(II) bispidine complexes

Also important to remark is that the Jahn-Teller axis is along the Cu-N7 bond (see Table 5.3) in all cases but that of $[Cu(N2Q2)(Cl)]^+$, where the Jahn-Teller axis is along the Cu-N3 bond and the Jahn-Teller stabilization is partially quenched due to the restraints of the rigid ligand backbone.
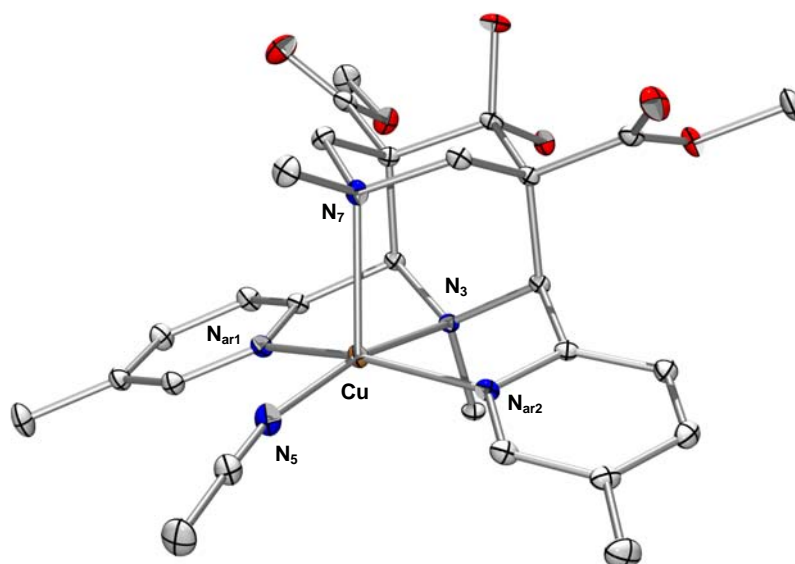
Fig. 5.19: Plot of the X-Ray structure of $[Cu(\mathbf{N2CQ2})(CH_3CN)_2]^{2+}$

An overview of copper(II) bispidone complexes with their redox potentials at 25°C in acetonitrile, TON in the aziridination reaction of styrene and EPR parameters in DMF:H_2O (3:2) are shown in Fig. 5.22.
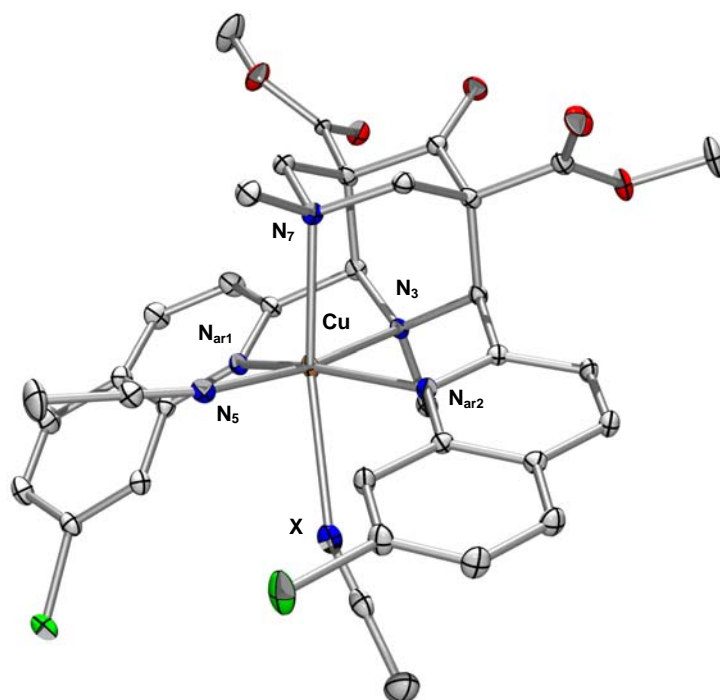
Fig. 5.20: Plot of the X-Ray structure of [Cu(**N2CQ2**)(CH$_3$CN)$_2$]$^{2+}$
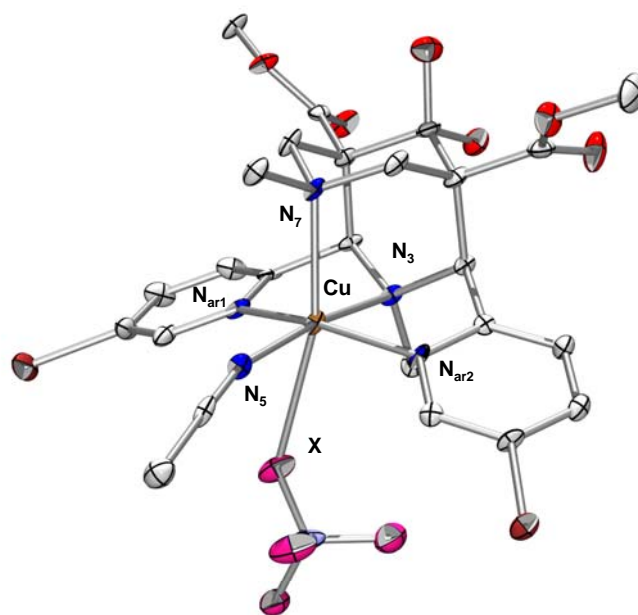
Fig. 5.21: Plot of the X-Ray structure of [Cu(**N25BrPy2**)(CH$_3$CN)(BF$_4$)]$^+$

Table 5.3

	[Cu(N2Py2)(CH$_3$CN)(OTf)]$^+$	[Cu(N26MePy2)(CH$_3$CN)(BF$_4$)]$^+$	[Cu(N2Q2)(F)]$^+$	[Cu(N2Q2)(Cl)]$^+$
Bond lengths(Å)				
Cu-N$_3$	2.0217(15)	1.9995(0.0031)	2.007(2)	2.149, 2.143(2)
Cu-N$_7$	2.3550(17)	2.3695(0.0029)	2.254(2)	2.131, 2.135(2)
Cu-N$_{ar1}$	1.9925(16)	2.0531(0.0032)	2.0872(19)	2.001, 2.033(2)
Cu-N$_{ar2}$	1.9982(16)	2.0722(0.0032)	2.0929(19)	2.019, 2.017(2)
Cu-N$_5$	1.9804(16)	1.9469(0.0035)	-	-
Cu-X	2.6078 (X = **O**Tf)	2.9111 (X = **F**BF$_3$)	1.8362(16) (X = **F**)	2.265, 2.255(1) (X = **Cl**)
N$_3$…N$_7$	2.9220	2.9344	2.9020	2.922, 2.913(2)
N$_{ar1}$…N$_{ar2}$	3.9415	4.0341	4.0645	3.992, 4.016(2)
Angles (°)				
N$_3$-Cu-N$_7$	83.40(6)	83.71(0.11)	85.67(7)	86.11, 85.85(6)
N$_3$-Cu-N$_{ar1}$	83.00(6)	80.89(0.12)	80.39(8)	82.80, 82.62(6)
N$_3$-Cu-N$_{ar2}$	81.44(6)	81.61(0.12)	80.05(8)	82.92, 82.52(6)
N$_3$-Cu-N$_5$(X)	175.41(6)	174.39(0.13)	176.98(7) (X = **F**)	109.14, 109.88(4) (X = **Cl**)
N$_7$-Cu-N$_{ar1}$	91.33(6)	98.91(0.11)	97.44(7)	88.55, 89.41
N$_7$-Cu-N$_{ar2}$	95.85(6)	95.62(0.11)	99.46(7)	91.14, 91.35
N$_7$-Cu-N$_5$(X)	100.40(6)	91.01(0.12)	96.59(7) (X = **F**)	164.69, 164.13 (X = **Cl**)
N$_{ar1}$-Cu-N$_{ar2}$	161.98(6)	155.82(0.12)	152.99(8)	165.70, 165.04(6)
N$_{ar1}$-Cu-N$_5$(X)	99.39(6)	98.10(0.13)	101.26(8) (X = **F**)	92.27, 92.33 (X = **Cl**)
Torsion angles (°)				
N$_{ar1}$-C-C-N$_3$	34.56	26.09	30.64	41.40, 42.32
N$_{ar2}$-C-C-N$_3$	-30.47	-29.89	-27.87	-44.18, -43.39

Table 5.3 (continued)

	[Cu(**N25MePy2**) (CH$_3$CN)]$^{2+}$	[Cu(**N25BrPy2**) (CH$_3$CN)(BF$_4$)]$^{2+}$	[Cu(**N2CQ2**) (CH$_3$CN)$_2$]$^{2+}$
Bond lengths(Å)			
Cu-N$_1$	2.0072(10)	2.010(5)	1.9872(14)
Cu-N$_2$	2.2443(11)	2.257(5)	2.3701(15)
Cu-N$_3$	1.9915(10)	2.022(5)	2.0899(14)
Cu-N$_4$	2.0070(10)	2.020(5)	2.1236(14)
Cu-N$_5$	1.9655(11)	1.957(5)	1.9673(15)
Cu-X	-	2.726(4) (X = **F**BF$_3$)	2.6341(17) (X = **N**CCH$_3$)
N$_1$…N$_2$	2.9037	2.9204	2.9181
N$_3$…N$_4$	3.9381	3.9695	4.1239
Angles (°)			
N$_1$-Cu-N$_2$	86.03(4)	86.19(19)	83.61(5)
N$_1$-Cu-N$_3$	82.45(4)	81.9(2)	79.33(6)
N$_1$-Cu-N$_4$	82.25(4)	81.31(19)	81.67(6)
N$_1$-Cu-N$_5$	168.40(4)	172.3(2)	169.93(6)
N$_2$-Cu-N$_3$	94.54(4)	92.70(18)	102.88(5)
N$_2$-Cu-N$_4$	97.20(4)	99.73(19)	88.86(5)
N$_2$-Cu-N$_5$	105.53(4)	101.5(2)	91.75(6)
N$_3$-Cu-N$_4$	159.97(4)	158.36(19)	156.31(6)
N$_3$-Cu-N$_5$	97.38(4)	98.6(2)	93.07(6)
N$_1$-Cu-X	-	96.87(16)	100.58(5)
Torsion angles (°)			
N$_3$-C-C-N$_1$	33.90	34.28	20.72
N$_4$-C-C-N$_1$	-33.96	-35.75	-35.76

Fig. 5.22: Overview of copper(II) bispidone complexes: redox potentials at 25°C in acetonitrile, TON in the aziridination reaction and EPR parameters in DMF:H_2O (3:2)

N2Py3o

E^0 = -603 mV

TON = 0

g_{par} = 2.230 / A_{par} = 175 G
g_{per} = 2.075

N2Pic6MePy

E^0 = -450 mV

TON = 3

g_{par} = 2.273 / A_{par} = 158 G
g_{per} = 2.060 / A_{per} = 9 G

Tri6MePy

E^0 = -94 mV

-

g_{par} = 2.295 / A_{par} = 152 G
g_{per} = 2.062 / A_{per} = 9 G

N26BrPy3o

E^0 = -389 mV

-

g_{par} = 2.258 / A_{par} = 168 G
g_{per} = 2.055 / A_{per} = 10 G

N2Q2Pyo

E^0 = -383 mV

-

g_{par} = 2.267 / A_{par} = 163 G
g_{per} = 2.058 / A_{per} = 9 G

N2Py2Qo

E^0 = -552 mV

-

g_{par} = 2.198 / A_{par} = 173 G
g_{per} = 2.042 / A_{per} = 25 G

N2Q3o

E^0 = -35 mV

-

g_{par} = 2.288 / A_{par} = 150 G
g_{per} = 2.060 / A_{per} = 6 G

N26MePicQ2

E^0 = -69 mV

-

g_{par} = 2.292 / A_{par} = 152 G
g_{per} = 2.060 / A_{per} = 9 G

N2Py2

E^0 = -413 mV

TON = 9

g_{par} = 2.245 / A_{par} = 172 G
g_{per} = 2.072

N26MePy2

E^0 = -94 mV

TON = 19

g_{par} = 2.245 / A_{par} = 165 G
g_{per} = 2.062

N2Q2

E^0 = -74 mV

TON = 17

N2CQ2

E^0 = +17 mV

-

N26BrPy2

E^0 = +53 mV

-

g_{par} = 2.305 / A_{par} = 156 G
g_{per} = 2.065 / A_{per} = 10 G

N25BrPy2

E^0 = -272 mV

-

g_{par} = 2.268 / A_{par} = 171 G
g_{per} = 2.060 / A_{per} = 10 G

N25MePy2

E^0 = -410 mV

-

g_{par} = 2.260 / A_{par} = 171 G
g_{per} = 2.054 / A_{per} = 10 G

N25MOXPy2

E^0 = -387 mV

-

g_{par} = 2.260 / A_{par} = 173 G
g_{per} = 2.056 / A_{per} = 9 G

5.3. Charge distribution calculations

5.3.1. Introduction

In recent years charge distribution calculations have become a powerful tool in the prediction and simulation of reactivity and thermodynamic properties of molecules (e.g. redox potentials), whether simple organic molecules, enzymes or metal complexes[54]. The representation of the electrostatic interactions of molecules via atomic point charges is, at present, the most commonly used approach in the construction of electrostatic force fields[55]. However, atomic charges are not observables and they cannot therefore be unambiguously determined by experiments or by quantum chemical calculations. For this reason, a number of different methods and approaches for the estimation of atomic point charges have been proposed. They are either estimated from experimental data or by quantum chemical calculations, but due to missing experimental reference data for many interesting molecules, the most common approach is the computational one. However, even within the quantum chemical approach, there is still debate as to the best way to calculate point charges.

There are two main groups within the quantum chemical approach:

- *Orbital-based methods*: Here, the charge is assigned according to the atomic orbital occupation. In the Mulliken approach[56] (the simplest and best established method), the overlap population between a pair of atoms is evenly divided, without taking into account differences in atom type, orbital coefficients, electronegativity, etc. To solve some of the problems of the Mulliken approach, the Löwdin[57] and NPA[58] methods, derivatives of the Mulliken approach, have been proposed.

- *Potential-based methods*: Here, the atomic charges are derived from a least-squares fit of the electrostatic potential (ESP), calculated over a large number of points around the molecule of interest (points p in Fig. 5.23). This approach is widely used and less basis set dependent than the orbital-based methods. The CHELP[59] (Charges from Electrostatic Potential), CHELPG[60], and Merz-Kollman[61] approaches are often used schemes in this area. The main difference between them is the choice of the points p around the molecule (Fig. 5.23). In the CHELP method, points are selected symmetrically on spherical shells around each atom. The Merz-Kollman scheme instead uses points on nested Connolly surfaces. In the CHELPG method, points are selected on a regularly spaced cubic grid with an over 10 times higher point density than for the other two methods (0.3 Å between the grid points).

Recently, it was suggested that the points p should be sampled randomly around the molecule to avoid any dependence on the choice of coordinate axes[54]. The electrostatic

potential methods do not include in the fit potential points within the van der Waals radii of the atoms, or points that are too far from the molecule. Unfortunately, the exclusion limits, as well as the van der Waals radii themselves, vary appreciably among the different methods. The Merz-Kollman scheme samples points at 1.4, 1.6, 1.8, and 2.0 times the van der Waals radius of the atoms. The CHELP method samples points at 2.5, 3.5, 4.5, 5.5, and 6.5 Å from each atom and excludes points within the van der Waals radius of any atom. The CHELPG method includes points between 0 and 2.8 Å plus the van der Waals radii. Several other schemes have been suggested, but normally no points within the van der Waals radii or more than 3.7 Å from all atoms are used in the corresponding fits. Naturally, this arbitrariness in the choice of the potential points will affect the resulting charges.
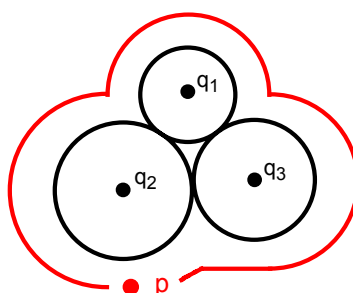
Fig. 5.23: Visualization of the fitting approach of the electrostatic potential (ESP) methodology

A popular methodology for the computation of these charges via quantum chemical calculations (ab initio, SCF calculations, semiempirical methods, or density functional computations) is the following[62]:

1. The charge density is obtained from the resulting wave function

$$V(r) = \sum_A \frac{Z_A}{|r - R_A|} - \sum_\mu \sum_\nu P_{\mu\nu} \int \frac{X_\mu(r_1)X_\nu(r_1)}{|r - r_1|} dr_1$$

2. The Coulomb field from this density is evaluated at the van der Waals radii of the atoms, where Z_A and R_A are the charge and the position of Ath nucleus, r_1 is the position of electron, $P_{\mu\nu}$ is the density matrix element and X_μ, and X_ν, are the basis functions used. For example, the Mulliken population is given by

$$q_A = Z_A - \sum_\mu \sum_\nu P_{\mu\nu} \int \frac{X_\mu(r_1)X_\nu(r_1)}{|r - r_1|} dr_1$$

3. The point charges are adjusted to reproduce this Coulomb field using a least-squares fitting procedure

$$V^C(r) = \sum_i \frac{q_i}{|r - R_i|} \qquad \sum_j \left[V(r_j) - V^C(r_j) \right]^2 = minimum$$

Here we report charge distribution calculations on the copper(II) acetonitrile complexes of a series of tetradentate bispidine-type ligands, using the CHELPG and Merz-Kollmann methodologies. In addition, geometries and relative energies (in cases where more than one isomer exists) are reported and discussed.

5.3.2. Computational Methods

All calculations were performed using the software package Gaussian03[63] for Linux running on the Opteron computer cluster Chi of the Chemistry Department of the University of Heidelberg. Geometry optimizations and frequency calculations were performed in the gas phase (no solvent effects were included), using the hybrid density functional B3LYP[64,65]. To reduce computational time, the ester groups on the ligand backbone were substituted by hydrogen atoms and the functional group at C9 was left in the ketone form (as found in the X-Ray structures of the free ligands). These approximations have been shown to have minimal effect on the properties of the corresponding metal complexes[66].

In order to test the basis set dependence of the chosen methods, the calculations were performed at two different levels of theory:

- "Low accuracy": 6-31G(d)[67] was used on all atoms
- "High accuracy":
    - TZVP[68] for Cu(II)
    - DZVP[69] for Br (due to the non-availability of a TZV[68] basis set for Br)
    - TZV for all other atoms (C, N, O, H, F, Cl)

Relative energies include zero-point corrections to the electronic energy term (the sum of the electronic and zero-point energies).

With regard to the charge distribution calculations, the default values for both methods (CHELPG and Merz-Kollman) were used, but the copper radius was set at 2.0 and 1.5 Å for CHELPG and Merz-Kollman, respectively. The reason for this difference is that the Merz-Kollman scheme samples points at 1.4 times the van der Waals radius of the atoms, while the CHELPG method samples points at the van der Waals radius. The methodology followed in the calculation of the atomic charges is the following: A geometry optimization of the corresponding copper(II) complex was performed at a low level of accuracy. Frequency calculations were performed on the optimized geometry to confirm that it is a minimum on the potential energy surface and the charges were then calculated as outlined above. From the low level geometry, a reoptimization at a higher level of accuracy was performed (with the corresponding frequency calculation) and the charges were recalculated.

5.3.3. Results and discussion

In order to investigate the effect that the position of substitution on the ligand has on the properties of the corresponding copper(II) complexes, calculations were performed on the complexes of all possible isomers of the methyl-, methoxy- and bromo-substituted N2Py2 derivatives. For the complexes with 4- (*p*-) and 5- (*m*-) substituted ligands, coordination of the co-ligand (acetonitrile) was assumed to take place trans to N3. Due the steric interaction of the substituents with the co-ligand in the 6- (*o*-) position, both coordination in the usual trans N3 position and coordination trans to N7 were considered for these complexes, and these are referred to as the 6- and 6-(trans) isomers, respectively. Calculations were also performed on selected isomers of the triflouromethyl-, cyano- and chloro- substituted ligands, but here only those isomers for which viable synthetic pathways exist were considered. For comparative purposes, the copper(II) complex with the unsubstituted N2Py2 ligand was also included in the calculations.
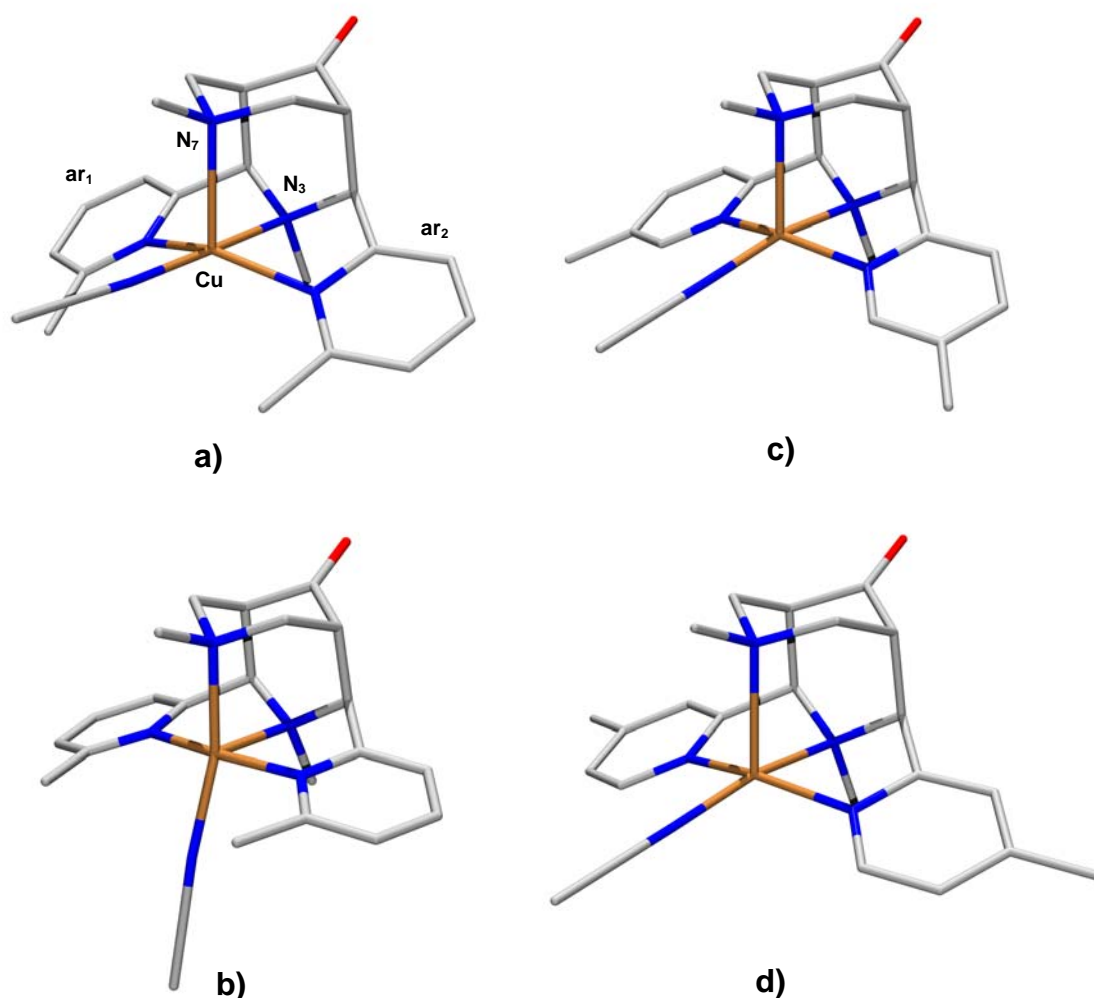
Fig. 5.24: Calculated structures of the copper(II) complexes of a) N26PyMe2, b) N26PyMe2 (trans), c) N25PyMe2 and d) N24PyMe2

The calculated geometries for both the low accuracy and high accuracy basis sets are given in Appendix A and the calculated structures for the methyl-substituted series are shown in Fig. 5.24. Where experimental structures exist these are compared to the calculated structures and the overall correspondence is good. Most of the calculated bond lengths lie within 0.05 Å of the experimental ones and the largest error in bond length is less than 0.1 Å. More importantly, the Jahn-Teller axis is correctly predicted to lie along the Cu-N7 bond in all calculated structures in which the acetonitrile is trans N3 disposed (the Cu-N7 bond lengths are between 0.2 and 0.4 Å longer than the Cu-N3 bond lengths). In the three trans complexes (acetonitrile trans to N7) one would expect the Jahn-Teller axis to lie along the Cu-N3 bond, with a partial quenching of the Jahn-Teller stabilization due to the restraints of the ligand backbone. Indeed, the Cu-N3 and Cu-N7 bond lengths lie within 0.1 Å of each other and for N26MePy2 the Cu-N7 bond are even slightly longer than the Cu-N3 bond.

With regard to the electronic properties of the different copper(II) complexes, not only the electronic charges are of importance, but also the relative energies of the different isomers. It is interesting to compare the effects of the basis set (level of accuracy) and the relative positions of the different residues in the aromatic ring (including the "normal" trans to N3 and the trans to N7 disposition of the coligand acetonitrile for o- substitution).
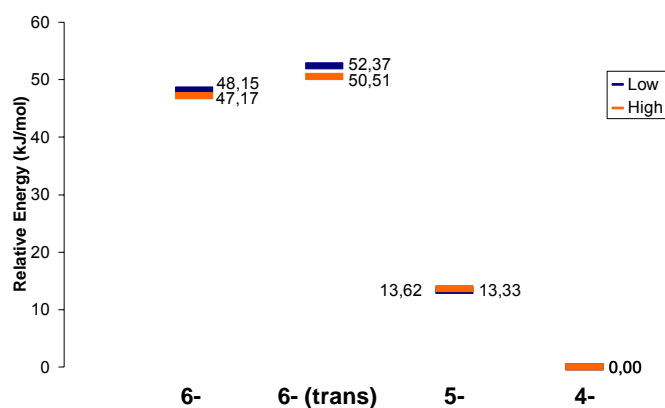
Fig. 5.25: Relative energies of the different isomers for the methyl-substituted ligands

Starting with the methyl series, the expected result was obtained. As the methyl group gets closer to the donor atom, the energy of the corresponding isomer increases, with a particularly large increase from m- to o- substitution (Fig. 5.25). These differences are quite large, both at the low and high level of accuracy, and the relative energies obtained at the

different levels of accuracy are close to identical. Another important result is that the two isomers of the *o-* substituted complex are very close in energy, with a slight preference for the electronically favourable trans N3 coordination of the acetonitrile molecule. This is in agreement with the crystal structure of the copper(II) acetonitrile complex of N26MePy2, in which the acetonitrile is coordinated trans to N3.

A similar tendency was observed for the *o-* and *p-* isomers of the methoxy derivatives (Fig. 5.26). The energy difference between the trans N3 and trans N7 coordination modes of the *o-* isomer is almost identical to that observed in the methyl series, and the *p-* isomer again has the lowest energy. It is interesting to note that the energy difference between the *o-* and *p-* isomers is much smaller that in the methyl series, an indication of how large the electronic stabilization of the electron donating methoxy- substituent in the *o-* position is. The *m-* isomer however, both at low and at high levels of accuracy, has a much higher energy than the others, despite the fact that the geometries of the *m-* and *p-* isomers are practically identical with respect to the metal centre (see Appendix A). A possible explanation is that the stabilizing +M effect is not felt by the nitrogen donor at the *m-* position, producing an even bigger destabilization than the purely steric effect induced by *o-* substitution.
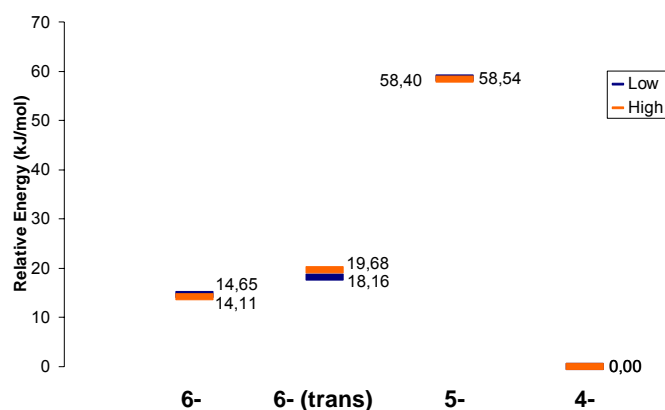
Fig. 5.26: Relative energies of the different isomers for the methoxy-substituted ligands

With regard to the bromo series (Fig. 5.27), the first remarkable result was the big difference between the low and high accuracy methods. The expected energetic sequence for the *o-* and *p-* isomers would be that observed in the methyl and methoxy series, but at the low level of accuracy, this order is inverted. By increasing the accuracy of the basis set to DZVP for bromine (the most accurate basis set available for bromine at the time of the calculations), the expected order was obtained. This extreme basis set dependence, not observed in the methyl and methoxy series, is probably due to the high electronegativity of bromine. The

more electronegative an element, the more important an accurate description of the electron density becomes and the greater the effect of additional basis and polarization functions.

A further interesting observation is that, while the energy difference between the trans N3 and trans N7 coordination modes of the *o*- isomer is similar to that of the previous two series (in the high level calculations), the energetic ordering of the two isomers is inverted. This may be related to the Jahn-Teller stabilization in the trans isomer, which is in turn related to the ratio of the Cu-N3 and Cu-N7 bond lengths (see Appendix A).
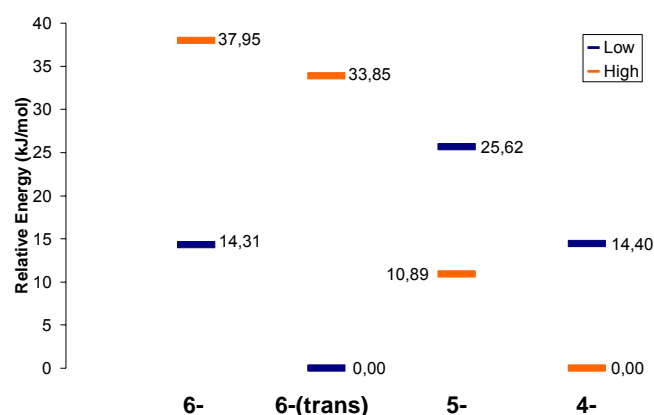
Fig. 5.27: Relative energies of the different isomers for the bromo-substituted ligands

The atomic charges of a broader range of 3,7-diazabicyclo[3.3.1]nonane derivatives were calculated. The investigated complexes are divided into two groups: complexes of ligands with donor substituents (N26MePy2, N26MOXPy2, N25MePy2, N25MOXPy2, N24MePy2, N24MOXPy2) and those of ligands with acceptor substituents (N25CF3Py2, N25CNPy2, N24CNPy2, N25ClPy2). The bromo substituted ligands were not included in the charge distribution calculations due to reliability issues caused by the lack of a defined van der Waals radius for bromine in the Gaussian03 package.

Before commenting on the results, it is important to explain what the calculated charges actually represent. The reported charges are those of the copper centre. A higher charge does not imply a reduced electron density on the copper centre, but that more electron density is donated to the copper centre by the ligand[70]. According to this, the charge on the copper centre should be higher in the donors group and lower in the acceptors group, than for the unsubstituted reference ligand N2Py2.

Beginning the discussion with the donors (the methyl and methoxy series), two important points must be mentioned, namely the differences obtained between low and high accuracy basis sets and the good agreement of the two methods (chelpgh and MKh) with the high

accuracy basis set. From the diagrams shown in Fig. 5.28 and Fig. 5.29, the need for accurate basis sets can be clearly observed. The lack of selectivity in the diagrams on the left hand side of the figures must be emphasized. The methyl group produces similar charge distributions, independent of its position in the ring, and in some cases with values close to or even lower that the unsubstituted N2Py2. A change to high accuracy (right hand side of Fig. 5.28 and Fig. 5.29) greatly improves the agreement of the methods. Here it is even possible to clearly order the trans N3 isomers (in the methyl and methoxy series) in the expected sequence of 6- > 4- > 5- > N2Py2 (unsubstituted analogue).
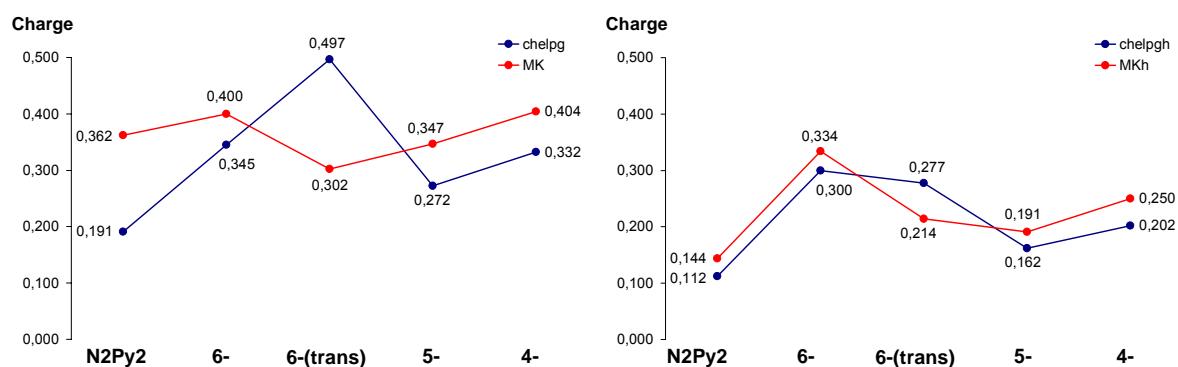
Fig. 5.28: Schematic representation of the charges of the different isomers within the methyl series: low accuracy (left) vs. high accuracy (right)
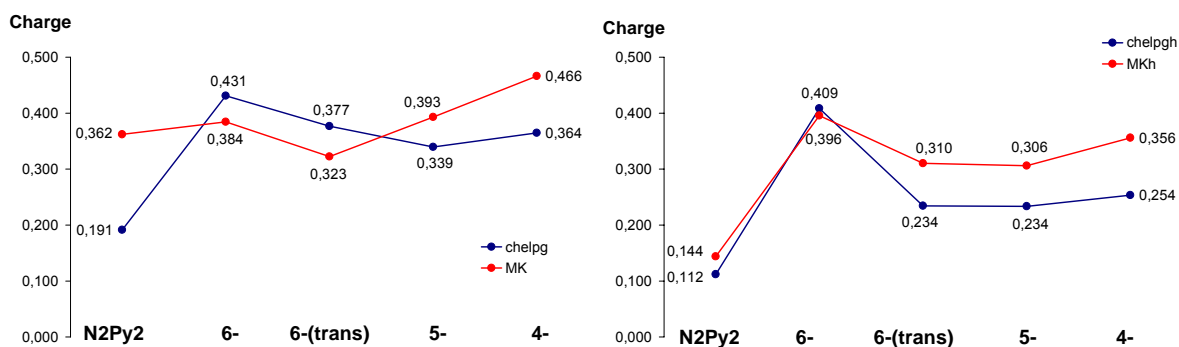
Fig. 5.29: Schematic representation of the charges of the different isomers within the methoxy series: low accuracy (left) vs. high accuracy (right)

When comparing the charge values of the methyl and methoxy series, a high accuracy basis set is again needed in order to obtain reasonable results. Here we see that, regardless of the position of substitution on the pyridine ring, each methoxy isomer donates more electron density to the copper center than its methyl analogue, in agreement with what one would expect on the basis of their electronic properties.

The results for the electron withdrawing groups (Cl-, CF_3- and CN-), can be explained in a similar way to those for the donating groups (Fig. 3.30). Yet again, high accuracy is required to obtain reasonable results, and in this case the Merz-Kollmann methodology seems to be slightly more efficient than CHELPG. An important difference between the electron donating and withdrawing groups is the relative values with respect to the unsubstituted N2Py2. The donating groups show a larger difference between the substituted and unsubstituted ligands than the acceptors, the latter showing in some cases charges very close to the reference value for N2Py2.
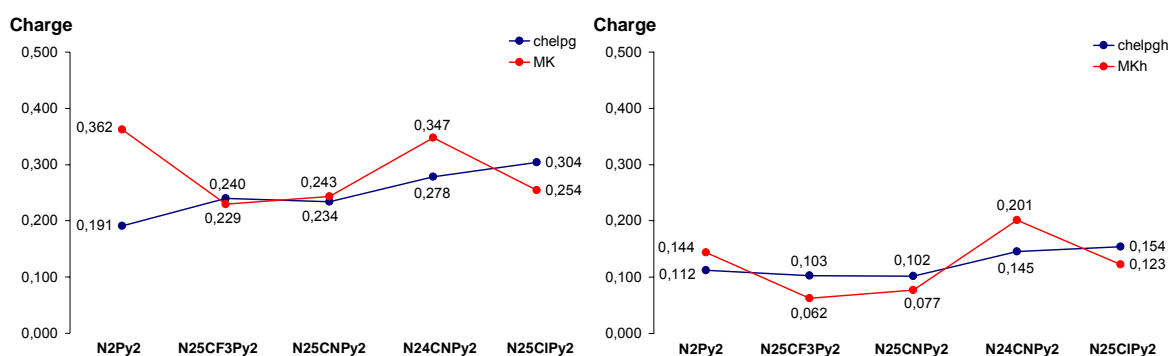
Fig. 5.30: Schematic representation of the charges of the different isomers within the acceptors series: low accuracy (left) vs. high accuracy (right)

The motivation for performing a systematic investigation of the charges of a range of copper(II) complexes with different substituted ligands, was to try to correlate them with their redox potentials. Unfortunately however, there are clear discrepancies between theory and experiment. The results of the charge distribution calculation for the donor group predict a clear influence of the electron donating capacity of both methyl and methoxy on the metal center (even in the *m*- position). From the obtained redox potentials however, we know that this is not always the case.

Focusing our attention on the 5- substituted derivatives and N2Py2, we see that the redox potentials of their copper(II) complexes are quite similar, that of N25MePy2 being almost identical to that of N2Py2 and that of N25OXPy2 not much higher. This implies that the electronic influence of the methyl group at the 5- position is negligible and that of methoxy very small. On the basis of the calculations, the copper(II) complexes of N25MePy2 and N25MOXPy2 should have even lower redox potentials than that of N2Py2, whereas in reality they are higher.

The trend between redox potential and charge on the copper(II) center is shown in Fig. 5.30. From these four points it is quite difficult to propose any kind of tendency, but if one were to fit a linear regression curve to the data, the question is whether the slope of the resulting line

would be correct. As discussed previously, the higher the charge at the copper(II) center, the higher the electronic density obtained from the ligand and the greater the stabilization of the oxidised form of the metal. Taking only electronic effects into consideration, an increase in the charge would therefore imply a decrease in the redox potential and a negative slope in Fig 5.31, which is exactly opposite of what is observed.
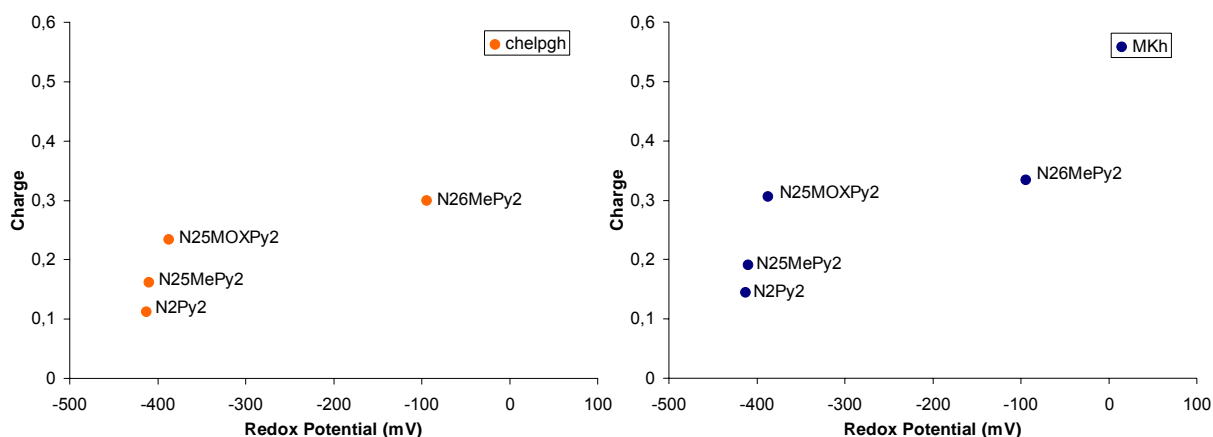
Fig. 5.31: Plot of the correlation between charges and redox potentials of selected copper(II) complexes: CHELPG (left) vs. Merz-Kollman (right)

In theory, the previously discussed acceptor groups, such as CF_3 or CN, should lie quite far to the right in Fig. 5.31, with fairly low charge values. Furthermore, N26MePy2 should not be directly compared to the other three (pure electronic effects), because of the aforementioned influence of the steric destabilization of the two methyl groups, on the redox potential of the copper(II) complex.

From these results, it is important to highlight the need for new copper(II) complexes with ligands containing electron donating as well as withdrawing groups at 4-, 5- or 6- positions, in order to obtain a better understanding of the relationship between redox potential and the charge calculations.

In summary, the charge calculations provide an interesting and chemically intuitive picture of the bonding in copper(II) bispidine complexes, which is however, not always in agreement with experiment. Possible reasons for this lack of correlation between experiment and theory could be effects such as solvation, which may influence the redox potentials, but are not included in the present theoretical model. A high level of theory is required to provide reasonable results for charge calculations, but has been shown to be less important for the geometries and relative energies of the complexes, with the exception of complexes with highly electronegative ligand substituents such as bromine.

6. Iron(II) complexes of 3,7-diazobicycle[3.3.1]nonane derivatives

6.1. Introduction

Iron, as well as copper, is an important metal in many fields of chemistry. Focusing our attention on a molecular level, various bioinorganic and synthetic catalytic systems are relevant, the iron proteins and enzymes being of great importance. From a bioinorganic point of view, important to mention are the transport and management of dioxygen, electron transfer and various catalytic reactions involving dioxygen or hydrogen peroxide. *Hemoglobin* plays an important role in the transport of dioxygen[71], while *superoxide dismutases* are responsible for the detoxification of the dangerous dioxygen species superoxide[71]. *Rubredoxin* and *ferredoxin,* both iron-sulfur clusters, are involved in electron transfer processes[71], while a large group of enzymes containing one or two iron centres, including various *dioxygenases*, *methane monooxygenase*, and *bleomycin*, perform many different kinds of oxidation reactions on a broad variety of organic substrates (including DNA)[19,72].

Within this broad scope of application of iron compounds, the oxidation reactions performed by iron enzymes and, more specifically, the oxygen activation reactions of the mononuclear non-heme enzymes, are of great interest to the present work[19].

A challenging task in molecular catalysis, either homo- or heterogeneously, is the selective oxidation of hydrocarbons. These kinds of processes are present in many biological systems and key industrial transformations involving the production of fine chemicals, either as important intermediates or as final products. Here, we concentrate our interest on the (di)hydroxylation and epoxidation of olefins.

The dihydroxylation of olefins, especially in its enantioselective form, has become an important step in many synthetic processes. Although the reaction has been known for many years, and the proposed mechanisms for different variations of the reaction are generally accepted[13,73,74], osmium tetraoxide (OsO_4) remains one of the most widely used and reliable oxidizing reagents available for the cis-hydroxylation of alkenes.
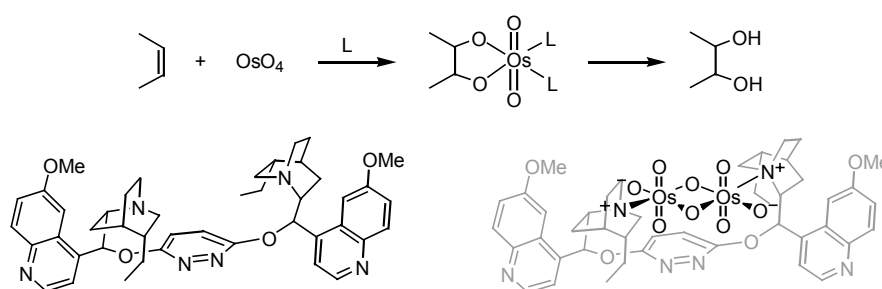
Fig. 6.1: Proposed general mechanism and cinchona alkaloid derivative

The generally proposed mechanism for cis-dihydroxylation of alkenes by osmium tetraoxide in the presence of a ligand L is shown In Fig. 6.1, along with one member of the successful cinchona alkaloid family of ligands[74] and its osmium complex[13]. The mechanism is well established and proceeds via the formation of an osmium(VI) intermediate which, upon reductive or oxidative hydrolysis, yields the corresponding cis-diol. Other secondary oxidants used in combination with osmium tetraoxide for the catalytic oxidation of alkenes are: tert-butyl hydroperoxide, *N*-methylmorpholine *N*-oxide, oxygen, sodium periodate, and sodium hypochlorite[12,73].

The complementary reaction to the dihydroxylation involving mononuclear iron(II) complexes, is the epoxidation of alkenes. Epoxidation by peracids has been known for almost 80 years and has found great application. Based on both experimental and theoretical investigations, a plausible route of interaction between the peroxygen unit, the carbonyl group of the peracid and the alkene has been postulated, although other mechanisms have also been suggested. This proposed mechanism is shown in Fig. 6.2[75].
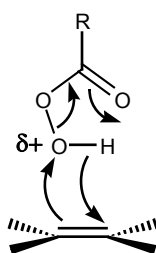
Fig. 6.2: Proposed mechanism for epoxidation of olefins by peracids

Epoxidation systems using hydrogen peroxide with catalytic amounts of "cheap", relatively non-toxic metals have been given increased attention in the past three decades and are potentially viable for large-scale production. The idea of hydrogen peroxide as a preferred oxidant to dioxygen, arises for environmental and security reasons (under certain circumstances, O_2/organic mixtures are known to spontaneously ignite)[76].

Ligands containing mixed pyridine and amine donors have been extensively investigated, particularly from the point of view of biomimetic, nonheme iron catalysts[15,17,77]. Although the activity of some of these complexes in epoxidation and/or dihydroxylation reactions using H_2O_2 as oxidant is quite modest (these iron catalysts are not synthetically useful because they yield only a few turnovers), the mechanistic details of these reactions involve multiple iron oxidation and spin states, as well as interesting intermediates, and are of great importance in gaining a better understanding of the workings of iron enzymes, as well as in the development of more active and selective catalysts.
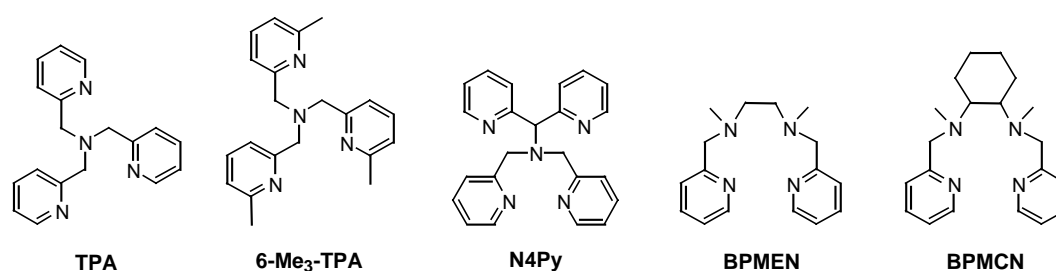
Fig. 6.3: Some popular ligands used in non-heme biomimetic catalysts

Mechanistic studies of hydrocarbon oxidation reactions by Que and co-workers, using the mainly tetradentate ligands shown in Fig. 6.3, suggest that these iron(II) complexes show similarities with the antitumor drug *bleomycin* (Fig. 6.4), which is responsible for DNA cleavage in cells. The key step in the activation of oxygen by bleomycin is the formation of a low-spin Fe(III)-OOH intermediate. This species, known as activated bleomycin (ABLM), is the last observable intermediate in the reaction mechanism[23].
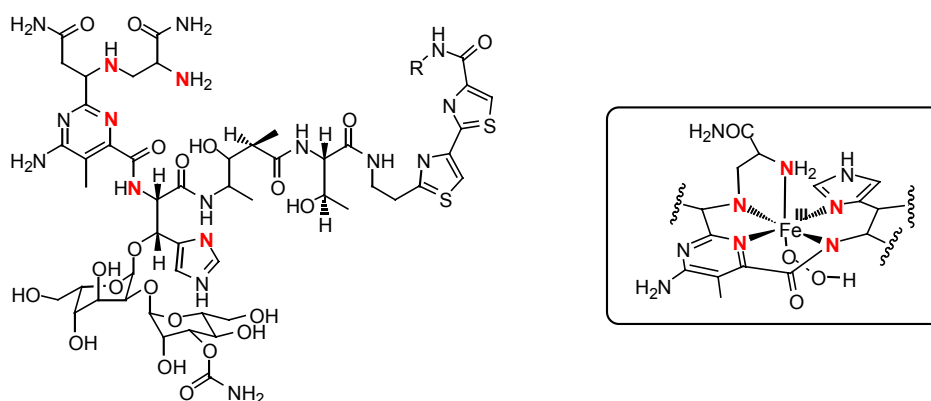
Fig. 6.4: *Bleomycin* and its Fe(III)-OOH complex (ABLM)

From the accumulated spectroscopic data (UV-Vis, Raman and EPR), it is clear that, for most of the complexes in this class, an Fe(II) precursor treated with excess of H_2O_2 leads to the formation of an Fe(III)-OOH intermediate (as with *Bleomycin*). Depending on the ligand, this species may have different spin states, which govern the reactivity of the corresponding active species. The key is then to investigate how this highly active intermediate evolves and, of course, to try to determine which intermediate species is responsible for the substrate oxidation.

The iron complex of the pentadentate ligand N4Py, for example, reacts with H_2O_2 to afford a low-spin Fe(III)-η^1-OOH intermediate with a hydroperoxo-to-Fe(III) charge transfer band at

548 nm. Deprotonation of this species yields the respective conjugate base with a lower energy charge-transfer band (685 nm). Spectroscopic studies agree that the corresponding formed species is the high-spin Fe(III) side-on peroxo derivative, but due to the lack of crystal structures for both the hydroperoxo and peroxo complexes, the exact structures of those compounds are still matter of discussion[78].

From kinetic and ^{18}O-labeling experiments performed on the tetradentate systems presented in Fig. 6.3, some common features can be found. On the basis of these experimental results and DFT studies[79], a high valent oxo/hydroxo species is proposed to be the highly reactive intermediate responsible for the cis-dihydroxylation and epoxidation (Fig. 6.5).
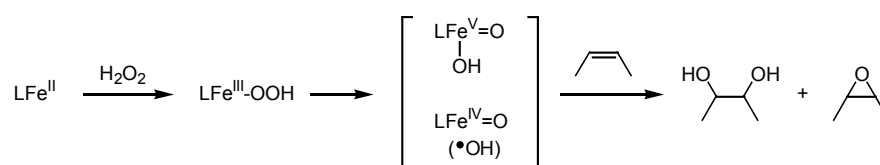
Fig. 6.5: Proposed simplified mechanism for non-heme iron(II) catalysts[79]

With regard to this group of iron catalysts, if one wishes to develop a selective epoxidation catalyst, it should be able to activate H_2O_2 without radical formation. Assuming the formation of an Fe(III)-OOH intermediate, the key step in producing an active species without forming radicals is how the O-O bond in the Fe^{III}-OOH complex cleaves. To avoid radical formation, cleavage must be heterolytic (Fig. 6.6). If this is not the case, the free radicals can initiate the so called Fenton-type chemistry[80,81], with the consequences of degradation of the catalytic species and/or incomplete consumption of the substrate.
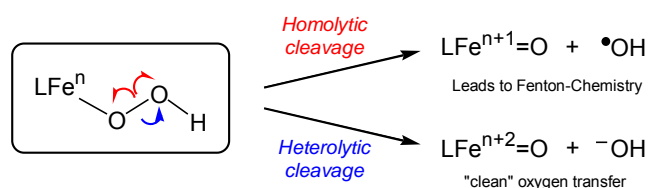
Fig. 6.6: Cleavage pathways for the O-O bond in the Fe^{III}-OOH intermediate

6.2. Catalytic oxidation of cyclooctene with iron(II) bispidones

The 3,7-diazabicyclo[3.3.1]nonane derivatives belong to the group, presented above, containing a combination of pyridine and tertiary amine donors. In particular, the rigid tetra- and pentadentate ligands have similar donor sets to TPA and N4Py (Fig. 6.3), the iron complexes of which represent the most active oxidation catalysts in non-heme iron chemistry. Despite certain structural differences, some analogy in mechanism and reactivity will be shown.

The most crucial structural aspect of bispidine coordination chemistry is emphasized in Fig. 6.7, where the coordination of different co-ligands within the three studied iron(II) complexes is shown. Important to note are the metal-ligand distances trans to N3 (equatorial, **E**) and trans to N7 (axial, **A**). In general, the metal-ligand distances trans to N3 are shorter than those trans to N7. Regarding the two pentadentate isomers, N2Py3o and N2Py3u, the coordination sites trans to N3 and trans to N7, respectively, are blocked by an additional pendant pyridine arm. When studying the stability of the Fe(III)-OOH and Fe(III)-OO complexes in terms of steric and electronic effects, it is important to consider the fact that only one coordination site for H_2O_2 binding is free, but in each case only **A** or **E**. From experimental and computational studies on $Cu^{II/I}$ derivatives and X-Ray crystal structures of the Fe(II) complexes[9], the Fe(III) and Fe(IV) complexes of N2Py3o and N2Py3u are expected to have different structural and electronic properties. In fact, when one considers the resonance Raman studies of the Fe(III)-OOH species of these ligands, while the O-O stretching vibration frequencies of the two intermediates are interestingly nearly identical, the Fe-O vibration of the complex where the hydroperoxo unit lies along **A** is shifted to lower energy by 12 cm^{-1} relative to the isomer where it lies along **E**, confirming a weaker and therefore more labile Fe-O bond for the N2Py3o complex[82]. From DFT computational results on the structures of the corresponding hydroperoxo complexes[82], the calculated Fe-O distances show the same tendency as all the previously mentioned experimental data with values of 1.88 Å for N2Py3o and 1.78 Å for N2Py3u.

N2Py2   N2Py3o   N2Py3u
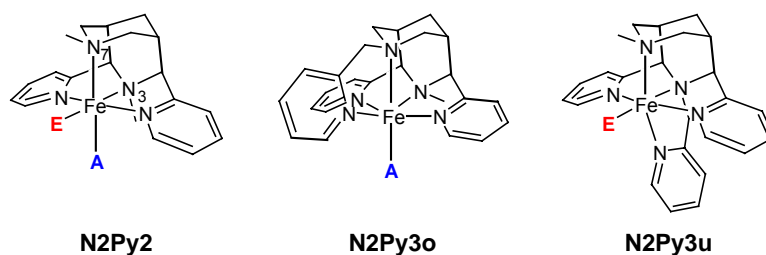
Fig. 6.7: Representation of the three studied iron(II) bispidine complexes

The discussed structural and electronic differences between the Fe(III)-OOH complexes of the two pentadentate isomers are supported by the properties of their conjugate bases[82]. Deprotonation of the Fe(III)-hydroperoxo intermediate of N2Py3u in methanol at -40°C (by addition of NaOMe) leads to a blue solution with an absorption maximum at 721 nm. Interestingly, this deprotonated species can be reprotonated with $HClO_4$. All UV-Vis titration spectra go through an isosbestic point at 650 nm, indicating the presence of a reversible acid-base equilibrium. The conjugate base of Fe(III)-OOH with N2Py3o as ligand is fairly unstable, showing no stable deprotonated intermediate at -40°C and affording exclusively an Fe(III) decomposition product. This deprotonation process can be successfully performed at temperatures much lower than is necessary for N2Py3u (-80°C), and a new chromophore with a broad absorption band centered at 760 nm can be observed, which is postulated to be the side-on peroxo complex of N2Py3o. The suggested side-on binding of the peroxo unit is supported by DFT calculated structures of the Fe(III)-peroxo complexes, which yield values of 1.91 and 1.98 Å for the Fe-O bond lengths (symmetrical, side on binding of O-O) and 1.41 and 1.36 Å for the O-O bond lengths, for N2Py3u and N2Py3o respectively.

Therefore, the low-spin hydroperoxo (six-coordinate) and the high-spin peroxo complexes (seven-coordinate) have relatively weak Fe-O bonds in the case of N2Py3o and stronger for N2Py3u. One would expect the strong interaction of the peroxo ligand with the Fe(III) center coordinated to N2Py3u to produce a weaker O-O bond, while the weaker interaction in the complexes with N2Py3o should lead to a stronger and less activated O-O bond.

In addition to the Fe(III) intermediates observed for N2Py3u and N2Py3o, a low-spin Fe(IV)-oxo intermediate has been isolated for N2Py3u. This species is characterised by an absorption maximum at 715 nm and is formed by the addition of excess H_2O_2 to the Fe(II) complex in acidic aqueous medium. It is interesting to note that here there is no evidence for the involvement of the corresponding Fe(III)-OOH intermediate, an indication of the complexity of the Fe(II)/H_2O_2 reaction surface[83].

The iron chemistry of the tetradentate ligand N2Py2 is less well understood than that of the pentadentate ligands N2Py3u and N2Py3o. In particular, the reaction of its Fe(II) complex with H_2O_2 yields no spectroscopically observable Fe(III) intermediates, although the Fe(III)-peroxo complex could be synthesized and characterized by the addition of KO_2 to the Fe(II) precursor in neutral aqueous medium[84]. While no Fe(III)-OOH intermediate has been characterised for N2Py2, an Fe(III)-OOR species (R = ^tBu) could be formed by the reaction of t-butylperoxide with the corresponding Fe(II) complex in acetonitrile or dichloromethane. Spectroscopic evidence indicates an equilibrium between the high spin and low spin species, which can be shifted by a change of solvent and/or temperature[85]. Due to lack of experimental information for the Fe(II)/H_2O_2 system of this ligand, a range of DFT

calculations have been performed. These support the experimental observation that no Fe(III) intermediates are formed and suggest the involvement of an Fe(II)/Fe(IV) pathway[86].

Once the fundamentals of the electronic and structural properties of the iron(II) complexes shown in Fig. 6.7 and its Fe(III) intermediates were understood, the catalytic activity in the reaction shown in Fig. 6.8 was tested[11].
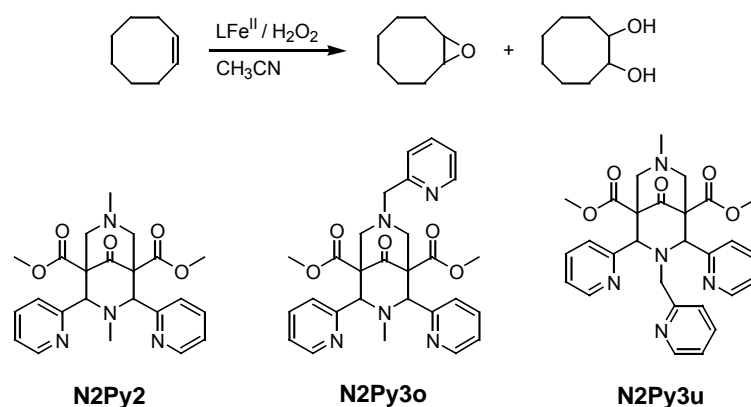
Fig. 6.8: Oxidation reaction and studied 3,7-diazabicyclo[3.3.1]nonane ligands

All experiments were performed at 25.0 °C, using acetonitrile or methanol as solvent, H_2O_2 as oxidant and cyclooctene as substrate (catalyst:H_2O_2:substrate = 1:10(100):1000). The product distributions and corresponding isotope labeling results are summarized in Tables 6.1 and 6.2.

Table 6.1: Product distribution

Ligand	Experimental conditions[a]	D+E[d,e]	D/E
TPA	[b]	7.4	1.2 : 1
6-Me$_3$-TPA	[b]	5.6	7 : 1
N4Py	[b]	0.6	0 : 1
N2Py3u	air (0.5 h)	1.2	0.1 : 1
	air (6 h)	6.8	< 0.1 : 1
	argon (0.5 h)	1.0	0.2 : 1
	PhIO[c], air	1.1	0 : 1
	PhIO[c], argon	0.6	0 : 1
N2Py3o	air (0.5 h)	5.0	0 : 1
	argon (0.5 h)	2.0	1 : 1
	PhIO[c], air	1.0	0 : 1
	PhIO[c], argon	0.4	0 : 1
	CH$_3$OH, air	1.9	0 : 1
	CH$_3$OH, argon	1.7	0 : 1
	cis-2-heptene[82]	1.9	0 : 1, 20% RC[87]
N2Py2	[b]	6.5	3.2 :1
	air (0.5 h)	3.8	1.6 : 1
	argon (0.5 h)	3.4	1.7 : 1
	cis-2-heptene[82]	7.0	1.6 : 1, 99% RC[87]

[a] 1000 eq. cyclooctene, 10 eq. H$_2$O$_2$, reacted for 0.5 h under air in CH$_3$CN at 298 K, unless otherwise noted

[b] ambient temperature

[c] oxidant: 1 eq. of Fe(IV)=O; no H$_2$O$_2$ used, i.e., stoichiometric reaction

[d] TON = 10 · µmol (product) / µmol (H$_2$O$_2$), 10 = max; the error limit for all data is approx. ±5% (relative) for TON

[e] diol is exclusively cis for TPA and 6-Me$_3$-TPA and a mixture of cis and trans for N2Py3o and N2Py3u, when observed

Table 6.2: Labeling data

Ligand	Experimental conditions[a]	% epoxide-^{18}O [c]			% 1,2-diol-^{18}O			
		$H_2^{18}O$	$H_2^{18}O_2$	$^{18}O_2$	$H_2^{18}O$		$H_2^{18}O_2$	
					$^{16}O^{16}O$	$^{16}O^{18}O$	$^{16}O^{18}O$	$^{18}O^{18}O$
TPA	H_2O_2, air	9	90	(1)	13[d]	86[d]	97[d]	3[d]
6-Me$_3$-TPA	H_2O_2, air	3	54	(43)	99[d]	1[d]	4[d]	96[d]
	H_2O_2, air	(0)	15	85				
	H_2O_2, argon	18	82	---	70[d]	30[d]	23[d]	77[d]
N2Py3o					50[e]	50[e]	56[e]	44[e]
	PhIO[b], air			55[f]				
	PhIO[b], argon	40[g]						
N2Py2	H_2O_2, air	0	45	55	92	8	0	100
	H_2O_2, argon	16	84	---	93	7	0	100

[a] 1000 eq. cyclooctene, 10 eq. H_2O_2, reacted for 0.5 h under air in CH_3CN at 298 K, unless otherwise noted

[b] oxidant: 1 eq. of Fe^{IV}=O; no H_2O_2 used, i.e., stoichiometric reaction

[c] values in parentheses are calculated by difference

[d] cis-diol

[e] trans-diol; cis : trans = 0.4 : 0.6

[f] 45% from PhIO

[g] 60% from PhIO

Pentadentate Ligands (N2Py3o and N2Py3u)

Epoxide formation

The extreme difference in catalytic activity obtained for the two isomers N2Py3o and N2Py3u under aerobic conditions is quite remarkable. After standard reaction time (see experimental part), the N2Py3u complex yields less than 1 TON of oxidation products (primarily epoxide, comparable to N4Py), while the N2Py3o complex is much more reactive, affording 5 TON of exclusively epoxide. This difference suggests that the N2Py3u-based catalyst is a rather poor catalyst compared to the N2Py3o complex. However, when the reactions are carried out over a longer period of time (6 hours), the product yield increases to about 7 TON[11], indicating that the N2Py3u-based catalyst is simply much slower in activating the oxidant (H_2O_2) and therefore needs about seven times longer to achieve a comparable product yield.
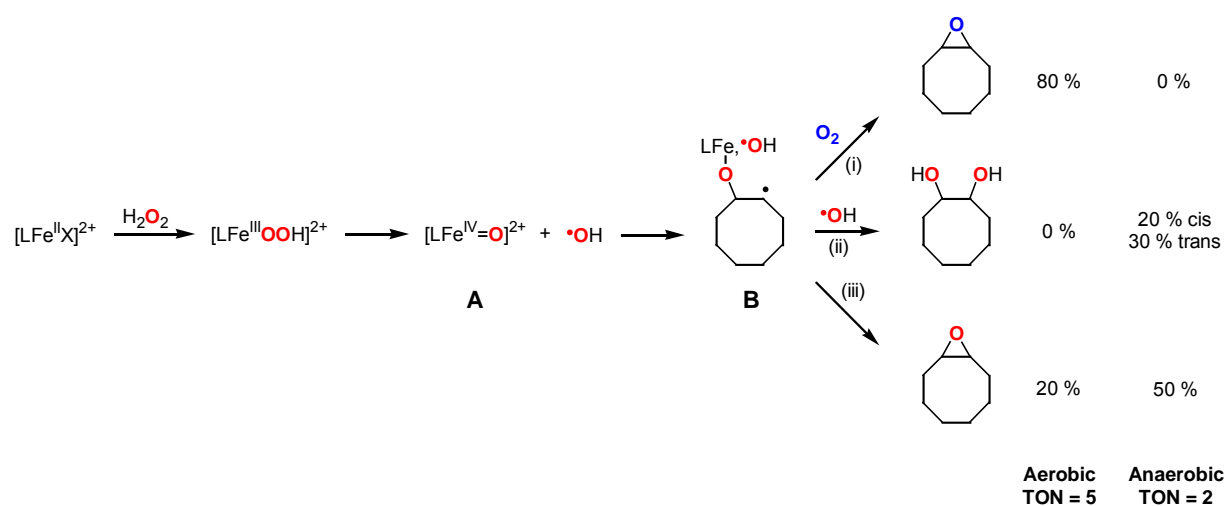
Fig. 6.9: Proposed mechanism for cyclooctene oxidation with the iron(II) complex of N2Py3o

Under strictly anaerobic conditions the N2Py3o-based catalyst exhibits a completely different reactivity: only 1 TON of epoxide is produced, suggesting that 80% of the epoxide produced in air is due to a mechanism whereby the oxygenation proceeds independently of the iron site. The necessity for the presence of oxygen indicates that this is a carbon-centered radical-based process, and this is supported by the $^{18}O_2$ labeling experiments, which indicate that the extra 80% (4 TON) of epoxide produced under aerobic conditions result from O_2 addition to a carbon-based (cyclooctene-derived) radical. It has been known for many years that for cyclooctene, this radical chain mechanism (autoxidation, pathway (i) in Fig. 6.9) yields epoxide as the main product, via addition of an initially formed alkyl peroxy radical to the C-C double bond[88]. The remaining 20% (1 TON) of epoxide, observed both under aerobic and anaerobic conditions (label from $H_2^{18}O_2$), is proposed to emerge from direct

transfer of the ferryl oxygen atom. The mechanism of formation of intermediate B (Fig. 6.9) could be either concerted or stepwise, consisting of an electron transfer in the first step, leading to the formation of a radical cation which then traps the emerging Fe(III)-O fragment. Once formed, intermediate B has three possible pathways for product formation. The mentioned ferryl oxygen atom transfer may occur as shown in (iii). This is supported by the observation that the epoxide oxygen atom under anaerobic conditions originates predominantly from $H_2^{18}O_2$ and to a minor extent from $H_2^{18}O$ (homolytic cleavage of the O-O bond in $[Fe(III)(OOH)]^{2+}$, the ferryl oxygen in the emerging Fe(IV)=O exchanges with H_2O with $t_{1/2} \leq 1h$). Using cis-2-heptene as substrate, it is important to remark that, under aerobic conditions, stereochemical scrambling takes place (Table 6.1), leading exclusively to epoxide. This indicates again the presence of carbon-based radicals in the mechanism.

In order to gain a better understanding of the reaction mechanism proposed in Fig. 6.9, some catalytic experiments were performed with the in-situ prepared $[Fe^{IV}=O]^{2+}$ species (characterised by UV-Vis and Mössbauer), produced from the reaction of the corresponding N2Py3u and N2Py3o iron(II) complex and iodosylbenzene[89] (PhIO). Epoxide is obtained as unique product both under aerobic (1.1 TON for N2Py3u against 1.0 TON for N2Py3o) and anaerobic conditions (0.6 TON for N2Py3u against 0.4 TON for N2Py3o)[11]. Under aerobic conditions, autooxidation, pathway (i), and ferryl oxygen transfer, pathway (iii) take place. In absence of oxygen, only reaction path (iii) is responsible for the production of the epoxide. It is known that complexes with M=O groups which attack at carbon-carbon double bonds yield M-O-C-C$^\bullet$ radical species such as intermediate B, which subsequently form metal-epoxide complexes[12,90]. The fact that no diol is formed when $[Fe(IV)=O]^{2+}$ is used directly as oxidant, indicates that hydrogen peroxide or a H_2O_2-derived species, such as OH radicals, are required for diol formation. This is in agreement with the labeling results using H_2O_2 as oxidant, which indicate that most of the oxygen atoms present in the cis- and trans-1,2-diol come from $H_2^{18}O_2$. This therefore supports the suggested pathway with Fe(III) intermediates and a caged radical pair (intermediate B).

Diol formation

The formation of 1,2-diol with the N2Py3o-based catalyst (1 TON, only under anaerobic conditions and only in MeCN), is the most amazing result of the present work. The cis- and the trans- isomers of the 1,2-diol are observed in a ratio of approximately 4:6, indicating a mechanism of formation different to the usual one involving an $[Fe(O)(OH)]^{n+}$-type species. In order to explain these results, it is necessary again to consider the presence of carbon based radicals in the mechanism of diol formation. Under aerobic conditions, carbon-based radicals are known to be quenched, and the absence of any diol formation under these conditions indicates that the diol is formed via a radical intermediate. This supposition is strongly

supported by the loss of stereoselectivity in the diol formation. Switching to MeOH as solvent, it is remarkable to observe the absence of any diol formation, suggesting that intermediate B traps O-based radicals (pathway (ii)) to form the diol, which are quenched in MeOH. The incorporation of solvent water into the diol product can be rationalized by solvent exchange at the $[Fe(IV)=O]^{2+}$ unit.

The mechanism for epoxidation and diol formation requires an intermediate B, with a lifetime long enough to trap O_2 and lead to autoxidation (pathway (i)). While B-type intermediates generally are proposed to be very short-lived[12,90], the observation of the loss of stereocontrol with 2-heptene indicates a somewhat extended lifetime; this indicates that the above-mentioned radical cation, preceding B, may be of importance. The presence of the proposed intermediate B can explain all results, but it is also possible that these are due to the formation of other carbon-based radicals (like allyl-radicals), leading to intermediates and products not yet discovered. Furthermore, it is impossible to exclude pathways with O-based radicals other than the extremely short-lived •OH, e.g., •OOH and other less reactive species (it is unlikely that free •OH radicals are directly involved in the olefin oxidation reaction, these are much too reactive in non-aqueous solutions[91,92])

The usual conditions for the experiments are: 25.0 °C, catalyst: H_2O_2: substrate = 1:10:1000 (for more details see experimental part). To investigate the influence of reaction time, temperature and amount of oxidant (in this case H_2O_2) on the yield/TON, the following experiments were performed for N2Py3o:
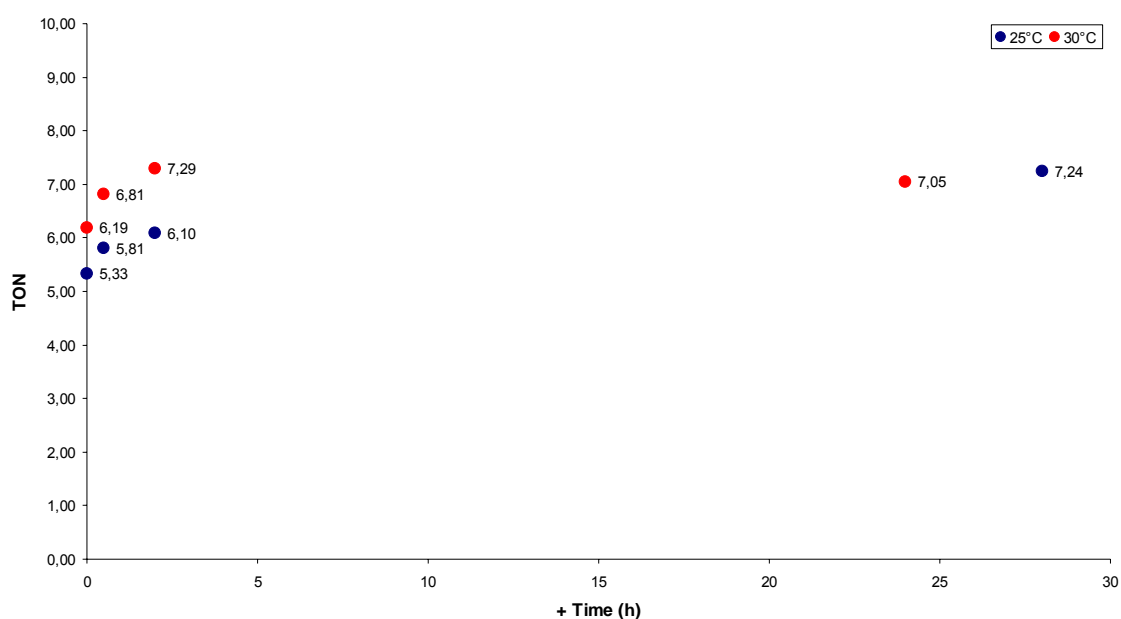
Fig. 6.10: Evolution of epoxide yield with time and temperature using 10 eq. of H_2O_2

To study the effect of reaction time, the normal experimental procedure was followed, but after the addition of the oxidant (H_2O_2), the reaction mixture was stirred for an additional amount of time before being quenched. In order to gain a better understanding of the process, the experiment was done at two different temperatures. Some interesting results were obtained (Fig. 6.10).

An increase in temperature should accelerate the reaction being studied and, as shown in Fig. 6.10, the tendency at higher temperature is exactly the same, but displaced to higher TONs. Interesting to note is the evolution of the TON with time under both temperatures. After a determined amount of time a TON_{max} is reached, which is the same for both temperatures (considering that the data is subject to ±5% error). However, as one would expect, this TON_{max} is reached faster at higher temperature.

Temperature and amount of oxidant are further key factors in this catalytic reaction. As shown in Fig. 6.10, the higher the temperature, the higher the yield (as expected). This is confirmed by the results shown in Fig. 6.11. In the same way, more oxidant should produce more product, and this is also shown to be the case in Fig. 6.11.
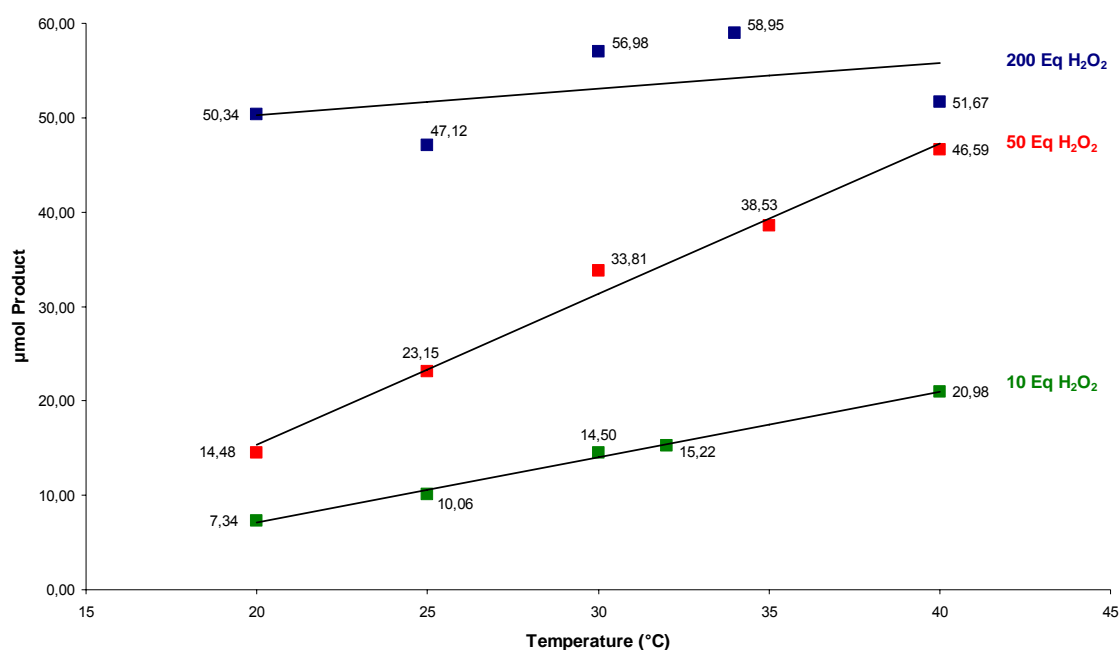
Fig. 6.11: Evolution of epoxide yield with the amount of oxidant (H_2O_2)

If we represent Fig. 6.11 in terms of TON, Fig. 6.12 is obtained, in which the sequence of Fig. 6.11 is very clearly inverted. This implies that, although more product (epoxide) is obtained at higher temperatures and higher concentrations of oxidant, the increase is not as much as expected considering the amount of H_2O_2 used (the relationship between eq H_2O_2 and TON is not linear). As discussed previously, the presence of free oxygen-based radicals

such as $^\bullet OH$ or $^\bullet OOH$ can produce the degradation of the catalytic species and it is likely that this is the case for the 3,7-diazabicyclo[3.3.1]nonane iron(II) complexes. The possibility also exists however, that the additional H_2O_2 simply requires more time to react than the experiments allowed.
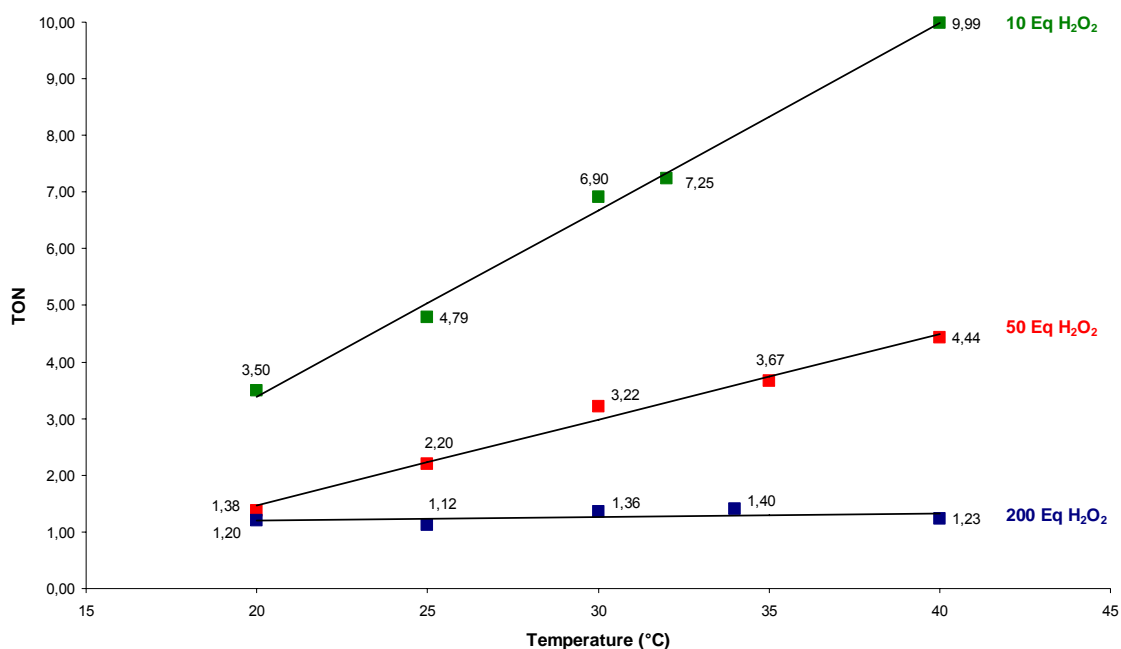
Fig. 6.12: Evolution of epoxide TON with the amount of oxidant (H_2O_2)

Tetradentate Ligands (N2Py2)

In terms of product distribution, the N2Py2 complex demonstrates a similar reactivity and selectivity to the complexes of the known tetradentate ligands presented in Fig. 6.3, with an epoxide:diol ratio of approximately 1:1 (slightly more diol than epoxide is formed). The most interesting result concerning the reactivity of N2Py2 is that the obtained yields under aerobic and anaerobic conditions are practically identical, implying the existence of an iron-based pathway for epoxide formation.

Epoxide formation

The results of the $^{18}O_2$ and $H_2^{18}O_2$ labelling experiments indicate that, under aerobic conditions, around 70% of the epoxide comes from O_2 and 30% from H_2O_2. This suggests that, as for N2Py3o, there are two possible mechanisms for the formation of the epoxide, one which requires oxygen (radical-based) and one which is independent of oxygen (iron-based). The important difference between N2Py2 and the pentadentate ligands is however, that the total yield of epoxide remains the same under aerobic and anaerobic conditions. A possible explanation is that both pathways originate from a common intermediate and are equally favourable, but that the radical-based pathway is faster, so that it forms more of the epoxide under aerobic conditions. In the absence of oxygen, the iron-based reaction simply replaces the radical-based reaction and the total yield remains the same.
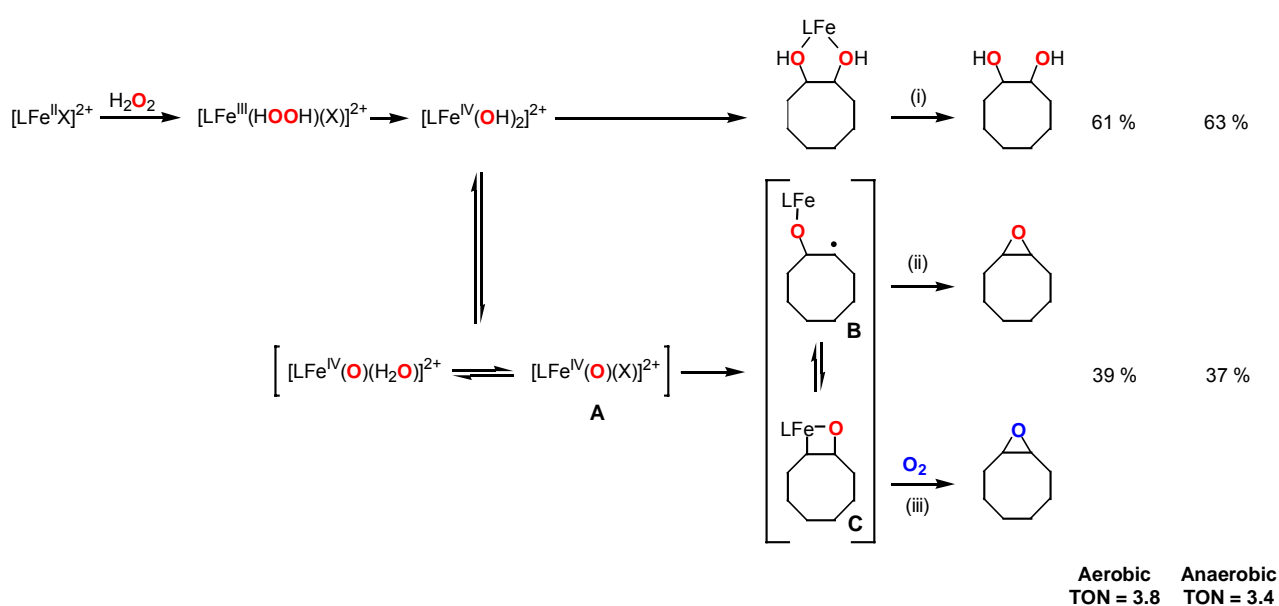
Fig. 6.13: Proposed mechanism for cyclooctene oxidation with the iron(II) complex of N2Py2

A tentative mechanism for the epoxidation and dihydroxylation with the N2Py2 based catalyst is shown in Fig. 6.13. It involves the formation of an active Fe(IV)-oxo species, via Fe(II)(HOOH) and Fe(IV)-dihydroxo intermediates. This species is analogous to intermediate **A** in the N2Py3o mechanism (Fig. 6.9), but is formed without the release of OH radicals. The analogue of intermediate **B** can then be formed in a similar way to that proposed for N2Py3o. Due to the lack of OH radicals, this species cannot form diol, as for N2Py3o, but follows pathways (ii) and (iii) to form epoxide originating from H_2O_2 and O_2 respectively.

In methanol, epoxide formation is strongly inhibited (TON under aerobic or anaerobic conditions approx. 0.5). This could be due to solvent coordination in the addition open site, which would inhibit the formation of the Fe(IV)-dihydroxo intermediate.

The most remarkable result of the labelling experiments is that even under strict anaerobic conditions, some oxygen from an alternative source to H_2O_2 is incorporated into the epoxide. A possible reason can be found in the experimental procedure. Even under anaerobic conditions, after the standard reaction time, the reaction is quenched with 1-methylimidazole, which contains some oxygen. If a stable enough intermediate exists, which can react with oxygen, this reaction can compete with the quenching reaction and form additional epoxide (after the standard reaction time). Intermediate **C**, which can be formed for N2Py2 but not for the pentadentate ligands N2Py3u and N2Py3o, due to the additional coordination site which is required, is one such candidate. This theory is supported by an additional experiment, in which labelled $^{18}O_2$ was added to the reaction mixture after the standard reaction time and together with the 1-methylimidazole[93]. Indeed, incorporation of this $^{18}O_2$ was observed in the epoxide, but not in the diol.

Diol formation

The most interesting result obtained from the ^{18}O-labeling experiments is that the entire label in the diol product comes from $H_2^{18}O_2$. This is contrast to tetradentate analogues like TPA (Fig. 6.3), for example, where a fraction of the diol product does not originate from the labelled $H_2^{18}O_2$, but from water. In this case the active catalyst was proposed to be a low-spin iron(III)-hydroperoxo complex with a water molecule coordinated in the additional open site, or the product of bond homolysis in this complex, an iron(V)-oxo-hydroxo complex. Density functional calculations[86] suggest an Fe(II)/Fe(IV) pathway for diol formation, where the active species is an Fe(IV)-dihydroxo species (pathway (i) of Fig. 6.13), formed by cleavage of the O-O bond in an Fe(II)(HOOH) precursor (Fig. 6.13). This proposal is supported by the doubly labelled diol in the $H_2^{18}O_2$ labelling experiments and the fact that no Fe(III) intermediates are observed in the reaction of H_2O_2 with the iron(II) complex of N2Py2.

As in the epoxidation, diol formation is completely inhibited in methanol. Again, this can be attributed to solvent coordination in the addition open site, which would inhibit the formation of the active Fe(IV)-dihydroxo species.

In order to obtain additional information and support all the previously mentioned mechanistic proposals, preliminary experiments with the catalysts based on N2Py2 and N2Py3o were also done with cis-heptene[87] (using the standard aerobic conditions described in chapter 6). With N2Py2 a TON of 3.4 and a diol:epoxide ratio of 0.6:1 were observed. The sterioselectivity (cis- vs. trans-heptene derivative, 100((cis-trans)/(cis+trans)) in both products was high (diol:>99%, epoxide>99%). With the pentadentate ligand N2Py3o the TON was 1.9 with selectively epoxide produced, but with a cis/trans selectivity of only 20%. This is a further support for the suggestion that ligand radical autoxidation pathways are of importance for N2Py3o, as dicussed previously in this chapter, while for N2Py2 mechanistic pathways explicitly involving the high-valent iron centre predominate.

7. Experimental part

Chemicals

All chemicals and dry solvents were directly obtained from Aldrich, Fluka and Merck and used without further purification.

IR

Infrared spectra were measured with a Perkin Elmer 16 PC FTIR instrument, using KBr pellets.

NMR

NMR spectra were measured with a Bruker AS200 instrument. The sweep frequency used for ^{1}H-NMR measurements was 200 MHz, and for ^{13}C-NMR it was 50.32 MHz. The program MestReC v.4.5.6.0 was used for the processing of the data.

UV-Vis

The UV-Vis spectra were obtained using a Varian Cary 1E spectrophotometer and a JASCO V-570 and quartz cuvettes of 1 cm path length. The speed of sweep was in all measurements between 30 and 50 nm/s.

EPR

EPR measurements were performed with a Bruker ELEXSYS E500 instrument in a mixture of DMF and water (3:2). The frozen solutions were measured at 125 K. The spin Hamiltonian parameters were all extracted directly from the original spectra.

Mass Spectrometry

Mass spectra were obtained from the Inorganic Chemistry Institute of the University of Heidelberg, using a Finnigan 8400 mass spectrometer with the FAB (fast atom bombardment) technique.

GC

GC measurements were performed with a Varian 3900 instrument with autosampler. The column used was a Phenomenex Zebron ZB-1701 (30 m. long with an internal diameter of 0.25 mm.). The temperature program used for cyclooctene was the following: 40°C for 5 minutes, increase to 200°C (Rate 12 °C/min), maintain for 5 minutes, increase to 240°C (Rate 35 °C/min) and maintain for 5 minutes.

GC-MS

GC-MS measurements were performed with a Fisons 8060 instrument coupled to a Fisons MD 800 mass detector. The column and temperature program for cyclooctene were the same as in the GC measurements.

Elemental analyses

Elemental analyses were obtained from the microanalysis laboratory of the Chemical Institute of the University of Heidelberg.

Cyclovoltammetry:

Cyclovoltammetric measurements were performed using a BAS 100B analyser using a three electrode cell composed of a glassy carbon working electrode, a Pt wire auxiliary electrode and a $Ag/AgNO_3$ reference electrode (0.01 M Ag^+ concentration). As electrolyte a 0.1 M acetonitrile solution of tetrabutylammonium tetrafluoroborate ($TBABF_4$) was used. The scan rate was 100 mV/s and the temperature 25°C.

Crystal structures

Crystal structures shown were determined in the Inorganic Chemistry Department of the University of Heidelberg by Dr. H. Pritzkow and Prof. Dr. H. Wadepohl, using a Siemens AED2 Diffractometer (with Mo-K_α radiation).

Compounds synthesized following methods described in the literature

Ligands
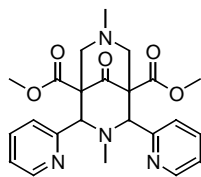
N2Py2[94]
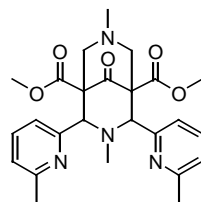
N26MePy2[94]
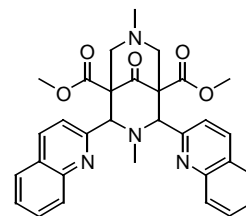
N2Q2[10]
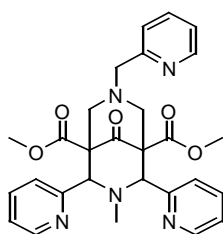
N2Py3o[94]
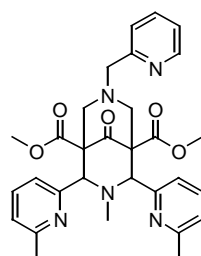
N2Pic6MePy[10]
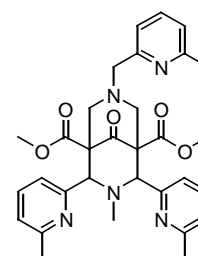
Tri6MePy[10]
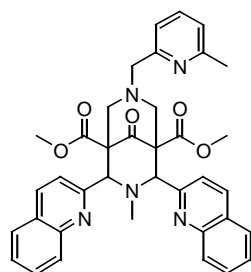
N26MePicQ2[10]
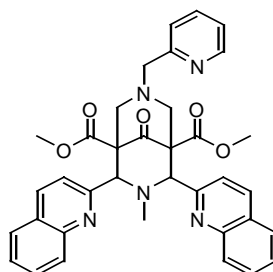
N2Q2Pyo[10]
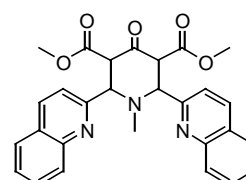
NQ2[10]
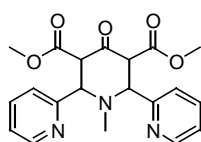
NPy2[94]

Other substances/precursors

N-tosyliminobenzyliodinane[95]

5-Methoxy-2-pyridinecarbaldehyde[35]

Iodosylbenzene[89]

7.1. Aldehyde and amine synthesis

General procedure for direct Br-Li exchange[36]

To a solution of 1 eq. of the correspondent bromo substituted pyridine in toluene at -78 °C was slowly added 1.2 eq. BuLi (2.5 M in hexanes). The reaction mixture is aged for 2 hours and after that time, 1.3 eq. of DMF is added. The solution is then stirred for a further 1 hour at the same temperature and subsequently warmed up to -10 °C. At this temperature the mixture is quenched with a saturated NH_4Cl aqueous solution and finally warmed to r.t. Separation of the organic phase, after evaporation of the solvent and column chromatography afforded the desired product.

7-chloro-2-quinolinecarbaldehyde

Following a literature known procedure[34], 4.95 g (27.9 mmol) 2-methyl-7-chloroquinoline, 3.10 g (27.9 mmol) SeO_2, 3.0 ml (0.17 mol) H_2O in 125 ml dioxane yield 4.8 g (90 %) product.

^{1}H-NMR (CDCl$_3$): 7.65 (dd, 1H, $^3J_{HH}$ = 8.7 Hz, $^4J_{HH}$ = 2.0 Hz, Ar-*H*), 7.86 (d, 1H, $^3J_{HH}$ = 8.7 Hz, Ar-*H*), 8.03 (d, 1H, $^3J_{HH}$ = 8.4 Hz, Ar-*H*), 8.20-8.35 (m, 2H, Ar-*H*), 10.22 (s, 1H, -C*H*O).

5-bromo-2-pyridinecarbaldehyde

Following the general procedure for direct Br-Li exchange, 5.0 g (21.1 mmol) 2,5-dibromopyridine, 10.0 ml (25.3 mmol) of a 2.5 M solution of BuLi in hexanes, 2.15 ml (27.6 mmol) DMF in 250 ml toluene yield after silica gel column chromatography 1.35 g (35 %) product.

R_f (hexane:ethylacetate 9:1 = 0.2). *^{1}H-NMR (CDCl$_3$)*: 7.85 (d, 1H, $^3J_{HH}$ = 8.3 Hz, Ar-*H*), 8.03 (d, 1H, $^3J_{HH}$ = 8.3 Hz, Ar-*H*), 8.86 (Bs, 1H, Ar-*H*), 10.04 (s, 1H, -C*H*O).

5-methyl-2-pyridinecarbaldehyde

Following the general procedure for direct Br-Li exchange, 5.0 g (29.1 mmol) 2-bromo-5-methylpyridine, 14.0 ml (34.9 mmol) of a 2.5 M solution of BuLi in hexanes, 2.90 ml (37.8 mmol) DMF in 350 ml toluene yield after silica gel column chromatography 1.55 g (45 %) product.

R_f (hexane:ethylacetate 7:3 = 0.2). *^{1}H-NMR (CDCl$_3$)*: 2.44 (s, 3H, C*H*$_3$-Ar), 7.67 (dd, 1H, $^3J_{HH}$ = 7.9 Hz, $^4J_{HH}$ = 0.7 Hz, Ar-*H*), 7.88 (d, 1H, $^3J_{HH}$ = 7.9 Hz, Ar-*H*), 8.61 (d, 1H, $^4J_{HH}$ = 0.7 Hz, Ar-*H*), 10.05 (s, 1H, -C*H*O).

4-methyl-2-pyridinecarbaldehyde

Following the general procedure for direct Br-Li exchange, 10.5 g (61.1 mmol) 2-bromo-4-methylpyridine, 28.0 ml (69.8 mmol) of a 2.5 M solution of BuLi in hexanes, 5.80 ml (75.6 mmol) DMF in 700 ml toluene yield after silica gel column chromatography 2.70 g (39 %) product.

R_f (hexane:ethylacetate 7:3 = 0.2). *^{1}H-NMR (CDCl$_3$)*: 2.37 (s, 3H, C**H**$_3$-Ar), 7.27 (Bd, 1H, ^{3}J$_{HH}$ = 5.0 Hz, Ar-**H**), 7.71 (Bs, 1H, Ar-**H**), 8.57 (d, 1H, ^{3}J$_{HH}$ = 5.0 Hz, Ar-**H**), 9.99 (s, 1H, -C**H**O).

2-(aminomethyl)-quinoline

Following a literature known procedure[33], 5.0 g (31.8 mmol) 2-quinolinecarbaldehyde in 15 ml ethanol, 2.2 g (31.8 mmol) hydroxylamine hydrochloride, 5.1 g (36.9 mmol) potassium carbonate in 30 ml water yield 5.1 g (95 %) 2-formaldoximoquinoline.

2.0 g (11.6 mmol) of this oxime were treated, following a literature known procedure[33], with 4.25 g (65.0 mmol) zinc dust in 25 ml trifluoroacetic acid to yield 1.05 g (57 %) 2-(aminomethyl)-quinoline.

^{1}H-NMR (CDCl$_3$): 2.60 (Bs, 2H, -N**H**$_2$), 4.16 (s, 2H, -C**H**$_2$-NH$_2$), 7.30-8.15 (m, 6H, Ar-**H**).

7.2. Ligand synthesis

General piperidone synthesis

To a solution of 2 eq of the correspondent aldehyde and 1 eq. dimethyl 1,3-acetonedicarboxylate in methanol under ice cooling, 1.2 eq. of a 41 % aqueous methylamine solution is slowly added. The red-orange to red-brown solution mixtures produce, when left stirring at r.t., a white to yellowish precipitate, which is filtered, washed with methanol and dried under vacuum.

N5MOX2

Following the general piperidone synthesis, 0.8 g (5.83 mmol) of 5-methoxy-2-pyridinecarbaldehyde, 0.30 ml (3.50 mmol) 41 % aqueous methylamine solution and 0.42 ml (2.92 mmol) dimethyl 1,3-acetonedicarboxylate in 3 ml methanol yield 350 mg (27 %) product.

Elemental analysis: Calculated: C: 59.59 H: 5.68 N: 9.48

Observed: C: 59.43 H: 5.90 N: 8.92

Mass (FAB nibeol), m/z: 444.0 [M+H]

^{1}*H-NMR (CDCl$_3$) (keto-form)*: 1.80 (s, 3H, CH_3-N), 3.70 (s, 6H, Ar-OCH_3), 3.92 (s, 6H, -OCH_3), 4.48 (d, 2H, $^3J_{HH}$ = 11.3 Hz, CH), 4.64 (d, 2H, $^3J_{HH}$ = 11.3 Hz, CH), 7.27 (dd, 2H, $^3J_{HH}$ = 8.5 Hz, $^4J_{HH}$ = 2.7 Hz, Ar-H), 7.49 (d, 2H, $^3J_{HH}$ = 8.5 Hz, Ar-H), 8.31 (d, 2H, $^4J_{HH}$ = 2.7 Hz, Ar-H).

^{13}*C-NMR (CDCl$_3$) (keto-form)*: 25.5 (1C, CH$_3$-N), 52.0 (2C, OCH_3), 55.5 (2C, Ar-OCH_3), 57.7 (2C, CH-N), 67.9, 69.3 (2C, CH-CO), 121.3, 124.7, 136.2, 149.4, 155.0 (10C, C_{Ar}), 168.5 (2C, COOCH$_3$), 200.7 (1C, C=O).

N5MePy2

Following the general piperidone synthesis, 1.55 g (12.8 mmol) of 5-methyl-2-pyridinecarbaldehyde, 0.65 ml (7.68 mmol) 41 % aqueous methylamine solution and 0.92 ml (6.40 mmol) dimethyl 1,3-acetonedicarboxylate in 5 ml methanol yield 910 mg (34 %) product.

Elemental analysis: Calculated: C: 64.22 H: 6.12 N: 10.21

Observed: C: 64.31 H: 6.10 N: 10.27

Mass (FAB nibeol), m/z: 412.2 [M]

^{1}*H-NMR (CDCl$_3$) (keto-form)*: 1.73 (s, 3H, C**H**$_3$-N), 2.30 (s, 6H, C**H**$_3$-Ar), 3.63 (s, 6H, Ar-OC**H**$_3$), 4.41 (d, 2H, ^{3}J$_{HH}$ = 11.2 Hz, C**H**), 4.59 (d, 2H, ^{3}J$_{HH}$ = 11.2 Hz, C**H**), 7.30-7.55 (m, 4H, Ar-**H**), 8.32-8.40 (m, 2H, Ar-**H**).

^{13}*C-NMR (CDCl$_3$) (keto-form)*: 18.2 (2C, Ar-**C**H$_3$), 33.7 (1C, **C**H$_3$-N), 52.0 (2C, O**C**H$_3$), 57.6 (2C, **C**H-N), 69.8 (2C, **C**H-CO), 123.9, 132.6, 137.3, 149.4, 154.5 (10C, **C**$_{Ar}$), 168.6 (2C, **C**OOCH$_3$), 200.7 (1C, **C**=O).

N5BrPy2

Following the general piperidone synthesis, 1.2 g (6.45 mmol) of 5-bromo-2-pyridinecarbaldehyde, 0.33 ml (3.87 mmol) 41 % aqueous methylamine solution and 0.47 ml (3.23 mmol) dimethyl 1,3-acetonedicarboxylate in 8 ml methanol yield 1.15 g (66 %) product.

Elemental analysis: Calculated: C: 44.39   H: 3.54   N: 7.76
                                          Observed: C: 44.11   H: 3.52   N: 7.66

Mass (FAB nibeol), m/z: 541.8 [M]

^{1}*H-NMR (CDCl$_3$) (enol-form)*: 2.26 (s, 3H, C**H**$_3$-N), 3.63 (s, 3H, -OC**H**$_3$), 3.73 (s, 3H, -OC**H**$_3$), 4.10-4.30 (m, 1H, C**H**), 4.30-4.50 (m, 1H, C**H**), 4.79 (s, 1H, C**H**-N), 7.10-7.20 (m, 2H, Ar-**H**), 7.60-7.80 (m, 2H, Ar-**H**), 8.50-8.70 (m, 2H, Ar-**H**), 12.46 (s, 1H, -O**H**).

^{13}*C-NMR (CDCl$_3$) (enol-form)*: 31.6 (1C, **C**H$_3$-N), 37.7 (1C, **C**H-N), 52.2, 52.7 (2C, O**C**H$_3$), 60.2 (C, **C**H-N), 97.7 (1C, -**C**=COH), 124.1, 124.8, 125.7, 138.9, 139.1, 139.5, 149.7, 150.1, 150,3 (10C, **C**$_{Ar}$), 155.8 (1C, -C=**C**OH), 167.2, 168.4 (2C, **C**OOCH$_3$).

N6BrPy2

Following the general piperidone synthesis, 10.0 g (53.8 mmol) of 6-bromo-2-pyridinecarbaldehyde, 2.73 ml (32.3 mmol) 41 % aqueous methylamine solution and 3.88 ml (26.9 mmol) dimethyl 1,3-acetonedicarboxylate in 25 ml methanol yield 11.2 g (82 %) product.

Elemental analysis: Calculated: C: 44.39   H: 3.54   N: 7.76
                                          Observed: C: 44.39   H: 3.53   N: 7.77

Mass (FAB nibeol), m/z: 541.8 [M]

^{1}*H-NMR (CDCl$_3$) (enol-form)*: 2.26 (s, 3H, C***H***$_3$-N), 3.63 (s, 3H, -OC***H***$_3$), 3.83 (s, 3H, -OC***H***$_3$), 4.04 (d, 1H, ^{3}J$_{HH}$ = 9.6 Hz, C***H***), 4.50 (d, 1H, ^{3}J$_{HH}$ = 9.6 Hz, C***H***), 4.80 (s, 1H, C***H***-N), 7.26-7.62 (m, 6H, Ar-***H***), 12.46 (s, 1H, -O***H***).

^{13}*C-NMR (CDCl$_3$) (enol-form)*: 31.6 (1C, ***C***H$_3$-N), 37.7 (1C, ***C***H-N), 52.2, 52.7 (2C, OCH$_3$), 60.2 (C, ***C***H-N), 97.7 (1C, -***C***=COH), 121.8, 123.0, 127.4, 138.6, 138.8, 139.1, 140.7, 140.8, 141.6, (10C, ***C***$_{Ar}$), 158.4 (1C, -C=***C***OH), 168.8 (2C, ***C***OOCH$_3$).

NCQ2 · 0.5 CH$_3$OH

Following the general piperidone synthesis, 5.40 g (28.2 mmol) of 7-chloro-2-quinolinecarbaldehyde, 1.43 ml (16.9 mmol) 41 % aqueous methylamine solution and 2.04 ml (14.1 mmol) dimethyl 1,3-acetonedicarboxylate in 20 ml methanol yield 5.1 g (65 %) product.

Elemental analysis: Calculated: C: 60.22   H: 4.43   N: 7.39

                           Observed: C: 60.23   H: 4.16   N: 7.49

Mass (FAB nibeol), m/z: 551.8 [M]

^{1}*H-NMR (CDCl$_3$) (keto-form)*: 1.78 (s, 3H, C***H***$_3$-N), 3.61 (s, 6H, Ar-OC***H***$_3$), 4.56 (d, 2H, ^{3}J$_{HH}$ = 11.2 Hz, C***H***), 5.21 (d, 2H, ^{3}J$_{HH}$ = 11.2 Hz, C***H***), 7.27-8.25 (m, 10H, Ar-***H***).

^{13}*C-NMR (CDCl$_3$) (keto-form)*: 30.7 (1C, ***C***H$_3$-N), 51.8 (2C, OCH$_3$), 61.1 (2C, ***C***H-N), 69.3 (2C, ***C***H-CO), 125.7, 125.9, 127.5, 128.3, 128.6, 135.1, 136.1, 147.2, 158.4 (18C, ***C***$_{Ar}$), 169.2 (2C, ***C***OOCH$_3$), 201.6 (1C, ***C***=O).

General bispidone synthesis

To a suspension of 1 eq. piperidone in methanol or ethanol is added, at r.t., 2.4 eq of a 37 % aqueous formaldehyde solution. Subsequently 1.2 eq. of the desired amine is added, and the resulting mixture is refluxed for 60 to 90 minutes. If the mixture produces when left standing at r.t. a white to yellowish precipitate, this is filtered, washed with methanol and dried under vacuum. If this is not the case, the resulting mixture is left open to dry. To the resulting resin, methanol, ethanol or even diethylether is added to favour the precipitation of the compound (sometimes an ultrasonic-bath is required). The resulting precipitate is then filtered and dried under vacuum.

N25MOX2 · 0.5 CH$_3$OH

Following the general bispidone synthesis, 0.75 g (1.7 mmol) N5MOX2, 0.31 ml (4.1 mmol) 37 % aqueous formaldehyde solution and 0.17 ml (2.0 mmol) 41 % aqueous methylamine solution in 6 ml methanol yield 320 mg (38 %) product.

Elemental analysis:	Calculated:	C: 59.52	H: 6.27	N: 10.89
	Observed:	C: 59.35	H: 6.02	N: 11.14

Mass (FAB nibeol), m/z: 499.0 [M]

^{1}*H-NMR (CDCl$_3$)*: 1.97 (s, 3H, CH_3-N), 2.26 (s, 3H, CH_3-N), 2.53 (d, 2H, $^2J_{HH}$ = 12.5 Hz, H6/H8 equatorial, CH_2), 3.04 (d, 2H, $^2J_{HH}$ = 12.5 Hz, H6/H8 axial, CH_2), 3.80 (s, 6H, Ar-OCH_3), 3.86 (s, 6H, -OCH_3), 4.64 (s, 2H, H2/H4, CH), 7.28 (dd, 2H, $^3J_{HH}$ = 8.7 Hz, $^4J_{HH}$ = 2.9 Hz, Ar-H), 7.93 (d, 2H, $^3J_{HH}$ = 8.7 Hz, Ar-H), 8.18 (d, 2H, $^4J_{HH}$ = 2.9 Hz, Ar-H).

^{13}*C-NMR (CDCl$_3$)*: 42.9, 44.5 (2C, CH$_3$-N), 52.4 (2C, OCH$_3$), 55.6 (2C, Ar-OCH$_3$), 60.7, 62.4 (2C, C-CO), 73.3 (2C, CH-N), 121.4, 123.9, 136.0, 150.8, 155.0 (10C, C_{Ar}), 168.7 (2C, COOCH$_3$), 203.8 (1C, C=O).

N25MePy2

Following the general bispidone synthesis, 0.8 g (1.9 mmol) N5MePy2, 0.37 ml (4.6 mmol) 37 % aqueous formaldehyde solution and 0.18 ml (2.3 mmol) 41 % aqueous methylamine solution in 5 ml methanol yield 430 mg (49 %) product.

Elemental analysis:	Calculated:	C: 64.36	H: 6.48	N: 12.01
	Observed:	C: 63.95	H: 6.39	N: 11.95

Mass (FAB nibeol), m/z: 467.0 [M+H]

^{1}*H-NMR (CDCl$_3$)*: 1.99 (s, 3H, C**H**$_3$-N), 2.24 (s, 3H, C**H**$_3$-N), 2.31 (s, 6H, C**H**$_3$-Ar), 2.49 (d, 2H, ^{2}J$_{HH}$ = 12.0 Hz, H6/H8 equatorial, C**H**$_2$), 3.00 (d, 2H, ^{2}J$_{HH}$ = 12.0 Hz, H6/H8 axial, C**H**$_2$), 3.81 (s, 6H, -OC**H**$_3$), 4.65 (s, 2H, H2/H4, C**H**), 7.56 (dd, 2H, ^{3}J$_{HH}$ = 8.0 Hz, ^{4}J$_{HH}$ = 2.0 Hz, Ar-**H**), 7.93 (d, 2H, ^{3}J$_{HH}$ = 8.0 Hz, Ar-**H**), 8.30-8.34 (m, 2H, Ar-**H**).

^{13}*C-NMR (CDCl$_3$)*: 18.2 (2C, Ar-**C**H$_3$), 43.0, 44.5 (2C, **C**H$_3$-N), 52.4 (2C, O**C**H$_3$), 60.7 (2C, **C**H$_2$-N), 62.2, (2C, **C**-CO), 73.6 (2C, **C**H-N), 123.0, 132.4, 137.0, 149.5, 155.9 (10C, **C**$_{Ar}$), 168.7 (2C, **C**OOCH$_3$), 203.8 (1C, **C**=O).

N26BrPy2

Following the general bispidone synthesis, 3.5 g (6.5 mmol) N6BrPy2, 1.16 ml (15.6 mmol) 37 % aqueous formaldehyde solution and 0.66 ml (7.8 mmol) 41 % aqueous methylamine solution in 30 ml methanol yield 1.93 g (50 %) product.

Elemental analysis:	Calculated:	C: 46.33	H: 4.06	N: 9.40
	Observed:	C: 46.35	H: 4.07	N: 9.46

Mass (FAB nibeol), m/z: 596.8 [M]

^{1}*H-NMR (CDCl$_3$)*: 2.10 (s, 3H, C**H**$_3$-N), 2.18 (s, 3H, C**H**$_3$-N), 2.46 (d, 2H, ^{2}J$_{HH}$ = 12.0 Hz, H6/H8 equatorial, C**H**$_2$), 2.77 (d, 2H, ^{2}J$_{HH}$ = 12.0 Hz, H6/H8 axial, C**H**$_2$), 3.89 (s, 6H, -OC**H**$_3$), 4.74 (s, 2H, H2/H4, C**H**), 7.41 (dd, 2H, ^{3}J$_{HH}$ = 7.7 Hz, ^{4}J$_{HH}$ = 0.8 Hz, Ar-**H**), 7.66 (t, 2H, ^{3}J$_{HH}$ = 7.7 Hz, Ar-**H**), 8.01 (dd, 2H, ^{3}J$_{HH}$ = 7.7 Hz, ^{4}J$_{HH}$ = 0.8 Hz, Ar-**H**)

^{13}*C-NMR (CDCl$_3$)*: 43.6, 44.4 (2C, **C**H$_3$-N), 52.6 (2C, O**C**H$_3$), 60.7 (2C, **C**H$_2$-N), 61.8 (2C, **C**-CO), 73.0 (2C, **C**H-N), 121.9, 127.3, 138.7, 141.4, 160.3 (10C, **C**$_{Ar}$), 168.1 (2C, **C**OOCH$_3$), 202.7 (1C, **C**=O).

N25BrPy2 · H$_2$O

Following the general bispidone synthesis, 1.06 g (1.96 mmol) N5BrPy2, 0.35 ml (4.7 mmol) 37 % aqueous formaldehyde solution and 0.2 ml (2.4 mmol) 41 % aqueous methylamine solution in 4 ml methanol yield 860 mg (74 %) product.

Elemental analysis:	Calculated:	C: 44.97	H: 4.27	N: 9.12
	Observed:	C: 45.37	H: 4.24	N: 9.15

Mass (FAB nibeol), m/z: 596.6 [M+H]

^{1}H-NMR (CDCl$_3$): 2.00 (s, 3H, C**H**$_3$-N), 2.23 (s, 3H, C**H**$_3$-N), 2.50 (d, 2H, ^{2}J$_{HH}$ = 12.8 Hz, H6/H8 equatorial, C**H**$_2$), 2.90 (d, 2H, ^{2}J$_{HH}$ = 12.8 Hz, H6/H8 axial, C**H**$_2$), 3.80 (s, 6H, -OC**H**$_3$), 4.70 (s, 2H, H2/H4, C**H**), 7.92 (d, 2H, ^{4}J$_{HH}$ = 0.9 Hz, Ar-**H**), 7.94 (d, 2H, ^{3}J$_{HH}$ = 2.1 Hz, Ar-**H**), 8.56 (dd, 2H, ^{3}J$_{HH}$ = 2.1 Hz, ^{4}J$_{HH}$ = 0.9 Hz, Ar-**H**).

^{13}C-NMR (CDCl$_3$): 43.2, 44.5 (2C, **C**H$_3$-N), 52.6 (2C, O**C**H$_3$), 60.6 (2C, **C**H$_2$-N), 61.8 (2C, **C**-CO), 73.1 (2C, **C**H-N), 120.1, 124.7, 139.2, 150.3, 157.4 (10C, **C**$_{Ar}$), 168.2 (2C, **C**OOCH$_3$), 202.8 (1C, **C**=O).

N2CQ2 · 0.5 H$_2$O

Following the general bispidone synthesis, 2.0 g (3.6 mmol) NCQ2, 0.64 ml (8.6 mmol) 37 % aqueous formaldehyde solution and 0.37 ml (4.3 mmol) 41 % aqueous methylamine solution in 15 ml ethanol yield 1.70 g (78 %) product.

Elemental analysis:	Calculated:	C: 60.40	H: 4.74	N: 9.09
	Observed:	C: 60.58	H: 4.53	N: 8.94

Mass (FAB nibeol), m/z:	606.9 [M]

^{1}H-NMR (CDCl$_3$): 2.11 (s, 3H, C**H**$_3$-N), 2.28 (s, 3H, C**H**$_3$-N), 2.50 (d, 2H, ^{2}J$_{HH}$ = 12.2 Hz, H6/H8 equatorial, C**H**$_2$), 2.92 (d, 2H, ^{2}J$_{HH}$ = 12.2 Hz, H6/H8 axial, C**H**$_2$), 3.92 (s, 6H, -OC**H**$_3$), 4.96 (s, 2H, H2/H4, C**H**), 7.51 (dd, 2H, ^{3}J$_{HH}$ = 8.6 Hz, ^{4}J$_{HH}$ = 2.1 Hz, Ar-**H**), 7.79 (d, 2H, ^{3}J$_{HH}$ = 8.6 Hz, Ar-**H**), 7.96 (d, 2H, ^{4}J$_{HH}$ = 2.1 Hz, Ar-**H**), 8.26 (d, 2H, ^{3}J$_{HH}$ = 8.6 Hz, Ar-**H**), 8.35 (d, 2H, ^{3}J$_{HH}$ = 8.6 Hz, Ar-**H**).

^{13}C-NMR (CDCl$_3$): 43.6, 44.4 (2C, **C**H$_3$-N), 52.6 (2C, O**C**H$_3$), 61.0 (2C, **C**H$_2$-N), 62.3 (2C, **C**-CO), 74.0 (2C, **C**H-N), 120.9, 126.1, 127.8, 128.3, 128.7, 135.5, 136.3, 147.9, 160.8 (18C, **C**$_{Ar}$), 168.3 (2C, **C**OOCH$_3$), 203.0 (1C, **C**=O).

N2Py2Qo · H$_2$O

Following the general bispidone synthesis, 1.5 g (3.9 mmol) NPy2, 0.7 ml (9.4 mmol) 37 % aqueous formaldehyde solution and 0.74 g (4.7 mmol) 2-(aminomethyl)quinoline in 15 ml methanol yield 0.60 g (28 %) product.

Elemental analysis:	Calculated:	C: 65.85	H: 5.70	N: 12.00
	Observed:	C: 66.06	H: 5.64	N: 11.72

Mass (FAB nibeol), m/z:	566.0 [M]

^{1}*H-NMR (CDCl$_3$)*: 1.95 (s, 3H, C**H**$_3$-N), 2.81 (d, 2H, ^{2}J$_{HH}$ = 12.2 Hz, H6/H8 equatorial, C**H**$_2$), 3.25 (d, 2H, ^{2}J$_{HH}$ = 12.2 Hz, H6/H8 axial, C**H**$_2$), 3.47 (s, 2H, N-C**H**$_2$-Ar), 3.80 (s, 6H, -OC**H**$_3$), 4.66 (s, 2H, H2/H4, C**H**), 6.90-7.20 (m, 4H, Ar-**H**), 7.50-7.85 (m, 3H, Ar-**H**), 7.90 (Bd, 3H, ^{3}J$_{HH}$ = 7.6 Hz, Ar-**H**), 8.10-8.25 (m, 2H, Ar-**H**), 8.40 (dd, 2H, ^{3}J$_{HH}$ = 4.9 Hz, ^{4}J$_{HH}$ = 1.0 Hz, Ar-**H**).

^{13}*C-NMR (CDCl$_3$)*: 43.1 (1C, **C**H$_3$-N), 52.5 (2C, O**C**H$_3$), 62.4 (2C, **C**-CO), 64.0 (1C, N-**C**H$_2$-Ar), 73.7 (2C, **C**H-N), 122.4, 122.8, 123.8, 126.6, 127.3, 127.5, 129.5, 129.7, 136.0, 136.3, 147.9, 149.0, 157.6, 158.3 (14C, **C**$_{Ar}$), 168.5 (2C, **C**OOCH$_3$).

N2Q3o · 0.5 H$_2$O

Following the general bispidone synthesis, 1.36 g (2.8 mmol) NQ2, 0.50 ml (6.7 mmol) 37 % aqueous formaldehyde solution and 0.53 g (3.4 mmol) 2-(aminomethyl)quinoline in 15 ml methanol yield 520 mg (28 %) product.

Elemental analysis:	Calculated:	C: 71.20	H: 5.38	N: 10.38
	Observed:	C: 70.95	H: 5.25	N: 10.33

Mass (FAB nibeol), m/z: 666.1 [M]

^{1}*H-NMR (CDCl$_3$)*: 2.05 (s, 3H, C**H**$_3$-N), 2.80 (d, 2H, ^{2}J$_{HH}$ = 12.0 Hz, H6/H8 equatorial, C**H**$_2$), 3.22 (d, 2H, ^{2}J$_{HH}$ = 12.0 Hz, H6/H8 axial, C**H**$_2$), 3.76 (s, 2H, N-C**H**$_2$-Ar), 3.90 (s, 6H, -OC**H**$_3$), 4.93 (s, 2H, H2/H4, C**H**), 7.40-8.40 (m, 18H, Ar-**H**).

^{13}*C-NMR (CDCl$_3$)*: 43.4 (1C, **C**H$_3$-N), 52.4 (2C, O**C**H$_3$), 62.6 (2C, **C**-CO), 63.9 (1C, N-**C**H$_2$-Ar), 74.1 (2C, **C**H-N), 121.0, 122.6, 126.5, 126.7, 127.3, 127.4, 127.5, 129.2, 129.4, 129.8, 136.0, 136.4, 147.4, 148.2, 157.3, 159.2 (27C, **C**$_{Ar}$), 168.4 (2C, **C**OOCH$_3$), 203.3 (1C, **C**=O).

N2Py3Lo · 0.5 H$_2$O

Following the general bispidone synthesis, 2.0 g (5.2 mmol) NPy2, 0.93 ml (12.5 mmol) 37 % aqueous formaldehyde solution and 0.75 ml (6.3 mmol) 2-(aminoethyl)pyridine in 20 ml methanol yield 1,26 g (46 %) product.

Elemental analysis:	Calculated:	C: 64.67	H: 5.99	N: 13.00
	Observed:	C: 64.46	H: 5.86	N: 12.85

Mass (FAB nibeol), m/z: 530.1 [M+H]

^{1}*H-NMR (CDCl$_3$)*: 2.02 (s, 3H, C**H**$_3$-N), 2.65 (d, 2H, ^{2}J$_{HH}$ = 12.5 Hz, H6/H8 equatorial, C**H**$_2$), 2.72-2.86 (m, 2H, C**H**$_2$-N), 2.86-3.02 (m, 2H, C**H**$_2$-N), 3.13 (d, 2H, ^{2}J$_{HH}$ = 12.5 Hz, H6/H8

axial, CH_2), 3.83 (s, 6H, -OCH_3), 4.74 (s, 2H, H2/H4, CH), 7.10-7.25 (m, 4H, Ar-H), 7.62 (dt, 1H, $^3J_{HH}$ = 7.6 Hz, $^4J_{HH}$ = 1.9 Hz, Ar-H), 7.76 (2H, $^3J_{HH}$ = 7.6 Hz, $^4J_{HH}$ = 1.9 Hz, Ar-H), 7.80 (Bd, 2H, $^3J_{HH}$ = 7.8 Hz, Ar-H), 8.50 (dd, 2H, $^3J_{HH}$ = 4.8 Hz, $^4J_{HH}$ = 0.9 Hz, Ar-H), 8.55 (dd, 1H, $^3J_{HH}$ = 4.7 Hz, $^4J_{HH}$ = 1.0 Hz, Ar-H).

^{13}C-NMR (CDCl$_3$): 43.3 (1C, CH$_3$-N), 52.5 (2C, OCH_3), 57.2, 58.6 (2C, N-CH$_2$-CH$_2$-Ar), 62.2 (2C, C-CO), , 73.7 (2C, CH-N), 121.4, 123.0, 123.2, 123.6, 136.5, 149.2, 149.3, 158.7, 159.7 (15C, C_{Ar}), 168.6 (2C, COOCH$_3$).

N26BrPy3o

Following the general bispidone synthesis, 3.5 g (6.5 mmol) N6BrPy2, 1.16 ml (15.5 mmol) 37 % aqueous formaldehyde solution and 0.80 ml (7.8 mmol) 2-(aminomethyl)pyridine in 20 ml methanol yield 1.6 g (35 %) product.

Elemental analysis:	Calculated:	C: 49.94	H: 4.04	N: 10.40
	Observed:	C: 49.63	H: 4.08	N: 10.28

Mass (FAB nibeol), m/z: 673.9 [M]

^1H-NMR (CDCl$_3$): 2.03 (s, 3H, CH_3-N), 2.64 (d, 2H, $^2J_{HH}$ = 12.5 Hz, H6/H8 equatorial, CH_2), 2.95 (d, 2H, $^2J_{HH}$ = 12.5 Hz, H6/H8 axial, CH_2), 3.50 (s, 2H, N-CH_2-Ar), 3.87 (s, 6H, -OCH_3), 4.68 (s, 2H, H2/H4, CH), 7.15-7.45 (m, 6H, Ar-H), 7.60-7.75 (m, 1H, Ar-H), 7.93 (dd, 2H, $^3J_{HH}$ = 7.2 Hz, $^4J_{HH}$ = 1.3 Hz, Ar-H), 8.71 (Bd, 2H, $^3J_{HH}$ = 4.8 Hz, Ar-H).

^{13}C-NMR (CDCl$_3$): 43.5 (1C, CH$_3$-N), 52.6 (2C, OCH_3), 62.0 (2C, C-CO), 63.3 (1C, N-CH$_2$-Ar), 73.0 (2C, CH-N), 122.4, 122.5, 124.6, 127.1, 136.4, 138.6, 141.2, 149.7, 156.6, 159.7 (15C, C_{Ar}), 168.1 (2C, COOCH$_3$), 202.6 (1C, C=O).

7.3. Synthesis of metal bispidone complexes

General procedure

To a suspension of 1 eq. of the ligand in acetonitrile at r.t. 1 eq. of the desired metal salt is added. If the metal salt is not well soluble in acetonitrile, the addition is performed as a solid. After 2-3 hours stirring at r.t., a clear solution is usually obtained, although in some cases the product precipitates. If this is not the case, the volume of the obtained solution is reduced by approximately half and ethylacetate or diethylether added to precipitate the metal complex. Once a precipitate is obtained, this is filtered and dried under vacuum.

[Cu(N26BrPy2)](BF$_4$)$_2$ · 3 H$_2$O · CH$_3$CN   (928,52 g/mol)

Following the general procedure for metal complexes, 200 mg (0.34 mmol) N26BrPy2 and 116 mg (0.34 mmol) Cu(BF$_4$)$_2$ · 6 H$_2$O yield g (%) product.

Elemental analysis:	Calculated:	C: 32.34	H: 3.58	N: 7.54
	Observed:	C: 32.15	H: 3.50	N: 7.18

Mass (FAB nibeol), m/z: 676.6 [LCu · H$_2$O]

CV $E_{1/2}$ (CH$_3$CN) = +56 mV ΔE = 171 mV i_c^P / i_a^P = 1,07

UV (CH$_3$CN) λ = 660 nm (ε = 52 l · cm^{-1} · mol^{-1}), λ = 1091 nm (ε = 30 l · cm^{-1} · mol^{-1})

EPR (DMF:H$_2$O - 3:2) $g_{||}$ = 2.305 ($A_{||}$ = 156 G), $g_\perp$ = 2.065 ($A_\perp$ = 10 G)

[Cu(N2Q3o)](BF$_4$)$_2$ · 5 H$_2$O (992.97 g/mol)

Following the general procedure for metal complexes, 106 mg (0.16 mmol) N2Q3o and 55 mg (0.16 mmol) Cu(BF$_4$)$_2$ · 6 H$_2$O yield 140 mg (88 %) product.

Elemental analysis:	Calculated:	C: 48.38	H: 4.57	N: 7.05
	Observed:	C: 47.96	H: 4.10	N: 6.86

Mass (FAB nibeol), m/z: 764.9 [LCu · 2H$_2$O], 745.9 [LCu · H$_2$O]

CV $E_{1/2}$ (CH$_3$CN) = -35 mV ΔE = 69 mV i_c^P / i_a^P = 1,04

UV (CH$_3$CN) λ = 632 nm (ε = 125 l · cm^{-1} · mol^{-1}), λ = 710 nm (ε = 133 l · cm^{-1} · mol^{-1}), λ = 1091 nm (ε = 94 l · cm^{-1} · mol^{-1})

EPR (DMF:H$_2$O - 3:2)   g$_{||}$ = 2.288 (A$_{||}$ = 150 G), g$_\perp$ = 2.060 (A$_\perp$ = 6 G)

[Cu(N2Py2Qo)](BF$_4$)$_2$ · 4 H$_2$O   (874.84 g/mol)

Following the general procedure for metal complexes, 164 mg (0.29 mmol) N2Py2Qo and 100 mg (0.29 mmol) Cu(BF$_4$)$_2$ · 6 H$_2$O yield 225 mg (89 %) product.

Elemental analysis: Calculated: C: 43.93   H: 4.49   N: 8.01
                            Observed: C: 43.83   H: 4.32   N: 8.00

Mass (FAB nibeol), m/z: 664.8 [LCu · 2H$_2$O], 645.8 [LCu · H$_2$O]

CV   E$_{1/2}$ (CH$_3$CN) = -552 mV ΔE = 70 mV   i$_c^P$ / i$_a^P$ = 1,15

UV (CH$_3$CN) λ = 630 nm (ε = 132 l · cm^{-1} · mol^{-1}), λ = 881 nm (ε = 60 l · cm^{-1} · mol^{-1})

EPR (DMF:H$_2$O - 3:2)   g$_{||}$ = 2.198 (A$_{||}$ = 173 G), g$_\perp$ = 2.042 (A$_\perp$ = 25 G)

[Cu(N25BrPy2)](BF$_4$)$_2$ · 3 H$_2$O · CH$_3$CN   (928.52 g/mol)

Following the general procedure for metal complexes, 200 mg (0.34 mmol) N25BrPy2 and 116 mg (0.34 mmol) Cu(BF$_4$)$_2$ · 6 H$_2$O yield 270 mg (85 %) product.

Elemental analysis: Calculated: C: 32.34   H: 3.58   N: 7.54
                            Observed: C: 32.13   H: 3.47   N: 7.34

Mass (FAB nibeol), m/z: 711.6 [LCu · 3H$_2$O], 675.1 [LCu · H$_2$O]

CV   E$_{1/2}$ (CH$_3$CN) = -272 mV ΔE = 77 mV   i$_c^P$ / i$_a^P$ = 1,42

UV (CH$_3$CN) λ = 633 nm (ε = 129 l · cm^{-1} · mol^{-1}), λ = 970 nm (ε = 30 l · cm^{-1} · mol^{-1})

EPR (DMF:H$_2$O - 3:2)   g$_{||}$ = 2.268 (A$_{||}$ = 171 G), g$_\perp$ = 2.060 (A$_\perp$ = 10 G)

[Cu(N25MOXPy2)](BF₄)₂ · 3 H₂O · CH₃CN   (830.78 g/mol)

Following the general procedure for metal complexes, 117 mg (0.23 mmol) N25MOXPy2 and
81 mg (0.23 mmol) Cu(BF₄)₂ · 6 H₂O yield 144 mg (73 %) product.

Elemental analysis:	Calculated:	C: 39.03	H: 4.73	N: 8.43
	Observed:	C: 39.39	H: 4.66	N: 8.12

Mass (FAB nibeol), m/z: 597.9 [LCu · 2H₂O], 579.1 [LCu · H₂O]

CV $E_{1/2}$ (CH₃CN) = -387 mV ΔE = 94 mV i_c^p / i_a^p = 3.03

UV (CH₃CN) λ = 627 nm (ε = 127 l · cm⁻¹ · mol⁻¹), λ = 929 nm (ε = 27 l · cm⁻¹ · mol⁻¹)

EPR (DMF:H₂O - 3:2) $g_{||}$ = 2.260 ($A_{||}$ = 173 G), $g_{\perp}$ = 2.056 ($A_{\perp}$ = 9 G)

[Cu(N25MePy2)](BF₄)₂ · 3 H₂O · CH₃CN   (798.78 g/mol)

Following the general procedure for metal complexes, 115 mg (0.25 mmol) N25MePy2 and
85 mg (0.25 mmol) Cu(BF₄)₂ · 6 H₂O yield 175 mg (88 %) product.

Elemental analysis:	Calculated:	C: 40.60	H: 4.92	N: 8.77
	Observed:	C: 41.04	H: 4.83	N: 8.78

Mass (FAB nibeol), m/z: 566.1 [LCu · 2H₂O], 547.0 [LCu · H₂O]

CV $E_{1/2}$ (CH₃CN) = -410 mV ΔE = 110 mV i_c^p / i_a^p = 2.55

UV (CH₃CN) λ = 624 nm (ε = 122 l · cm⁻¹ · mol⁻¹), λ = 920 nm (ε = 25 l · cm⁻¹ · mol⁻¹)

EPR (DMF:H₂O - 3:2) $g_{||}$ = 2.260 ($A_{||}$ = 171 G), $g_{\perp}$ = 2.054 ($A_{\perp}$ = 10 G)

[Cu(N2CQ2)](BF₄)₂ · 3 H₂O   (898.68 g/mol)

Following the general procedure for metal complexes, 200 mg (0.33 mmol) N2CQ2 and 114
mg (0.33 mmol) Cu(BF₄)₂ · 6 H₂O yield 240 mg (81 %) product.

Elemental analysis:	Calculated:	C: 41.43	H: 3.81	N: 6.23
	Observed:	C: 41.85	H: 3.89	N: 6.34

Mass (FAB nibeol), m/z: 707.8 [LCu · 2H$_2$O], 688.8 [LCu · H$_2$O]

CV $E_{1/2}$ (CH$_3$CN) = +17 mV ΔE = 85 mV i_c^P / i_a^P = 1,30

UV (CH$_3$CN) λ = 735 nm (ε = 99 l · cm^{-1} · mol^{-1}), λ = 1030 nm (ε = 57 l · cm^{-1} · mol^{-1})

[Cu(N26BrPy3o)](BF$_4$)$_2$ · 3 H$_2$O   (964.55 g/mol)

Following the general procedure for metal complexes, 157 mg (0.23 mmol) N26BrPy3o and 80 mg (0.23 mmol) Cu(BF$_4$)$_2$ · 6 H$_2$O yield 198 mg (89 %) product.

Elemental analysis:	Calculated:	C: 34.87	H: 3.45	N: 7.26
	Observed:	C: 34.85	H: 3.66	N: 7.26

Mass (FAB nibeol), m/z: 772.8 [LCu · 2H$_2$O], 753.8 [LCu · H$_2$O]

CV $E_{1/2}$ (CH$_3$CN) = -389 mV ΔE = 75 mV i_c^P / i_a^P = 1,16

UV (CH$_3$CN) λ = 642 nm (ε = 73 l · cm^{-1} · mol^{-1}), λ = 957 nm (ε = 16 l · cm^{-1} · mol^{-1})

EPR (DMF:H$_2$O - 3:2) $g_{||}$ = 2.258 ($A_{||}$ = 168 G), $g_{\perp}$ = 2.055 ($A_{\perp}$ = 10 G)

[Cu(N2Py3Lo)](BF$_4$)$_2$ · H$_2$O   (784.76 g/mol)

Following the general procedure for metal complexes, 209 mg (0.39 mmol) N2Py3Lo and 136 mg (0.39 mmol) Cu(BF$_4$)$_2$ · 6 H$_2$O yield g (%) product.

Elemental analysis:	Calculated:	C: 44.38	H: 4.24	N: 8.92
	Observed:	C: 44.55	H: 4.28	N: 9.16

Mass (FAB nibeol), m/z: 610.0 [LCu · H$_2$O]

CV   Multiple redox processes difficult to interpret

UV (CH$_3$CN) λ = 602 nm (ε = 123 l $\cdot$ cm^{-1} $\cdot$ mol^{-1}), λ = 890 nm (ε = 34 l $\cdot$ cm^{-1} $\cdot$

mol^{-1})

EPR (DMF:H$_2$O - 3:2) $g_{||}$ = 2.211 (A$_{||}$ = 176 G), $g_{\perp}$ = 2.060 (A$_{\perp}$ = 37 G)

7.4. General procedure for the catalytic experiments

Aziridination of styrene[96]

Under an argon atmosphere, to a solution of 1 eq. of the metal complex (0.02 mmol) in absolute acetonitrile (2 mL), 2 eq. PhINTs (0.40 mmol), styrene (1 mL) is added. The mixture is then allowed to warm to 25 °C in a water bath. To this mixture styrene is added. After 7 hours, the mixture is passed through a short neutral aluminium oxide column and washed with ethylacetate. After evaporation of the solvents, the resulting oil is recrystallized from hexane and diethylether. The crystallized product is the pure aziridination product.

Oxidation of cyclooctene

0.3 mL of a 70 mM H_2O_2 solution in MeCN (or MeOH) is delivered by syringe pump over 30 min at 25 °C under argon (or in air) to a vigorously stirred MeCN (or MeOH) solution (2.7 mL) containing the iron catalyst and the cyclooctene (previously distilled); the resulting concentrations are 0.7 mM iron catalyst, 7.0 mM H_2O_2 and 0.70 M olefin. The solution is stirred for 5 min after the addition of H_2O_2 is completed. 1-methylimidazole (0.1 mL, to quench the reaction) and acetic anhydride (1 mL, to form the corresponding ester from the diol) are added, followed by the addition of ice. After extraction with $CHCl_3$, the organic extract is washed successively with 1 M H_2SO_4 (1.0 mL), saturated aqueous $NaHCO_3$ and water. Naphtalene is added to the organic extract as internal standard for the GC analysis.

For the GC analysis, a previous calibration for cyclooctene was performed. For this, ten different samples containing cyclooctene, 1,2-cis-cyclooctenediacetate and cyclooctenone in various concentrations within the range of the reactivity of the catalytic system were used.

In experiments with $H_2^{18}O$, $H_2^{18}O$ (42 μL, 0.70 M) is added to the catalyst solution prior to the injection of H_2O_2 (experiments with the same amount of natural abundance H_2O were also made and shown not to have any influence on the product distribution). In experiments with $H_2^{18}O_2$, 70.0 mM $H_2^{18}O_2$ (diluted with MeCN (or MeOH) from a 2 % $H_2^{18}O_2$ / H_2O solution, $H_2^{18}O_2/H_2^{16}O_2$ = 9:1) is used. Experiments with $^{18}O_2$ were performed with $^{18}O_2$-saturated solutions. $Fe^{IV}=O$ solutions in MeCN were prepared with excess solid PhIO to afford, after filtration of the unreacted PhIO, the desired solutions; the concentration of $Fe^{IV}=O$ was determined spectrophotometrically. All experiments were run at least in duplicate and subjected to GC analysis (GC/MS for the labelling experiments). For comparison with published data, all yields are reported as TON = 10 μmol product)/μmol {Fe}; for most experiments (10 equivalents of H_2O_2) the maximum TON (without autoxidation) is therefore 10.0. The GC was calibrated with the pure epoxide and cis-diol derivative products. No other

major products were detected, except for the trans-diol in one set of experiments, which had the same mass and fragmentation pattern as the cis-diol, but a slightly different retention time. Due to relatively small yields the error limit for all data is approx. ±5% (absolute) for TON and ±5% (relative) for labelling percentages.

8. Literature

[1]   P. Comba, *Coord. Chem. Rev.*, **1999**, 182, 343

[2]   P. Comba, L. Fabbrizi, *Chemistry at the Beginning of the Third Millenium*, **2000**, Sprinter, Heidelberg, 94

[3]   P. Comba, B. Nuber, A. Ramlow, *J. Chem. Soc. Dalton Trans.*, **1997**, 347

[4]   S. Kuwata, Doktorarbeit, Ruprecht-Karls Universität Heidelberg, **2005**

[5]   C. Bleiholder, H. Börzel, P. Comba, R. Ferrari, A. Heydt, M. Kerscher, S. Kuwata, G. Laurenczy, G. A. Lawrance, A. Lienke, B. Martin, M. Merz, B. Nuber, H. Pritzkow, *Inorg. Chem.*, **2005**, 44, 8145

[6]   P. Comba, M. Kerscher, M. Merz, V. Müller, H. Pritzkow, R. Remenyi, W. Schiek, Y. Xiong, *Chem. Eur. J.*, **2002**, 8, 5750.

[7]   P. Comba, M. Merz, H. Pritzkow, *Eur. J. Inorg. Chem.*, **2003**, 1711

[8]   P. Comba, A. Hauser, M. Kerscher, H. Pritzkow, *Angew. Chem.*, **2003**, 115, 4675

[9]   H. Börzel, P. Comba, K. S. Hagen, Y. D. Lampeka, A. Lienke, M. Merz, H. Pritzkow, L. V. Tsymbal, *Inorg. Chim. Acta*, **2002**, 337, 407

[10]   P. Comba, C. López de Laorden, H. Pritzkow, *Helv. Chim. Acta*, **2005**, 88, 647

[11]   M. R. Bukowski, P. Comba, A. Lienke, C. Limberg, C. López de Laorden, R. Mas-Ballesté, M. Merz, L. Que, Jr., *Angew. Chem. Int. Ed.*, **2005**, submitted

[12]   C. Limberg, *Angew. Chem.*, **2003**, 115, 6112

[13]   E. J. Corey, M. C. Noe, S. Sarshar, *J. Am. Chem. Soc.*, **1993**, 115, 3828

[14]   K. Chen, L. Que, Jr., Angew. Chem. Int. Ed., **1999**, 38, 15, 2227

[15]   M. Costas, A. K. Tipton, K. Chen, D. H. Jo, L. Que, Jr., *J. Am. Chem. Soc.*, **2001**, 123, 27

[16]   K. Chen, M. Costas, J. Kim, A. K. Tipton, L. Que, Jr., *J. Am. Chem. Soc.*, **2002**, 124, 12

[17]   K. Chen, M. Costas, L. Que, Jr., *J. Chem. Soc., Dalton Trans.*, **2002**, 672

[18]   J. Y. Ryu, J. Kim, M. Costas, K. Chen, W. Nam, L. Que. Jr., *Chem. Comm.*, **2002**, 12, 1288

[19]   E. I. Solomon, T. C. Brunold, M. I. Davis, J. N. Kemsley, S.K. Lee, N. Lehnert, F. Neese, A. J. Skulan, Y. S. Yang, J. Zhou, *Chem. Rev.*, **2000**, 100, 235

[20]   A. L. Feig, S. J. Lippard, *Chem. Rev.*, **1994**, 94, 759

[21]   L. Que, Jr., R. Y. N. Ho, *Chem. Rev.*, **1996**, 96, 2607

[22]   B. Meunier, S. De Visser, S. Shaik, *Chem. Rev.*, **2004**, 104, 9, 3947

[23]   F. Neese, J. M. Zaleski, K. L. Zaleski, E. I. Solomon, *J. Am. Chem. Soc.*, **2000**, 122, 11703

[24]   T. E. Westre, K. E. Loeb, J. M. Zaleski, B. Hedman, K. O. Hodgson, E. I. Solomon, *J. Am. Chem. Soc.*, **1995**, 117, 1309

[25]   D. A. Evans, M. M. Faul, M. T. Bilodeau, *J. Am. Chem. Soc.* **1994**, 116, 2742

[26]   H. Kwart, A. A. Kahn, *J. Am. Chem. Soc.,* **1967**, 89, 1951

[27]   Z. Li, R. W. Quan, E. N. Jacobsen, *J. Am. Chem. Soc.*, **1995**, 117, 5889

[28]   P. Brandt, M. J. Södergren, P. G. Andersson, P.-O. Norrby, *J. Am. Chem. Soc.*, **2000**, 122, 8013

[29]   C. Mannich, P. Mohs, *Chem. Ber.*, **1930**, 63, 608

[30]   K. W. Merz, R. Haller, *Pharmaceutica Acta Helvetiae*, **1963**, 442

[31]   R. Haller, *Arzneimittelforschung*, **1965**, 11/15, 1327

[32]   T. Siener, U. Holzgrabe, S. Drosihn, W. Brandt, *J. Chem. Soc. Perkin Trans. 2*, **1999**, 1827

[33]   H. A. Goodwin, F. Lions, *J. Am. Chem. Soc.*, **1959**, 81, 6420

[34]   W. M. Tadros, H. A. Shoeb, M. A. Kira, F. Yousif, E. M. Ekladios, S. A. Ibrahim, *Indian J. Chem.*, **1975**, 13, 1366

[35]   M. Adamczyk, R. E. Reddy, *Tetrahedron: Asymmetry*, **2001**, 12, 1047

[36]   X. Wang, P. Rabbat, P. O´Shea, R. Tillyer, E. J. J. Grabowski, P. J. Reider, *Tetrahedron Letters*, **2000**, 41, 4335

[37]   G. P. Gardini, *Tethraedron Letters*, **1972**, 40, 4113

[38]   V. Snieckus, *Chem. Rev.*, **1990**, 90, 879

[39]   W. W. Parham, R. M. Piccirilli, *J. Org. Chem.*, **1977**, 42, 257

[40]   C. S. Giam, J. L. Stout, *J. Chem. Soc., Chem. Commun.*, **1969**, 142

[41]   P. Gros, Y. Fort, *Eur. J. Org. Chem.*, **2002**, 3375

[42]   M. Schlosser, *J. Organomet. Chem.*, **1967**, 8, 9

[43]   L. Lochmann, *Eur. J. Inorg. Chem.*, **2000**, 6, 1115

[44]   D. Cuperly, P. Gros, Y. Fort, *J. Org. Chem.*, **2002**, *67*, 238

[45]   A. B. P. Lever, E. I. Solomon, *Inorganic Electronic Structure and Spectroscopy*, **1999**, John Wiley & Sons, Oxford

[46]   B. L. Vallee, R. J. P. Williams, *Biochemistry*, **1968**, 59, 498

[47]   N. Kitajima, Y. Moro-oka, *Chem. Rev.*, **1994**, 94, 737

[48]   H. Börzel, P. Comba, C. Katsichtis, W. Kiefer, A. Lienke, V. Nagel, H. Pritzkow, *Chem. Eur. J.*, **1999**, 5, 1716

[49]   H. Börzel, P. Comba, K. S. Hagen, M. Kerscher, H. Pritzkow, M. Schatz, S. Schindler, O. Walter, *Inorg. Chem.*, **2002**, 41, 5440

[50]   P. Comba, W. Schiek, Coord. *Chem. Rev.*, **2003**, 238-239, 21

[51]   H. A. Jahn, E. Teller, *Proc. Roy. Soc. Lond. (A)*, **1937**, 161, 220

[52]   I. B. Bersuker, *Chem. Rev.*, **2001**, 1018, 1067

[53] M. Charton, *J. Am. Chem. Soc.*, **1964**, 86, 10, 2033

[54] E. Sigfridsson, U. Ryde, *J. Comp. Chem.*, **1998**, 19, 377

[55] W. L. Jorgensen, *Acc. Chem. Res.*, **1989**, 22, 184

[56] R. S. Mulliken, *J. Chem. Phys.*, **1962**, 36, 3428

[57] P.-O. Löwdin, *Adv. Quantum Chem.*, **1970**, 5, 185

[58] A. E. Reed, R. B. Weinstock, F. A. Weinhold, *J. Chem. Phys.*, **1985**, 83, 735

[59] L. E. Chirlain, M. M. Francl, *J. Comput. Chem.*, **1987**, 6, 894

[60] C. M. Breneman, K. B. Wiberg, *J. Comp. Chem.*, **1990**, 11, 361

[61] U. C. Sing, P. A. Kollman, *J. Comp. Chem.*, **1984**, 5, 129

[62] J. G. Lee, R. A. Friesner, *J. Phys. Chem.*, **1993**, 97, 3515

[63] M. J. Frisch, G. W. Trucks, H. B. Schlegel, G. E. Scuseria, M. A. Robb, J. R. Cheeseman, J. A. Montgomery, Jr., T. Vreven, K. N. Kudin, J. C. Burant, J. M. Millam, S. S. Iyengar, J. Tomasi, V. Barone, B. Mennucci, M. Cossi, G. Scalmani, N. Rega, G. A. Petersson, H. Nakatsuji, M. Hada, M. Ehara, K. Toyota, R. Fukuda, J. Hasegawa, M. Ishida, T. Nakajima, Y. Honda, O. Kitao, H. Nakai, M. Klene, X. Li, J. E. Knox, H. P. Hratchian, J. B. Cross, C. Adamo, J. Jaramillo, R. Gomperts, R. E. Stratmann, O. Yazyev, A. J. Austin, R. Cammi, C. Pomelli, J. W. Ochterski, P. Y. Ayala, K. Morokuma, G. A. Voth, P. Salvador, J. J. Dannenberg, V. G. Zakrzewski, S. Dapprich, A. D. Daniels, M. C. Strain, O. Farkas, D. K. Malick, A. D. Rabuck, K. Raghavachari, J. B. Foresman, J. V. Ortiz, Q. Cui, A. G. Baboul, S. Clifford, J. Cioslowski, B. B. Stefanov, G. Liu, A. Liashenko, P. Piskorz, I. Komaromi, R. L. Martin, D. J. Fox, T. Keith, M. A. Al-Laham, C. Y. Peng, A. Nanayakkara, M. Challacombe, P. M. W. Gill, B. Johnson, W. Chen, M. W. Wong, C. Gonzalez, and J. A. Pople, **2003**, Gaussian 03, Revision B.03, Gaussian, Inc., Pittsburgh PA

[64] A.D.J. Becke, *J. Chem. Phys. B*, **1993**, 98, 5648

[65] Lee, W. Yang, R.G. Parr, *Phys. Rev. B*, **1988**, 37, 785

[66] P. Comba, B. Martin, A. Prikhod´ko, H. Pritzkow, H. Rohwer, *Comptes Rendus Chimie*, **2005**, 88, 647

[67] V. Rassolov, J.A. Pople, M. Ratner, T.L. Windus, *J. Chem. Phys.*, **1998**, 109, 1223

[68] A. Schäfer, C. Huber and R. Ahlrichs, *J. Chem. Phys.*, **1994**, 100(8), 5829

[69] N. Godbout, D. R. Salahub, J. Andzelm, E. Wimmer, *Can. J. Chem.*, **1992**, 70, 560

[70] J. B. Levy, *Structural Chemistry*, **1999**, 10, 2, 121

[71] S. J. Lippard, J. M. Berg, *Bioanorganische Chemie*, **1995**, Spektrum Akademischer Verlag GmbH, Heidelberg

[72] J. J. R. Fraústo da Silva, R. J. P. Williams, *The Biological Chemistry of the Elements*, **1991**, Clarendon Press, Oxford

[73] M. Schröder, *Chem. Rev.*, **1980**, 80, 187

[74]   W. Amberg, Y. L. Bennani, R. K. Chadha, G. A. Crispino, W. D. Davis, J. Hartung, K. S. Jeong, J. Y. Ogino, T. Shibata, K. B. Sharpless, *J. Org. Chem.*, **1993**, 58, 844

[75]   K. A Jørgensen, *Chem. Rev.*, **1989**, 89, 3

[76]   B. S. Lane, K. Burgess, *Chem. Rev.*, **2003**, 103, 7

[77]   P. D. Oldenburg, A. A. Shteinman, L. Que, Jr., *J. Am. Chem. Soc.*, **2005**, 127, 45, 15672

[78]   G. Roelfes, V. Vrajmasu, K. Chen, R. Y. N. Ho, J.-U. Rohde, C. Zondervan, R. M. la Crois, E. P. Schudde, M. Lutz, A. L. Spek, R. Hage, B. Feringa, E. Münck, L. Que, Jr., *Inorg. Chem.*, **2003**, 42, 2639

[79]   A. Bassan, M. R. A. Blomberg, P. E. M. Siegbahn, L. Que, Jr., 2005, 117, 2999

[80]   H. J. H. Fenton, *J. Chem. Soc.*, **1894**, 65, 899

[81]   C. Walling, *Acc. Chem. Res.*, **1975**, 8, 125

[82]   M. R. Bukowski, P. Comba, C. Limberg, M. Merz, L. Que, Jr., T. Wistuba, *Angew. Chem. Int. Ed.*, **2004**, 43, 1283

[83]   J. Bautz, M. Bukowski, A. Stubna, A. Lienke, P. Comba, E. Münck, L. Que Jr., *Angew. Chem.*, in preparation

[84]   M. Bukowski, unpublished results

[85]   J. Bautz, P. Comba, L. Que Jr., *Inorg. Chem.*, in preparation

[86]   H. Rohwer, unpublished results

[87]   M. Merz, Doktorarbeit, Ruprecht-Karls Universität Heidelberg, **2002**

[88]   D. E. van Sickle, F. R. Mayo, R. M. Arluck, *J. Am. Chem. Soc.*, **1965**; 87, 4824.

[89]   H. Saltzman, J. G. Sharekin, *Org. Synth.*, **1963**, 43, 60

[90]   T. A. van den Berg, J. W. de Boer, W. R. Browne, G. Roelfes, B. L. Feringa, *J.Chem. Soc., Chem. Comm.*, **2004**, 2550

[91]   P. Neta, R. H. Schuler, *J. Phys. Chem.*, **1975**, 79,1

[92]   G. V. Buxton, C. L. Greenstock, W. P. Helman, A. B. Ross, *J. Phys. Chem.*, **1988**, 513

[93]   J. Bautz, unpublished results

[94]   A. Samhammer, U. Holzgrabe, R. Haller, *Arch. Pharm.*, **1989**, 322, 551

[95]   Y. Yamada, T. Yamamoto, M. Okawara, *Chemistry Letters*, **1975**, 361

[96]   J. A. Halfen, J. M. Uhan, D. C. Fox, M. P. Mehn, L. J. Que, *Inorg. Chem.*, **2000**, 39, 4913

[97]   A. Robert, F. Benoit-Vical, O. Dechy-Cabaret, B. Meunier, *Pure Appl. Chem.*, **2001**, 73, 7, 1173

[98]   D. J. Sullivan, Jr., I. Y. Gluzman, D. G. Russell, D. E. Goldberg, *Proc. Natl. Acad. Sci.*, **1996**, 93, 11865

[99]   S. Girault, P. Grellier, A. Berecibar, L. Maes, P. Lemière, E. Mouray, E. Davidoud Charvet, C. Sergheraert, *J. Med. Chem.*, **2001**, 44, 1658

[100]   S. R. Meshnick, T. E. Taylor, S. Kamchonwongpaisan, *Microbiol. Rev.*, **1996**, 60, 301

[101]   A. Robert, O. Dechy-Cabaret, J. Cazelles, B. Meunier, *Acc. Chem. Res.*, **2002**, 35, 167

[102]   G. H. Posner, J. N. Cumming, P. Ploypradith, C. H. Oh, *J. Am. Chem. Soc.*, **1995**, 117, 5885

[103]   A. V. Pandey, H. Bisht, V. K. Babbarwal, J. Srivastava, K. C. Pandey, V. S. Chauhan, *Biochem. J.*, **2001**, 355, 333

Appendix A:

Crystal data and calculated structures

of the copper(II) complexes

Crystal data

	[Cu(**N2Q3o**)(CH$_3$CN)]$^{2+}$	[Cu(**N2CQ2**)(CH$_3$CN)$_2$]$^{2+}$	[Cu(**N25MePy2**)(CH$_3$CN)]$^{2+}$	[Cu(**N25MePy2**)(CH$_3$CN)(BF$_4$)]$^+$
Empirical formula	C$_{42}$H$_{40}$B$_2$CuF$_8$N$_6$O$_6$	C$_{37}$H$_{37}$B$_2$Cl$_2$CuF$_8$N$_7$O$_5$	C$_{27}$H$_{39}$B$_2$CuF$_8$N$_5$O$_8$	C$_{25}$H$_{29}$B$_2$Br$_2$CuF$_8$N$_5$O$_6$
M$_r$	961.96	967.80	798.79	892.51
Temperature (°K)	100(2)	100(2)	100(2)	100(2)
Wavelength (Å)	0.71073	0.71073	0.71073	0.71073
Crystal system	Triclinic	Monoclinic	Triclinic	Monoclinic
Space group	P -1	$P\,2_1/c$	P -1	$C\,2/c$
Unit cell dimensions: a (Å) α(°)	11.0938(8) / 84.469(2)	15.4862(13)	11.7884(6) / 107.6020(10)	21.582(3)
b (Å) β(°)	13.1601(9) / 80.1140(10)	13.0418(11) / 118.594(4)	11.8821(6) / 105.5540(10)	11.8963(11) / 104.604(3)
c (Å) γ(°)	14.6098(11) / 74.1640(10)	22.7423(16)	13.9001(7) / 105.9100(10)	26.109(2)
Volume (Å^3)	2018.8(3)	4033.0(6)	1648.69(14)	6486.8(11)
Z	2	4	2	8
Density (calculated) (Mg·m^{-3})	1.583	1.594	1.609	1.828
Absorption coefficient (mm^{-1})	0.637	0.765	0.764	3.232
F_{000}	986	1972	822	3544
Crystal size (mm^3)	0.30 • 0.10 • 0.10	0.25 · 0.25 · 0.25	0.30 • 0.25 • 0.25	0.20 • 0.15 • 0.10
Θ range for data collection (°)	1.42 to 27.48	1.50 to 32.04	1.66 to 32.01	1.61 to 27.10
Index ranges	-14 <= h <= 14, -16 <= k <= 17, 0 <= l <= 18	-23 <= h <= 22, -19 <= k <= 0, -32 <= l <= 21	-17 <= h <= 16, -17 <= k <= 16, 0 <= l <= 20	-27 <= h <= 26, 0 <= k <= 15, 0 <= l <= 33
Reflections collected	39144	100717	29595	82753
Independent reflections	9251 [R$_{int}$ = 0.0624]	13582 [R$_{int}$ = 0.0620]	11209 [R$_{int}$ = 0.0297]	7162 [R$_{int}$ = 0.0728]
Completeness to Θ = 30.00	99.9 %	100.0 %	100.0 %	100.0 %
Absorption correction	Semi-empirical from equivalents	Semi-empirical from equivalents	Semi-empirical from equivalents	Semi-empirical from equivalents
Max. and min. transmission	0.9391 and 0.8320	0.8318 and 0.8318	0.8320 and 0.8032	0.7234 and 0.5529
Refinement method	Full-matrix least-squares on F^2	Full-matrix least-squares on F^2	Full-matrix least-squares on F^2	Full-matrix least-squares on F^2
Data / restraints / parameters	9251 / 64 / 611	13582 / 1 / 599	11209 / 0 / 470	7162 / 0 / 449
Goodness-of-fit on F^2	0.903	1.083	1.197	1.126
Final R indices [$I > 2\Theta(I)$]	R1 = 0.0483, wR2 = 0.1387	R1 = 0.0434, wR2 = 0.1062	R1 = 0.0352, wR2 = 0.0996	R1 = 0.0717, wR2 = 0.1531
R indices (all data)	R1 = 0.0691, wR2 = 0.1537	R1 = 0.0691, wR2 = 0.1170	R1 = 0.0432, wR2 = 0.1033	R1 = 0.0895, wR2 = 0.1603
Rms residual density, larg.diff.peak;hole	0.089, 2.034 and -0.572 e·Å^{-3}	0.095, 1.164 and -0.569 e·Å^{-3}	0.086, 0.646 and -0.347 e·Å^{-3}	0.163, 1.120 and -1.386 e·Å^{-3}

Calculated structures of the copper(II) complexes of selected tetradentate bispidine ligands using low accuracy basis sets

	N26MePy2 trans	N24MePy2	N26MOXPy2	N26MOXPy2 trans	N25MOXPy2	N24MOXPy2	N26BrPy2	N26BrPy2 trans	N24BrPy2	N25CF3Py2	N25CNPy2	N24CNPy2	N25ClPy2
Bond lengths(Å)													
$Cu-N_3$	2.120	2.030	2.013	2.162	2.020	2.032	2.013	2.189	2.032	2.029	2.026	2.027	2.025
$Cu-N_7$	2.202	2.292	2.324	2.169	2.286	2.297	2.359	2.153	2.287	2.283	2.283	2.276	2.274
$Cu-N_{ar1}$	2.028	2.023	2.080	2.020	2.038	2.017	2.084	1.994	2.027	2.031	2.032	2.037	2.037
$Cu-N_{ar2}$	2.028	2.023	2.080	2.020	2.038	2.017	2.083	1.994	2.027	2.031	2.032	2.037	2.037
$Cu-N_5$	2.035	1.997	1.963	2.014	1.997	2.001	1.959	2.041	1.995	1.993	1.994	1.992	1.992
$N_3…N_7$	3.026	3.007	3.007	3.011	3.004	3.007	3.016	3.033	3.007	3.003	3.005	3.004	3.001
$N_{ar1}…N_{ar2}$	4.027	3.949	4.000	3.997	3.970	3.940	3.972	3.951	3.952	3.964	3.961	3.967	3.970
Angles (°)													
N_3-Cu-N_7	88.87	87.93	87.48	88.08	88.26	87.78	86.88	88.59	88.02	88.08	88.21	88.36	88.35
N_3-Cu-N_{ar1}	83.55	81.28	79.87	82.08	81.29	81.39	79.40	82.52	81.20	81.16	81.21	81.06	81.13
N_3-Cu-N_{ar2}	83.55	81.28	79.87	82.08	81.29	81.39	79.39	82.52	81.20	81.16	81.22	81.06	81.12
N_3-Cu-N_5	116.62	165.78	178.85	117.09	167.12	165.64	175.57	105.88	165.43	163.80	165.75	165.64	164.66
N_7-Cu-N_{ar1}	92.03	98.75	101.68	92.03	99.44	98.58	103.14	91.85	98.95	98.65	99.09	99.37	99.13
N_7-Cu-N_{ar2}	92.03	98.75	101.69	92.03	99.43	98.59	103.31	91.84	98.94	98.64	99.08	99.38	99.13
N_7-Cu-N_5	154.51	106.29	93.67	154.83	104.63	106.58	88.70	165.53	106.55	108.12	106.05	106.00	106.99
$N_{ar1}-Cu-N_{ar2}$	166.38	154.73	148.16	163.50	153.80	155.10	144.87	164.49	154.35	154.74	154.21	153.59	154.04
$N_{ar1}-Cu-N_5$	90.96	96.21	99.88	91.56	96.32	96.12	101.74	90.08	96.18	95.97	96.19	96.26	96.07
Torsion angles (°)													
$N_{ar1}-C-C-N_3$	44.05	32.82	28.29	43.74	32.47	33.05	24.57	44.51	32.78	32.89	32.70	32.60	32.91
$N_{ar2}-C-C-N_3$	-44.05	-32.82	-28.29	-43.74	-32.47	-33.05	-24.49	-44.54	-32.78	-32.90	-32.70	-32.59	-32.91

Calculated structures of the copper(II) complexes of selected tetradentate bispidine ligands using high accuracy basis sets

	N26MePy2 trans	N24MePy2	N26MOXPy2	N26MOXPy2 trans	N25MOXPy2	N24MOXPy2	N26BrPy2	N26BrPy2 trans	N24BrPy2	N25CF3Py2	N25CNPy2	N24CNPy2	N25ClPy2
Bond lengths(Å)													
Cu-N_3	2.159	2.060	2.039	2.207	2.048	2.062	2.023	2.200	2.061	2.056	2.054	2.057	2.053
Cu-N_7	2.226	2.352	2.357	2.192	2.342	2.356	2.345	2.171	2.347	2.336	2.325	2.334	2.329
Cu-N_{ar1}	2.042	2.040	2.120	2.038	2.059	2.033	2.165	2.060	2.044	2.051	2.058	2.055	2.055
Cu-N_{ar2}	2.042	2.040	2.120	2.038	2.059	2.033	2.165	2.060	2.044	2.051	2.058	2.055	2.056
Cu-N_5	2.088	2.029	1.976	2.052	2.059	2.034	1.975	2.051	2.026	2.018	2.019	2.021	2.01993
$N_3…N_7$	3.061	3.037	3.020	3.047	3.030	3.039	3.016	3.053	3.035	3.028	3.026	3.032	3.026
$N_{ar1}…N_{ar2}$	4.056	3.999	4.101	4.033	4.031	3.988	4.135	4.082	4.005	4.017	4.028	4.021	4.025
Angles (°)													
N_3-Cu-N_7	88.54	86.72	86.46	87.71	87.04	86.64	86.98	88.62	86.79	86.92	87.19	87.09	87.10
N_3-Cu-N_{ar1}	83.44	81.37	79.61	81.88	81.28	81.50	78.92	82.43	81.28	81.13	81.05	81.13	81.15
N_3-Cu-N_{ar2}	83.44	81.37	79.61	81.88	81.28	81.50	78.94	82.43	81.28	81.13	81.05	81.13	81.15
N_3-Cu-N_5	110.94	169.97	178.47	110.32	170.65	170.11	178.96	106.83	169.39	167.95	167.93	169.52	168.33
N_7-Cu-N_{ar1}	91.73	96.91	99.58	91.50	97.54	96.80	102.47	91.82	97.07	96.99	97.28	97.44	97.20
N_7-Cu-N_{ar2}	91.73	96.91	99.59	91.50	97.54	96.81	102.42	91.82	97.08	96.99	97.28	97.44	97.20
N_7-Cu-N_5	160.52	103.30	95.07	161.97	102.31	103.25	91.98	164.56	103.82	105.13	104.88	103.40	104.57
N_{ar1}-Cu-N_{ar2}	166.35	157.16	150.64	163.35	156.23	157.49	145.50	164.33	156.82	156.71	156.28	156.16	156.51
N_{ar1}-Cu-N_5	90.57	97.20	100.11	91.09	97.30	97.11	101.28	90.27	97.16	97.10	97.12	97.27	97.12
Torsion angles (°)													
N_{ar1}-C-C-N_3	44.14	33.56	29.97	44.32	33.32	33.90	25.29	45.75	33.45	33.30	33.61	33.40	33.68
N_{ar2}-C-C-N_3	-44.14	-33.56	-29.86	-44.32	-33.32	-33.90	-25.35	-45.75	-33.44	-33.30	-33.61	-33.40	-33.67

Experimental vs. calculated* geometric parameters for the copper(II) complexes of selected tetradentate bispidine ligands

	[Cu(N2Py2)(CH₃CN)(OTf)]⁺			[Cu(N26MePy2)(CH₃CN)]²⁺			[Cu(**N25MePy2**)(CH₃CN)]²⁺			[Cu(**N25BrPy2**)(CH₃CN)(BF₄)]⁺		
	X-Ray	**Low**	**High**	**X-Ray**	**Low**	**High**	**X-Ray**	**Low**	**High**	**X-Ray**	**Low**	**High**
Bond lengths(Å)												
Cu-N₃	2.022	2.026	2.056	1.999	1.998	2.028	2.007	2.026	2.055	2.010	2.027	2.053
Cu-N₇	2.356	2.283	2.343	2.369	2.323	2.366	2.244	2.284	2.343	2.257	2.282	2.340
Cu-N_ar1	1.993	2.032	2.048	2.053	2.101	2.133	1.991	2.033	2.051	2.022	2.033	2.053
Cu-N_ar2	1.998	2.032	2.048	2.072	2.101	2.133	2.007	2.033	2.051	2.020	2.033	2.053
Cu-N₅	1.980	1.995	2.025	1.947	1.977	2.008	1.965	1.995	2.026	1.957	1.993	2.021
Cu-X	2.608 (X = **O**Tf)	-	-	-	-	-	-	-	-	2.726 (X = **F**BF₃)	-	-
N₃…N₇	2.922	3.005	3.034	2.934	3.011	3.031	2.904	3.004	3.032	2.9204	3.002	3.028
N_ar1…N_ar2	3.941	3.961	4.013	4.034	4.025	4.111	3.938	3.964	4.018	3.9695	3.966	4.022
Angles (°)												
N₃-Cu-N₇	83.40	88.20	86.94	83.71	88.01	86.87	86.03	88.13	86.93	86.19	88.13	86.90
N₃-Cu-N_ar1	83.00	81.21	81.31	80.89	80.14	79.87	82.45	81.25	81.33	81.90	81.22	81.25
N₃-Cu-N_ar2	81.44	81.22	81.30	81.61	80.14	79.87	82.25	81.24	81.33	81.31	81.22	81.25
N₃-Cu-N₅	175.41	165.75	169.89	174.39	179.87	179.47	168.40	165.65	169.43	172.30	164.58	168.96
N₇-Cu-N_ar1	91.33	99.08	97.19	98.91	103.01	101.09	94.54	99.01	97.13	92.70	98.87	97.08
N₇-Cu-N_ar2	95.85	99.08	97.20	95.62	103.01	101.07	97.20	99.02	97.13	99.73	98.87	97.08
N₇-Cu-N₅	100.40	106.05	103.17	91.01	92.12	92.60	105.53	106.23	103.64	101.50	107.30	104.14
N_ar1-Cu-N_ar2	161.98	154.22	156.73	155.82	146.55	148.92	159.97	154.33	156.86	158.36	154.51	156.78
N_ar1-Cu-N₅	99.39	96.19	97.21	98.10	99.82	100.24	97.38	96.17	97.12	98.60	96.02	97.13
Torsion angles (°)												
N_ar1-C-C-N₃	34.56	32.70	33.44	26.09	26.32	27.63	33.90	32.77	33.63	34.28	32.90	33.55
N_ar2-C-C-N₃	-30.47	-32.70	-33.44	-29.89	-26.33	-27.63	-33.96	-32.76	-33.62	-35.75	-32.90	-33.55

* All calculations were performed with the B3LYP functional. Low: 6-31G(d)[64] ; High: TZVP[65] for Cu(II), DZVP for bromine and TZV for all other atoms

Appendix B:
Antimalarial activity of
3,7-diazabicyclo[3.3.1]nonane derivatives

Antimalarial activity

Malaria has become one of the major diseases of humankind. Indeed, WHO estimated that, in 1998, there were 273 million cases of malaria and more than 1 million deaths because of it[97]. Furthermore, as international travel becomes more common, malaria is no longer confined to the tropical zones of the world, and imported malaria is becoming an increasingly serious problem. Another problem is the resistance to existing anti-malarial drugs. However, despite the desperate need for new treatments, malaria is not a priority for the pharmaceutical industry, basically due to economic reasons.

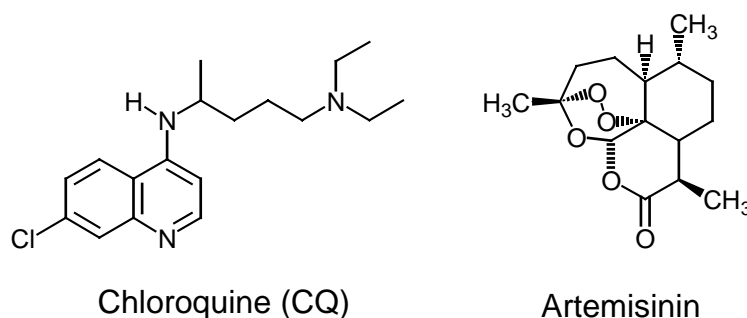

Chloroquine (CQ)   Artemisinin

Fig. 9.1: Most famous drugs against malaria

Antimalaria drugs can be divided into two main groups, the quinoline analogues and the artemisinin derivatives. Chloroquine (see Fig. 9.1) was introduced in the mid-forties; the drug was cheap, non-toxic, and active against all strains of malaria parasites. In 1994, CQ was the third most widely consumed drug in the world after aspirin and paracetamol[97]. The mode of action of the quinoline analogues is still not completely understood, but it is thought to interfere with the function of the food vacuole in the mature stages of the erythrocytic parasite. Within these acidic vacuoles, haemoglobin is the degradation product of proteases as supply of amino acids for the parasite. In this process however, toxic heme moieties are released, which the parasite detoxifies by forming polymers known as hemozoin. The Chloroquine antimalarial activity is believed to result from its interference in this polymerization process[97-99].

Artemisinin (derived from *Artemisia annua*) derivatives are the fastest active antimalarial drugs[100]. Artemisinin (see Fig. 9.1) belongs to the so-called endoperoxide-containing antimalarial agents and this type of compound has been used for almost two decades. The absence of any drug resistance in this rather long period is quite remarkable. However, the half-life of most of the Artemisinin derivatives is quite short (3–5 h). The key factor in the pharmacological activity of these compounds is related to the reactivity of the peroxide function within the parasite[97,101,102]. When purified hemozoin is incubated in the presence of artemisinin under similar pH conditions as in the parasite vacuole (pH = 5), the amount of

hemozoin is reduced, indicating that hemozoin may be distroyed by interaction with the endoperoxide-drug, resulting in an increase of free heme in the vacuole[103].

Because of the relative ease of implementation of bispidone type ligands and the structural similarities with Chloroquine, quinoline-derived and other already available and known bispidones were tested against diverse protozoan parasites, showing a relative low activity in comparison with already established drugs like Chloroquine.

Screen	Control Drug	ED_{50} (µg/ml)
P.falciparum 3D7	Chloroquine	0.0013
T.b.rhodesiense STIB900	Pentamidine	0.002

Compound ID	Parasite	% Inhibition (µg/ml)						ED_{50} µg/ml	Toxicity ED_{50} µg/ml
		30	10	3	1	0.3	0.1		
N2Py2	T.b.rhodesiense STIB900	89.9	12.9	2.4	0			16.68	39.9
	P.falciparum 3D7	-169.4	2.3	-184.4	11.3			>30	
N2Q2	T.b.rhodesiense STIB900	99.5	99.3	64.2	19.7			2.37	15.0
	P.falciparum 3D7	-160.4	2.3	-11.6	-96.7			>30	
N2Py3o	T.b.rhodesiense STIB900	98.9	98.7	29.8	3.0			4.05	11.3
	P.falciparum 3D7	84.4	74.6	42.0	31.7			3.5	
N2Q2Pyo	T.b.rhodesiense STIB900	99.9	99.5	94.0	41.0			1.26	87.7
	P.falciparum 3D7	97.3	90.1	58.5	39.9			1.9	
Tri6MePy	T.b.rhodesiense STIB900	40.4	4.1	1.9	0			>30	>30
	P.falciparum 3D7	41.0	26.7	-8.7	12.3			>30	
N26MePicQ2	T.b.rhodesiense STIB900	99.4	99.1	87.9	18.3			1.78	5.9
	P.falciparum 3D7	103..1	97.7	59.3	10.6			2.8	
N26BrPy3o	T.b.rhodesiense STIB900	39.5	0	0.2	0			>30	<0.3®
	P.falciparum 3D7	16.8	9.0	17.7	22.2			>30	
N2Q2DMEA	T.b.rhodesiense STIB900	97.0	98.3	22.7	0.3			4.3	0.39
	P.falciparum 3D7	74.0	35.6	42.4	-5.6			11.7	

® to be repeated

While the activity is quite low in comparison with Chloroquine, it is nonetheless interesting to compare the change in activity (the concentration causing 50% inhibition ED_{50}) with different backbone modifications. Tetradentate ligands (N2Py2 and N2Q2) are less active than all pentadentate ligands and among these the quinoline analogue N2Q2 is much more active against T.b.rhodesiense STIB900 than the pyridine one. Between N2Py3o and N2Q2Pyo the same trend could be observed, the quinoline containing compound (N2Q2Pyo) is slightly more active than the pyridine analogue (N2Py3o). Remarkable is also the fact that

N26BrPy3o is quite inactive but almost non-toxic (this experiment which needs to be reproduced).

The fact that the quinoline containing derivatives are slightly more active than the pyridine-containing compounds seems to point in the direction of the Chloroquine mechanism of action, although it may also be possible that artemisinin chemistry (iron chemistry) is involved in the process.

As can be seen from the preceeding dicussion, bispidone type compounds are not particularly active, or even non-toxic (quite high ED_{50} values), but it has been shown that with a rational tuning of the structure, promising new lead structures of this family might be used to introduce this kind of compounds to the interesting field of the antimalarial drugs.

Erklärungen gemäß § 8 (3) b) und c) der Promotionsordnung:

a) ich erkläre hiermit, dass ich die vorgelegte Dissertation selbst verfasst und mich keiner anderenfalls der von mir ausdrücklich bezeichneten Quellen und Hilfen bedient habe,

b) ich erkläre hiermit, dass ich an keiner anderen Stelle ein Prüfungsverfahren beantragt bzw. die Dissertation in dieser oder anderer Form bereits anderweitig als Prüfungsarbeit verwendet oder einer anderen Fakultät als Dissertation vorgelegt habe.

Heidelberg, den 24.01.2006 ……………………………………

Carlos López de Laorden